EXPERIMENTAL STUDIES OF MAGNETOHYDRODYNAMICS IN A LABORATORY SCALE HALL-HEROULT CELL

by

MANEESH CHANDRA SRIVASTAVA

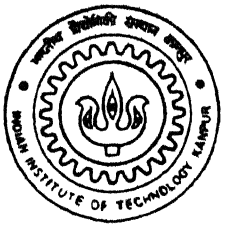

DEPARTMENT OF MATERIALS AND METALLURGICAL ENGINEERING

INDIAN INSTITUTE OF TECHNOLOGY, KANPUR

JULY, 1998

EXPERIMENTAL STUDIES OF MAGNETOHYDRODYNAMICS IN A LABORATORY SCALE HALL-HEROULT CELL

A Thesis Submitted
In Partial Fulfilment of the Requirements
for the Degree of
MASTER OF TECHNOLOGY

by
MANEESH CHANDRA SRIVASTAVA

to the
DEPARTMENT OF MATERIALS AND METALLURGICAL ENGINEERING
INDIAN INSTITUTE OF TECHNOLOGY, KANPUR
JULY, 1998

Entered In System

DEDICATED TO

My Parents

my source of inspiration

CERTIFICATE

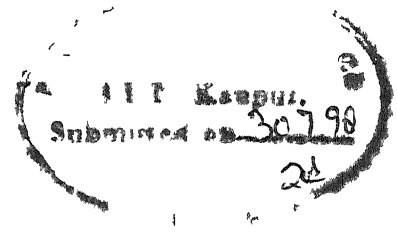

This is to certify that the thesis entitled " **Experimental Studies of Magnetohydrodynamics in a Laboratory Scale Hall-Heroult Cell**" by *Maneesh Chandra Srivastava* has been carried out under our supervision, and this has not been submitted elsewhere for a degree

(Dr S P Mehrotra)
Professor
Department of Materials & Metallurgical Engineering
Indian Institute of Technology, Kanpur

(Dr Rajiv Shekhar)
Associate Professor
Department of Materials & Metallurgical Engineering
Indian Institute of Technology, Kanpur

Dated July, 1998

ACKNOWLEDGEMENT

In my journey through a problematic path the light of right direction and destiny has come from my supervisors Dr S P Mehrotra and Dr Rajiv Shekhar Their invaluable suggestions and innovative ideas have made it possible for me to sail through all the predicament situations My sense of gratitude knows no bound for their mountain high patience they have offered me in all my mistakes and for their help in all parts of the study

I would like to express my sincere thanks to my labmates Brijesh Singh, P S S Raju, M H Umranikar, Alok Dobriyal, Manish, Nandan, Anoop, Tanmoy, Satyam Suwas for their valuable help and active cooperation during my stay at IIT Kanpur

I would like to express my sincere thanks to Mr K S Tripathi and Mr S Agnihotri for their help and support through out the experimental work

I express my sincere thanks to Mr G P Bajpai for his suggestions and active participation during the compilation of the thesis

Finally, I would like to offer my sincere thanks to my family members and relatives for their inspiration and encouragement in this study

July, 1998
Kanpur

Maneesh Chandra Srivastava

TABLE OF CONTENTS

LIST OF FIGURES

LIST OF TABLE

ABSTRACT

Production of aluminium is an energy intensive process Worldwide th research on aluminium is focused on the design of Hall cells for reducing energ consumption Unfortunately, it is very difficult to conduct experiment on laboratory sca models of Hall cell at actual conditions because of (a) the corrosive nature of the electroly and (b) high level of heat losses Consequently, one strategy adopted in investigations of Ha cells is to set up "low temperature" simulated cells Data from the simulated cell is used develop mathematical model that is subsequently used in the design and optimization industrial Hall-Heroult cells

The present investigation is carried out with the prime objective of generatir magnetic and velocity field distribution in a laboratory scale simulated cell Initially, a sing anode Hall cell was fabricated and experiments were carried out at the actual operatir condition with the aim of gaining familiarity with cell operation Though the secondary ai was fulfilled but the idea of recording magnetic field measurements in a multi-anode Hall ce was abandoned owing to the high operating temperature in the range of 1000^{o}C and th corrosive fluoride environment prevailing in the cell

Later a low temperature simulated Hall cell was designed and fabricate Readings of magnetic fields at temperatures below 100^{o}C were recorded in all the thre directions The trend is in accordance with expectation and match well with the findings other investigators

CHAPTER 1

INTRODUCTION

The electrolytic cell designed by Hall and Heroult independently, towards the end of nineteenth century is universally used for aluminium production In the electrolytic process, purified alumina dissolved in cryolite is electrolysed at temperature around 960^{o}C Current enters the cell from top through the bus-bar connected to carbon anodes, passes through the fluoride bath containing dissolved alumina and exits from the bottom through the collector bars fitted in the cathodic carbon block constituting the pot

Design of a typical industrial Hall cell is shown in the Fig 1 1 Barring a few variations in number of anodes, dimension of the cell, change from soderberg anode to prebaked anodes, minor changes in bus-bar design, changes in alumina charging systems, switching over from low to high amperage cells, minor changes in bath chemistry, better refractory and other construction materials, the design of the Hall cell during its existence for almost one hundred years has remained unchanged

1 1 CELL OPERATION

The operating parameters of the cell which are generally to be controlled for stable operation are current density bath temperature, bath composition, bath density, anode design and the interpolar distance Each of these parameters has its own influence over the process Many a times, a cell becomes unstable due to bad control of some of the parameters, particularly the bath composition During the electrolysis there is continuous depletion of alumina in the bath and finally a stage is reached when the alumina content of bath drops to a value ranging from 1 to 2 wt%, depending on current density, temperature, bath convection, electrolyte composition, shape and surface condition of the anode, etc [1] The bath suddenly begins to exhibit poor wettability on the anode The gas bubbles which are released at the anode are no longer washed away by the electrolyte resulting in formation

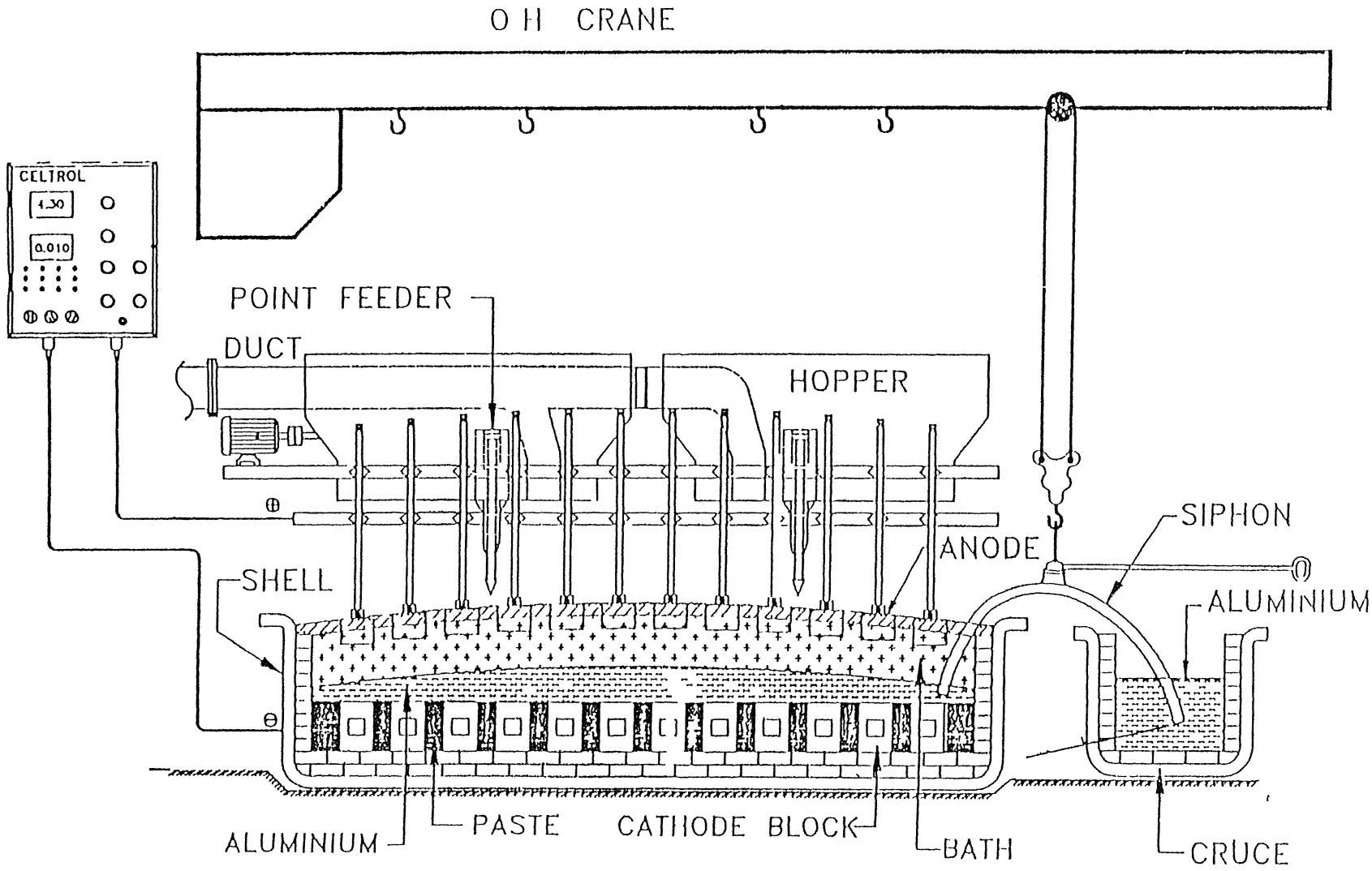

Figure1 1 Working System of a Pot Cell (open view)

of a continuous gas film around the anode surface This gives rise to significant increase in anode resistance which is indicated by the cell voltage shooting up This phenomenon is generally referred to as 'anode effect' Excess alumina in the bath also causes severe problems, particularly, if it exceeds the solubility limit of alumina in the fluoride bath Undissolved alumina which is heavier than both the electrolyte and the molten aluminium settles at the bottom of the cell i e below aluminium and forms a muck This also increases the cell resistance and adversely affects the current flow from the cell to the collector bar Undissolved alumina also finds its place at metal electrolyte interface because of high aluminium electrolyte interfacial tension This has been confirmed by the analysis of bath of the interface region [2] A density induced flow is set up at the interface of metal and electrolyte causing dispersion of alumina accumulated there The topic on bath chemistry and bath density has been dealt with in some detail in chapter 2 The problems arising due to over and under feeding of alumina are very well taken care of in modern cells which are being operated at lower alumina content and anode effects are avoided by trend analyzers of the control systems which sense the resistance of the cell and feed the appropriate amount of alumina according to the bath requirement [3]

1 2 CURRENT AND ENERGY EFFICIENCIES IN HALL CELLS

Although traditionally the Hall cells have been operated at around 1A/cm^2, trend in modern cells is to operate at lower current densities (cd), typically 0 8 A/cm^2, and higher currents ranging from 180 kA to 250 kA Significant improvements in cell operations in modern cells have been possible due to better magnetic design of the electrical conductor bus components, application of state-of-the-arts hardware and software computer systems for the control and management of cell operations with alumina point feeders, operating with a low ratio or high excess aluminium fluoride electrolyte chemistry There has been a three fold increase in the cell life over the last forty years Besides improvements in life, there have been significant lowerings in the voltage drops through cathodes typically being reduced by 0 15 V and energy consumption by 0 5 kWH/kg Al produced [4]

Though the current efficiency (CE) of the cell is almost touching 95 % in most of commercial cells, specific energy consumption of good cells remain as high as 12 9 kWH/kg against theoretical value of 6 2 kWH/kg as shown in Fig 1 2 [5] The reason behind

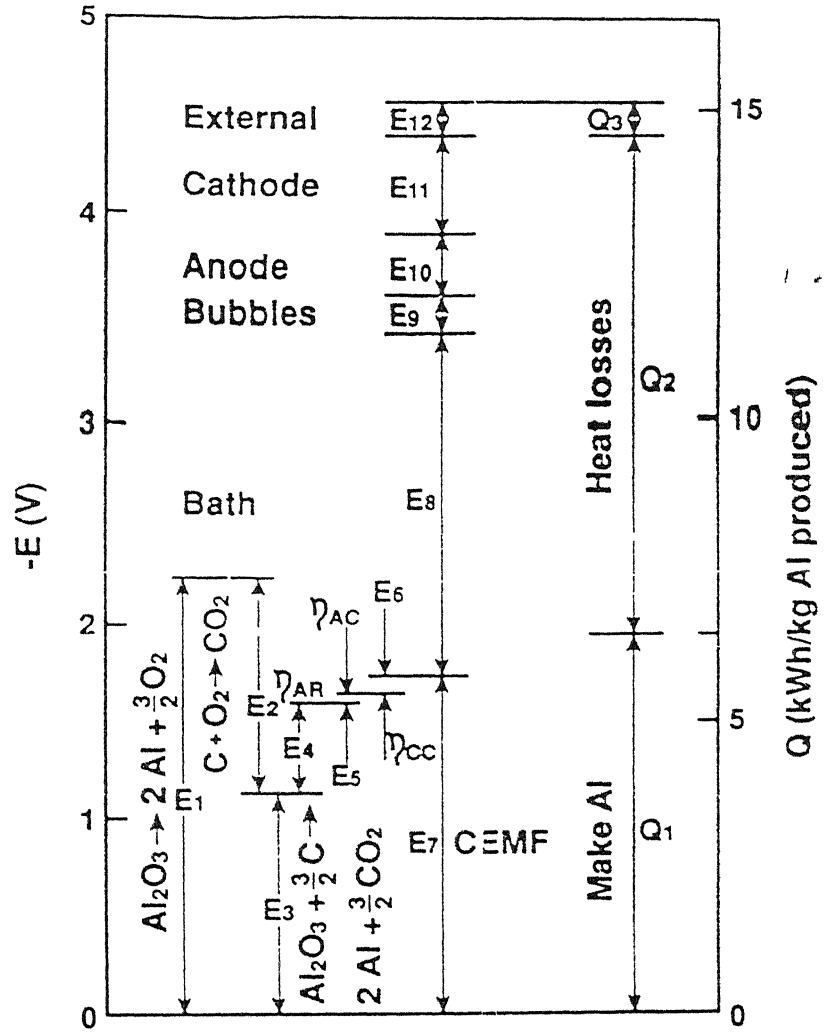

Figure1 2 Typical voltage distribution and energy requirement in a Hall-Heroult cell.

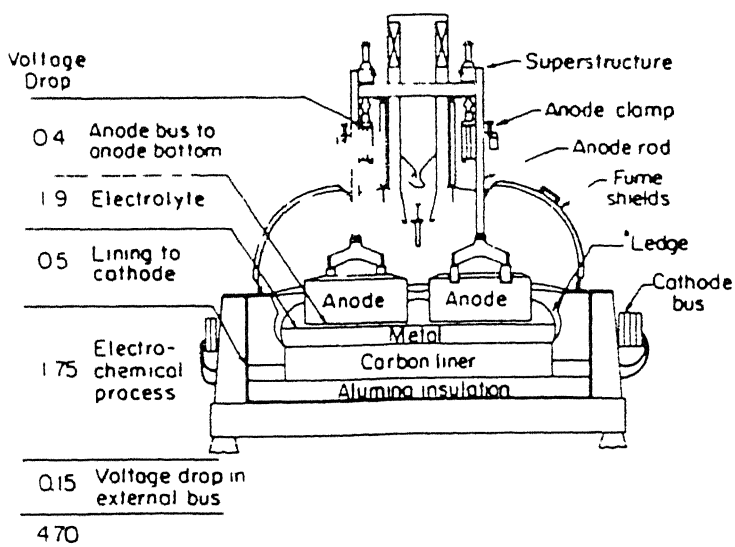

Figure1 3 Cross section of the Hall-Heroult Cell circuit approximate Voltage drops across various plate

this higher energy consumption may be directly linked with voltage drops across the anode stem, stubs, carbon lining and electrolytic bath, apart from electrochemical decomposition potential of alumina appropriate to the physicochemical state of the cell as shown in Fig 1 3 Energy consumption rates are proportional to these voltage drops, major efforts towards improvement of cell performance is in terms of lowering energy consumption There is not much scope of any significant reduction in voltage drops across the anode stem, stubs, connecting cables, and carbon lining, as the technology in terms of materials used in these components and their fabrication has more or less been optimized As most modern cells generally maintain an optimum bath composition, there is not much scope of lowering the electrochemical decomposition potential either The only candidate which has a reasonable scope of further lowering is the voltage drop across the electrolytic bath contained between the anode and cathode Therefore, any meaningful effort in the direction of further lowering the energy consumption has to concentrate on this aspect The voltage drop across the electrolyte bath of optimum concentration essentially depends on the anode-cathode distance (ACD), and any attempt to lower this voltage drop will require reducing the ACD However, reducing the ACD beyond a limit, increases the probability of short circuiting between the anode and molten aluminium, which acts as cathode after the initial stages of electrolysis Furthermore, smaller ACD causes reduced rate of electrical generation of heat in the cell which in turn cools down the cell and hampers the normal operation So in the process of jacking up the energy efficiency (EE), one may land up in a much worse situation This adverse effect of lowering the ACD can only be taken care of by improving the cell insulation design to achieve a heat balance at the lower ACD, and good control over the metal-cryolite interface by better control of magnetohydrodynamics of the cell which reduces oscillations at this interface

1 3 ROLE OF MAGNETOHYDRODYNAMICS IN HALL CELLS

Large currents of the order of 150kA-250kA flow through a Hall cell Large magnetic fields are produced due to the current in the cell as well as the current in the neighbouring cells This magnetic field on interacting with the current flowing in the cell gives rise to large magnetic forces and torques which provide motion to the conducting melt esp aluminium pad present at the bottom The electromagnetic forces acting within the aluminium causes its motion in horizontal direction which leads to formation of waves at the

metal/bath interface [6 7] Waves developed in the aluminium pad which apart from resulting in momentary shortcircuiting to the anode, produce erosion of the carbon lining of the cell by increasing the dissolution rate of aluminium carbide and by mechanical abrasion enhanced by the undissolved alumina frequently present

The efforts of technology experts are aimed at maintaining a quietened metal/bath interface by reducing the electromagnetic torques created in the cell by altering the basic design of the cells especially the bus-bar design, using mathematical modelling techniques The greatest effort, however, is to minimize the vertical magnetic field because it interacts with the horizontal currents and creates swirls and instability in the molten aluminium pad

1 4 OBJECTIVE OF PRESENT INVESTIGATION

One of the primary aims of researchers and technology experts, engaged in aluminium extraction research, has been to increase the energy efficiency of the Hall cell from its present level of around 48% to as high a value as possible The oscillating interface caused by large electromagnetic forces developed in the bath due to large currents flowing through the cell is one of the major factors responsible for higher energy consumption in the cell

One of the convenient methodologies to work towards the design of an energy efficiency improvement is through the judicious use of mathematical models, based on thermal balance and fluid flow considerations, and incorporating operating conditions as close as possible to the real cell rather than actually introducing the changes in the cell design and monitoring their effects on the cell performance Unfortunately, the mathematical models already developed are facing a paucity of reliable plant/experimental data in published literature against which they can be validated

Hence, the present study, aims at carrying out investigations in several stages In the first stage, a single anode cell is designed, fabricated and operated to observe the effect of various process parameters on the performance of the cell and generate magnetic and velocity data for validating the mathematical model being developed A large multi-

anode cell is then to be fabricated and operated Magnetic and velocity fields at various operating parameters are to be recorded in the multi-anode cell

The probe to be used for measuring the magnetic fields has limitations on the temperature of about 75^{o}C, up to which it can be safely used Fabrication of a good and reliable cooling system is essential to make measurements at temperatures around 1000^{o}C This has not been possible with the facilities existing in our laboratory Moreover, the single anode Hall cell is not able to exactly simulate the real Hall cell as (i) the amount of aluminium collected at the bottom of the cell is not sufficiently large to make a flat pool over the base plate, (ii) current and energy efficiencies are low, (iii) due to large surface area to volume ratio, heat losses are large requiring external heating It was, therefore, decided to fabricate a low temperature simulated multi-anode Hall cell using Wood's alloy and measure magnetic fields at various locations within the cell operated under different operating conditions It is hoped that these measurements would be useful in validating the mathematical model being developed to predict the fluid flow behaviour induced by the electromagnetic field

1 5 LAYOUT OF THE THESIS

The report comprises of eight chapters After this first introductory chapter, the second chapter is on literature review which deals with the relevant literature on various aspects of cell operation and latest developments made in the field Scope of the present investigation is presented in the third chapter Fourth chapter deals with the design, fabrication and operational aspect of a single anode Hall type cell Results and discussion on the single anode cell are presented and discussed in detail in the fifth chapter The design, fabrication and operation of a simulated low temperature multi-anode cell is discussed in the sixth chapter Results and discussion of low temperature simulated experiments have been presented in the seventh chapter Eighth chapter gives the summary and conclusions of the complete work done both on single anode Hall type cell operated at normal operating condition of real cells and low temperature multi-anode simulated Hall cell

CHAPTER 2

LITERATURE REVIEW

In this chapter, a brief review of literature on Hall-Heroult cell has been presented The topic comprises of the main operating parameters which affect the performance of the cell, particularly, bath temperature, bath chemistry, bath impurities, bath density, anode related factors, cathode design and construction, cathode refractory materials and magnetohydrodynamics of the cell The resistance based control for proper cell operation, along with its various corrective actions has been dealt with in some detail Various steps which control system takes up during abnormal situation, particularly, quenching of anode effects have also been described In the last section of this chapter, discussion is focused on current status of mathematical model pertaining to various aspects of cell operation

2 1 OPERATING VARIABLES AFFECTING PERFORMANCE OF HALL CELL

2 1 1 BATH TEMPERATURE

The thermal balance of the cell largely depends on the bath temperature and the liquidus temperature The liquidus temperature gives information about bath composition, the bath temperature, more importantly superheat, determines the current efficiency Temperature of bath to be maintained depends more on the superheat than the bath temperature itself [8]

Lower superheat, in general, results in higher current efficiency (CE) but decreased alumina solubility, which may lead to sludge formation The sludge gives rise to horizontal current components which interact with the magnetic field and cause an unstable metal pad

On the other hand, an excessively high superheat leads to a fall in current efficiency, increases thermal losses and increases anode carbon consumption For every 4°C rise in the bath temperature above the normal 960°C, the current efficiency falls by about 1% With increasing temperature, the extent of side reactions and rate of dissolution of the metal in the bath increase Decrease in temperature, however, does not improve the CE indefinitely [9]

Better control of temperature leads to reduction of thermal cycling of bath as well as of cathode blocks, and results in stable ledges, increase in cell life, and lesser turbulence due to reduced temperature gradients

Several attempts have been made to measure bath temperature as accurately as possible by different types of thermocouple The following conclusions have been drawn by Zhuxian, Jingjiang and Xiaoli at various locations in the Soderberg cell [10]

1 The bath temperature is usually 3-7°C higher than that of the metal

2 The bath temperature under the anode is 5-10°C higher than outside the anode region

3 The bath temperature at the current exit side is 2-3°C higher than at current entry side

It has also been observed that before the onset of an anode effect the bath temperature usually increases by 5-10°C It reaches a maximum of 1060-1080°C during the anode effect, and it takes about an hour to restore the original temperature after the quenching of the anode effect

Thermal effects associated with alumina feeding are also important The most probable value for the heat of dissolution in electrolytes has been found to be 100 and 120 kJ/mol of alumina As the alumina dissolves the superheat changes and consequently, the heat transfer rate varies Thermal effects associated with an alumina feeding cycle are dependent on the feeding technology (i e ,side or centre break, or point fed) used in a smelter

[11,12,13] The overall thermal effect associated with any feeding operation depends on

- the amount of alumina added
- the immersion time of the crust breaking mechanism
- the amount of crust broken during the break
- the average temperature of the "cold" alumina discharged
- the phase of the alumina
- the heat of solution
- heat of secondary reactions and processes associated with volatile

Bath temperature has a very strong influence on volatilization of electrolyte Vapours over Hall bath have the composition $NaAlF_4$ (sodium tetra fluoro aluminate) [14,15] Bath vapour pressure increases with decreasing bath ratio and increasing temperature At higher operating temperature, the surrounding atmosphere in the pot room has dense fumes of vaporised bath Additions of calcium fluoride, magnesium fluoride, lithium fluoride and alumina all decrease vapour pressure, though the alumina addition has the greatest effect

Significant amounts of convective and radiative heats are lost from the cell during its operation at around $960^{o}C$ To decrease the proportion of these losses, the trend these days is to go for bigger and bigger cells This is the classic surface area to volume story - as the size increases, the ratio decreases

Thermal balance in the cell has to be maintained such that a frozen layer of electrolyte, also known as ledge, forms on the sides of the cell to resist the corrosive action of the fluoride electrolyte The ledge thickness varies along with the height of the cell as shown in Fig 2 1, which in turn is controlled by providing appropriate thermal insulation on the sides of the cell Two liquid phases (molten electrolyte and molten aluminium) having very different heat transfer coefficients contact the frozen layer As aluminium is denser than the electrolyte, normally no frozen layer of the latter should be expected below the electrolyte/metal interface However, due to interaction of magnetohydrodynamics and the capillary action, some electrolyte is always able to reach the side walls of the cell with the metal pad to form a frozen layer

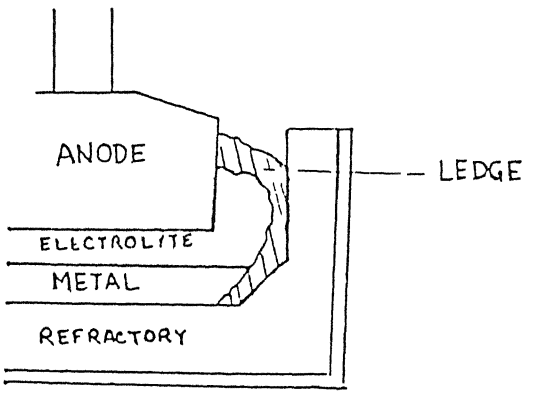

Figure2 1 Schematic Diagram of ledge in Hall Cell

Increased variable	Al_2O_3 solubility	Electrical conductivity	Density	Viscosity	Liquid temperature	Metal solubility	Surface tension	Vapour pressure
CaF_2	↓	↓	↑	↗	↓	↓	↑	↓
AlF_3	↓	↓	↓	↓	↘	↓	↓	↑
LiF	↓	↑	↓	↓	↓	↓	↑	↓
MgF_2	↓	↓	↑	↑	↓	↓	↑	↓
NaCl	↓	↑	↓	↓	↓	↓	↓	
NaF	↷	↑	↘	↘	↘	↑	↑	↓
Al_2O_3	—	↓	↓	↗	↓	↓	↘	↓
Temperature	↑	↑	↓	↓	—	↑	↓	↑

The qualitative effect of various additives on the properties of cryolite An up arrow indicates that this additive increases this property a down arrow indicates the converse A curved arrow indicated that the effect is highly non linear with concentration

Figure2 2 The qualitative effect of various additives on the properties of cryolite [1]

2 1 2 BATH CHEMISTRY

Normally, the bath consists of cryolite, alumina, calcium fluoride, aluminium fluoride Sometimes the additions of lithium fluoride and magnesium fluoride may also be made Constituents other than cryolite and alumina are called additives and are added to improve the chemical and physical properties of the electrolyte, to lower the cell operating temperature, to decrease the vapour pressure of the electrolyte so as to reduce its vapour losses to increase the electrical conductivity of the electrolyte to enable either greater interelectrode distance or a lowering of the cell voltage (to improve energy efficiency), to reduce fog formation or redissolution of aluminium in cryolite The qualitative effects of various additives on the properties of cryolite is shown in Fig 2 2 Modern cells operate with bath containing 10-12 wt% AlF_3, 3 5-6 wt% CaF_2 and 3% alumina [16,17,18]

2 1 2 1 BATH RATIO

The ratio of NaF/AlF_3, known as the bath ratio, plays an important role The bath ratio slightly less than three is considered to be optimum A higher NaF content reduces the current efficiency apparently due to an increase in the concentration of sodium ions and the deposition of sodium on the cathode

2 1.2.2 CALCIUM FLUORIDE

Calcium Fluoride (CaF_2) is a neutral additive in most cryolite baths It is maintained at 4-7 wt% in industrial baths Most CaF_2 comes as an impurity in the alumina from the Bayer's Process In this range, it has the beneficial effect of lowering the freezing point of the cryolite bath by about 12-20^{o}C However, its concentrations greater than 8-10 wt% causes excessive wave formation, with subsequent local events of short circuiting and/or dispersion of metal Calcium fluoride increases electrolyte density resulting in poorer phase separation between the electrolyte and metal

2 1 2 3 ALUMINIUM FLUORIDE

Aluminium Fluoride (a Lewis acid) is the most commonly used bath additive and it increases the acidity of the bath It improves the current efficiency by

1) reducing the solubility of sodium, aluminium, lithium in the electrolyte which is in equilibrium with the metal pad,
2) lowering the liquidus temperature of the cryolitic bath and consequently the bath temperature, and
3) lowering the bath density

Aluminium Fluoride (AlF_3) has the undesirable effects of decreasing the electrical conductivity and alumina solubility of the bath In modern cells where higher percentage of AlF_3 is being used, the negative aspect of reduced conductivity, hence higher voltage drop across the bath is neutralized by using very large anodes that significantly reduce the anode current density Thus, both the anode over voltage and the bath voltage drop are lowered The decreased solubility of alumina does not pose a big problem because the modern automatic control devices installed in the cell, regulate the alumina feed rate depending on the solubility of alumina in the bath at the operating temperature and composition There is a growing tendency to operate the pots at lower Al_2O_3 content to minimise the problems arising due to Al_2O_3 accumulation at the metal/bath interface or at the bottom of the cell

Higher AlF_3, however, results in higher fluoride emissions from the cells Modern fume recovery systems capture and recycle the fluorides in reduction plants

2 1 2 4 LITHIUM FLUORIDE

When added to cryolite, lithium fluoride behaves very much like sodium fluoride, (a Lewis base) It tends to increase the basicity of the bath and increases the bath ratio [19] It is primarily used to improve the cell performance by increasing the electrical conductivity of the modern cryolitic bath and decreasing the bath operating temperature

Plant operational results [19], obtained using a combined lithium-modified low

ratio (LMLR) bath in a modern 180 kA prebake cells, show that the addition of lithium within a specific composition range is beneficial in decreasing the cell voltage and unit energy consumption It also results in a significant improvement in the cell voltage stability However, the current efficiency decreases with increase in LiF concentration, apparently as a consequence of the corresponding decrease in AlF_3 content The physicochemical properties of low ratio bath and lithium fluoride bath is given in Table 2 1 and performance data for the low ratio bath and lithium fluoride bath is given in Table 2 2

2 1 2 5 ALUMINA

Alumina is the most important raw material used in the electrolytic process, where it acts as a solute in the molten cryolite based bath Apart from this primary function, being on the surface crust, it also provides an additional seal, absorbs gases which are evolved through the crust, and provides heat insulation

Both alumina depletion as also its excess amount cause the cell to go unstable As alumina content falls below 2 wt%, a phenomenon referred to as "anode effect" takes place During this effect, the current falls to almost zero and electrolysis stops Reduced alumina content of the bath (below 2 wt%) drastically reduces its wetting characterstics of the bath as a result of which gases formed/released at the anode (CF_4, C_2F_6, CO etc) [20 21] are no longer washed away from the anode surface forming a continuous gas film around the anode Because of the formation of this electrically insulating gas film the resistance of the anode is significantly increased in anode effect Anode effects are undesirable because of extra energy consumption, overheating of the cells, and the generation of the unwanted fluorine containing anode exhaust gases Anode effect can also occur at higher alumina content, if current density is higher than the critical current density (ccd)

On the other hand when the alumina content increases beyond the dissolution limit undissolved alumina tends to accumulate on the bottom of the cells, forming the sludge This sludge is undesirable since it disrupts the current path in the cell, giving rise to unstable cell operation In addition, it makes the maintenance of constant alumina content of the bath more difficult

Electrolyte Properties	Low Ratio	1% LiF LMLR	2% LiF Bath	3% LiF Bath
Bath Operating Temperature C	956	958	953	947
Freezing Point C	954	948	938	937
Bath Superheat C	2	10	15	10
Density, g/cm	2 1213	2 1236	2 1359	2 1436
Electrical Conductivity, ohm cm ^{1}	2 1251	2 1809	2 2767	2 3499
Alumina Solubility, wt %	6 2	6 2	6 0	5 6
Bath Vapor Pressure torr	4 1	3 7	2 5	2 0
Equilibrium Metal Solubility, wt %	0 320	0 327	0 359	0 367

Table 2 1 Physico-Chemical Properties of Low Ratio Bath and LiF-Modified Baths [19]

	Low Ratio	1% LiF LMLR	2% LiF Bath	3% LiF Bath
Months	12	12	5	3
Number Cells	240	240	18	18
Amperage kA	181 1	181 6	180 3	179.3
Resistance, μ ohm	14 14	13 82	12 95	13 14
Current Eff , %	94 47	94 15	93 24	91 96
Volts/Cell	4 210	4 160	3 984	4 006
KWH/kg Al DC	13 28	13 15	12 75	12 99
Instability, μ ohm	> 0 20	0 14	0 15	0 14
Anode Effects/PD	0 15	0 18	0 23	0 22
Cathode Drop, V	0 430	0 440	0 426	0 417
Bath Tap kg/PD	159	94	11	62

Table 2 2 Performance Data for Low Ratio and LiF-Modified Bath [19]

The period of alumina dissolution depends on several factors, such as convection and wave action on the bath surface, and also on the ability of the alumina to fluidize and spread out on the bath surface The agitation of the bath caused by the evolution of gas (CO and CO_2) and the magnetic stirring effect produced by the current flowing through the bath from the anode to the cathode lining of the cell help in maintaining fresh additions of alumina in suspension long enough for dissolution in the bath

2 1 3 BATH IMPURITIES

Besides the basic electrolyte and substances specifically added to improve its physico-chemical and electrochemical properties some other constituents originate as well from the anode material and from the raw materials used for the preparation of the electrolyte These constituents take an active part in the electrochemical process Impurities can also arise from cathodic carbon lining and the steel tools which are used during cell operation

The main impurities are metallic oxides B_2O_3, P_2O_5, sulphates and sulphide of alkali metals Depending on their character, these impurities may influence the electrolysis in several ways

(i) reaction with the electrolyte constituents, causing modified bath composition,
(ii) interaction with the anode carbon and/or with the cathode lining,
(iii) impurities with a lower decomposition potential than alumina can be decomposed electrolytically and the product can contaminate the aluminium produced

Different impurity oxides have different solubility levels in cryolite and alumina mixture These oxides dissolve in cryolite by one of two schemes They may form a simple eutectic with no interaction or alternatively they may react with the cryolite Generally the dissolution of an oxide in cryolite takes place according to the following scheme

$$2Na_3AlF_6 + 3MeO = 3MeF_2 + 6NaF + Al_2O_3$$

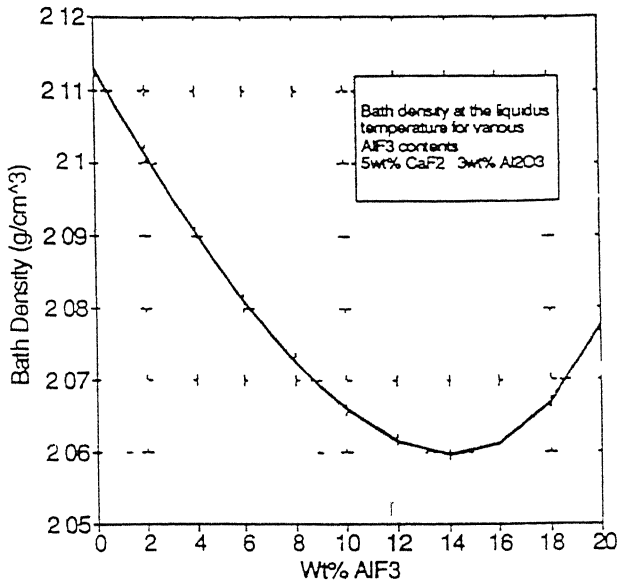

Figure2 3 Density of $Na_3AlF_{6-}AlF_3$ melts as a function of the AlF_3 content at their liquidus temperature

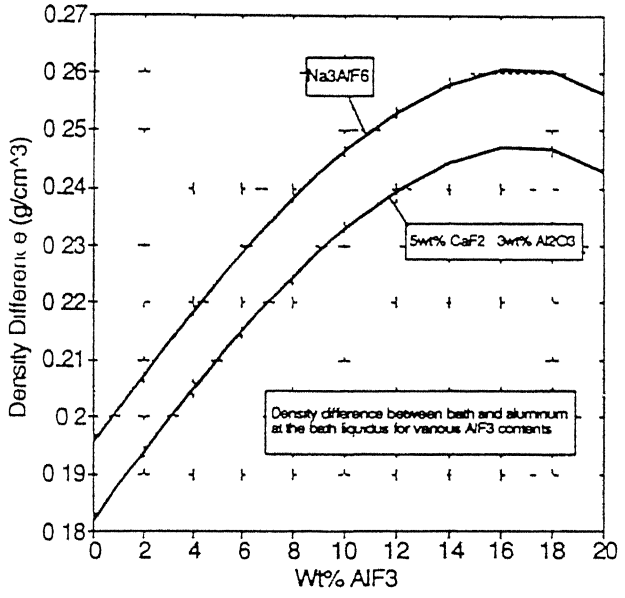

Figure2 4 Density difference between liquid aluminium and cryolite melts as a function of the AlF_3 content for cryolite and cryolite containing 5 wt% CaF_2 and 3 wt% Al_2O_3 respectively

The new formed Al_2O_3 can react with additional cryolite or with unreacted MeO

All oxides (Li_2O, Na_2O, K_2O, MgO, CaO, BaO, SiO_2, TiO_2, P_2O_5) are surface active and improve the wetting of carbon by melt As a result of improved wetting of carbon, it may be assumed that the impurities would impede the separation of the carbon froth from the electrolyte This in turn, increases the ohmic resistance of the electrolyte and eventually disturbs the the normal working of the cell This presumption has been confirmed in the industrial cell where it is observed that P_2O_5 and V_2O_5 are most dangerous admixtures from this point of view The concentration of P_2O_5 in the carbon froth is three to five times higher than in the electrolyte

2 1 4 BATH DENSITY

The lower the bath density, higher is the rate of separation of the metal liberated from the bath Theoretically, the bath density can be lowered by using a high AlF_3/NaF ratio, as shown in Fig 2 3, however, the detrimental effects of increasing AlF3 have been discussed earlier Maximum density difference is observed at 16 wt% AlF_3 as shown in Fig 2 4, which leads to shorter anode to cathode distance

For a given superheat, the aluminium/bath density difference decreases with increasing CaF_2, increases with increasing Al_2O_3, and decreases slightly with increasing LiF content

The bath density is related to bath temperature [22] as

$$\rho_{bath}(g/cm^3) = 3\text{-}0\ 006(AlF_3)\text{-}0\ 009(Al_2O_3)+0\ 004(CaF_2)\text{-}(0\ 009)T(^oC)$$

The density of aluminium is related as

$$\rho_{Al}(g/cm^3) = 2\ 561\text{-}(0\ 000272)T(^oC)$$

Density variations lead to ledge and bottom crust formation and Al_2O_3 density induced flow

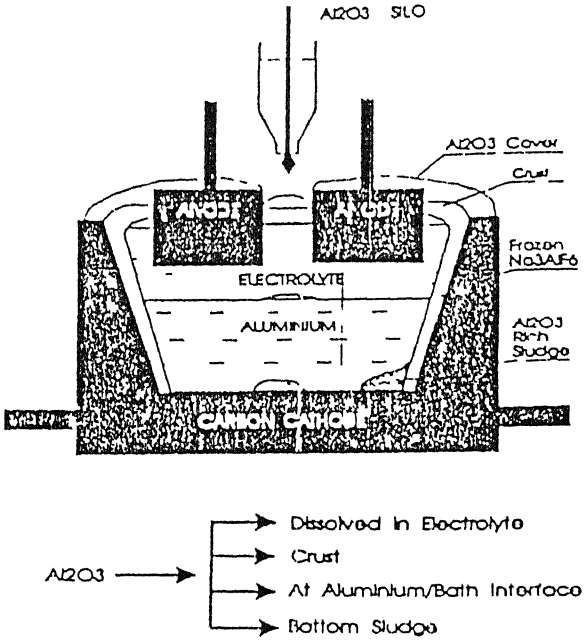

Figure 2.5 Schematics of the dissolution behaviour of alumina upon addition to the Hall-Heroult Cell [23]

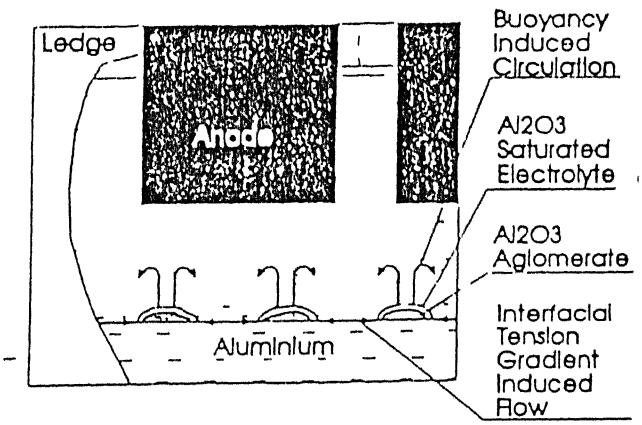

Figure 2.6 Schematics of the buoyancy induced circulation upon dissolution of alumina at the Al/Bath interface [23]

2 1 4 1 LEDGE AND BOTTOM CRUST FORMATION

Liquid adjacent to the ledge has lower temperature and higher AlF_3 content than the bulk bath [2] The corresponding density difference leads to an intense fluid motion and/or formation of mushy zone, which greatly affects the heat transfer coefficient Composition induced fluid motion may be of importance under the following situations

1) formation of side ledge
2) ledge melting during anode effects
3) ledge freezing during anode change
4) bottom crust formation

2 1 4 2 ALUMINA DENSITY INDUCED FLOW

On adding alumina to the cell, the undissolved part in the form of agglomerates, remain at the bath/metal interface as shown in Fig 2 5, due to high Al/electrolyte interfacial tension [23] This phenomena of excess Al_2O_3 being accumulated over metal has also been reported by Schadinger [24] Chemical analysis of the bath above the metal pool in industrial cells shows an alumina content of 16 wt% while the bulk bath contains only 4wt% Al_2O_3 Kent [25] has also reported the similar observation As the bath density at the alumina saturation side is less than at the cryolite side, liquid fraction surrounding the agglomerates rich in alumina moves causing alumina dispersion as shown in Fig 2 6 Due to increased bath alumina content in the vicinity of the alumina agglomerates, the local interfacial tension is higher than the average value This induces an interfacial tension driven flow, promoting further removal of alumina This interfacial tension and buoyancy induced flow leads to reduced current efficiency due to the increased transport of aluminium away from the boundary layer The liquid forced upwards is richer in dissolved metallic in addition to alumina Accumulation of Al_2O_3 at metal/bath interface is restricted with good feeding practice and computer control and low bath alumina content These findings are also substantiated by investigations carried out at Pechiney where also the current efficiency was seen to increase with decreasing Al_2O_3 content

2 1 5 ANODE RELATED FACTORS

Major anode related factors that affect the economics of an aluminium smelting cell are the factors contributing to

(1) the cell voltage drop,

(2) anode carbon consumption above the theoretical value (0 33 kg of anode per kg of aluminium produced, at 100% current efficiency)

The cell voltage drop from anode bus to anode bottom is about 0 4 V [26] This value could be cut down further only when the present material of anode, calcined petroleum coke is improved on or is replaced by a better conducting material [27]

The excess anode carbon consumption factor has components both above and below the bath Air oxidation or "air burning" occurs above the bath level Below the bath component may be further subdivided into selective oxidation of anode components resulting in carbon "dust" in the bath, and chemical reaction of anode material with oxygen to form carbon dioxide Anode density is considered to be a general indicator of anode quality and, more directly, has an influence on the frequency of anode replacement

Optimum economic Hall cell is somewhat handicapped by the consumable anode Anodes are replaced as they near complete consumption Since the carbon anodes are consumed by the anodic reaction (evolution of CO_2 gas at the anode) at the rate of 2cm/day, one anode per day per cell needs to be changed Through this consumable anode, several impurities also get introduced into the bath As the anode is consumed, the ACD changes and it has to be readjusted to maintain the stability of the process

Replacement of an anode after its life of 10-20 days in the cell gives rise to an abnormal situation When a cold anode is installed in the anode bus, it does not carry current immediately, because of the resistive contact between the anode and its stub and a frozen layer of electrolyte at its bottom surface After a few hours, when the new anode is heated up, the frozen layer of the electrolyte melts, and the normal current flow begins This problem is, however, aggravated in the modern cells due to magnetic field compensation,

which reduces heat transfer to the newly installed anode If a large lump of crust is frozen at the bottom surface of the anode, it may take several days to remelt In the intervening period, some portion of the same anode is oxidised, thus leading to a carbon spike which shorts the metal pad as a consequence of anode beam movement To minimise such an effect, a bath-cleaning grab has been designed to remove any lumps of crust resting in the zone of the cell where an anode is being changed

2 1 6 CATHODE DESIGN AND CONSTRUCTION

Cryolite used in the process is very corrosive and attacks the expensive refractories It is often advantageous to use a frozen layer as a container for the molten material Variations in liquid-solid heat transfer coefficient with position in the cell require corresponding variations in the thermal conductance of insulation behind the frozen layer, in order to maintain an adequate protective layer without excessive thickness at any location

Earlier the cathode carbon was formed as a monolithic mass from an anthracite pitch matrix, often above a bed of alumina insulation These cathodes were extremely porous and had a high sodium up-take capacity, resulting in rapid failure

The failure or degradation of a cathode is usually reflected by an increase in cell voltage, pick up of iron, or the cell leaking The failure of the lining is the result of at least one of the four basic causes cracks generated through thermal or mechanical stresses, erosion, cracking through stresses generated by chemical reactions within materials, and oxidation by penetrating air [28,29,30,31,32]

To overcome these shortcomings of earlier cathode material and design, several improvements have been made By preforming the cathode mix into extruded blocks, higher densities (and lower porosities) are achieved Further, these blocks can be baked to higher temperatures, thus improving the crystallisation order and ensuring dramatically reduced sodium up take

In modern preformed cathode blocks, as shown in Fig 2 7,[33,34] the sides

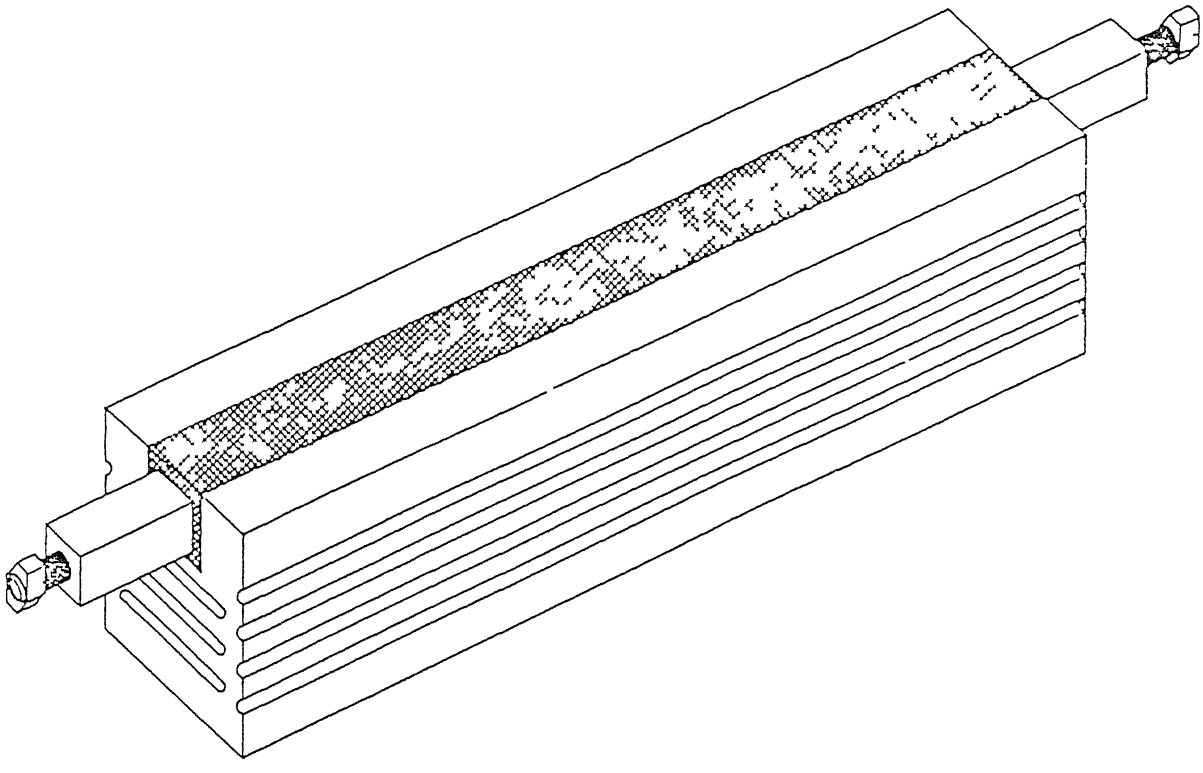

1	MATERIAL OF CATHOD BLOCK	–	ANTHRACITE
2	CATHODE BLOCK SIZE	–	1625x410x356 mm
3	GROVE SIZE	–	5"x5"
4	COLLECTOR BAR SIZE	–	2310x100x100 mm
5	WEIGHT OF BLOCK	–	328 Kgs
6	WEIGHT OF COLLECTOR BAR	–	125 Kgs
7	NO OF CATHODE BLOCK PER POT	–	PLANT#1 12 Nos
		–	PLANT#2 13 Nos

Figure2 7 Cathode block

of the graphitic blocks can be machined to close tolerances and the blocks pressed and glued together, minimising the possibility of defects being generated during start-up [33,34] This, in turn, leads to long cell lives The quality and longevity of the seals around the current collector bars to inhibit the ingress of air into the cathode lining needs to be improved Stuffing boxes at the entries for the collector bars prevent air burn of the back side of the carbon side wall Since it has been demonstrated that the oval collector bar slot design allows an improvement in electrical contact between the steel current-carrying collector bar and the carbon, thereby lowering cell voltages, techniques have been developed to extrude the blocks to that section when required Moreover, to restrain the bowing and heaving of cathode lining, strong steel shells may be used to provide lesser shell distortions

Improvements in cathode design are usually carried out through computer modelling, which may give a precise prediction of thermal performance These changes have the objectives of reducing heat losses, reducing cathode voltage drops, improving cell stability and operation, and increasing cell life In order to preserve heat balance and voltage savings, heat must be conserved in the cathode This means an increase in thermal insulation in the lower sidewall and under the blocks The thermal resistance of the upper side walls needs to be decreased

There has been a three fold increase in cell life over last fifty years Besides improvements, in life, there have been significant lowerings in the voltage drops through cathodes, typically being reduced by 0 15 V and energy consumption by 0 5 kWh/kg Al produced In achieving gains in performance, there have been several notable changes, including the improved quality of cathode carbon such as semigraphitized cathode blocks, reduced thermal cycling during cell operation, application of better insulating materials, better cell designs for thermal balance, better cathode designs to minimize degradation reactions, and improved cell start-up procedure

2 1.7 CATHODE REFRACTORY MATERIALS

To meet the needs of new and energy efficient Hall cells, new refractories and modified versions of old refractories have been introduced

Three major types of refractories are typically utilized in cathodes high-temperature refractory materials (HTR), low thermal conductivity insulation, and silicon carbide bricks During cell start-up and operations, refractories have to be structurally and chemically stable over the entire cathode temperature range Firebricks, low cement castables, and dry barrier refractory are used as HTRs Fireclay bricks, moler bricks, calcium silicate and diatomaceous silica blocks, vermiculite blocks and alumina have been used as low thermal conductivity insulation [36,37] Cell location of the cathode lining is shown in Fig 2 8 and comparasion of brick and castables is given in Table 2 3

2 1 8 MAGNETOHYDRODYNAMICS IN HALL CELLS

Fluid flow is very important for design and control of Hall cells The flow in the electrolyte governs the transport of reduced species, dissolution rate of alumina, convection in the bath Waves develop in the aluminium pad which apart from resulting in momentary shortcircuiting to the anode, produce erosion of the carbon lining of the cell by increasing the dissolution rate of aluminium carbide [29] and by mechanical abrasion enhanced by the undissolved alumina frequently present The latter mechanism is often accentuated by discontinuities at joints between carbon blocks that create turbulence in the aluminium which results in the formation of potholes Electrolyte and aluminium velocities at the sides of the cell influence the heat transfer coefficients that governs the thickness of the ledge Movement of the aluminium pad is caused mainly by the electromagnetic action in the aluminium and to a small extent by an interfacial drag of the moving electrolyte [7,38]

Magnetic field generated by large currents flowing through the cell (of the order of 150kA-250kA) interact in turn with the current producing the field and gives rise to Lorentz force according to the right hand thumb rule [1] The force per unit volume is given by

$$F_V = JxB$$

where J is current density and B is magnetic field vector The direction of the force is at mutual right angles to the current and magnetic field as shown in the Fig 2 9

The longitudinal component of magnetic field produces little trouble, but

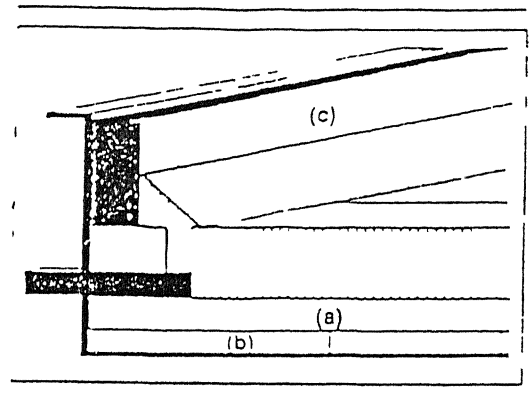

Cell locations of the cathode lining refractories (a) High temperature refractory (b) Lightweight insulation (c) SiC brick

Figure2 8 Cell locations of the cathode lining refractories [36]

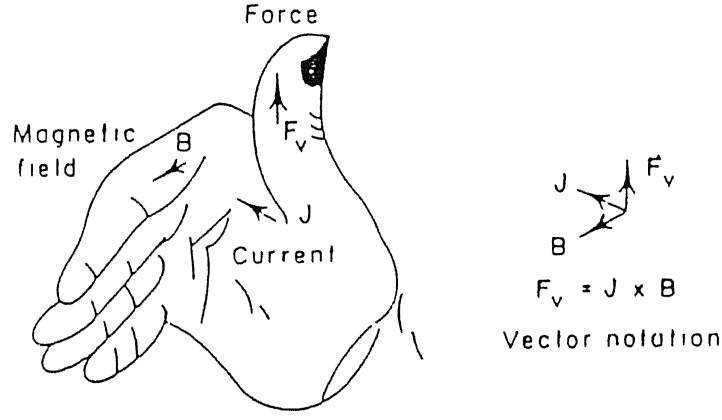

Figure2 9 Right hand thumb rule showing force direction as a function of current and magnetic field

Property	Heavy-Duty Fireclay Bricks	Low-Water Castables
Max Service Temp (°C)	2 650–3 200	2 800–3 200
Bulk Density (g/cm³)	2 20–2 30	2 21–2 68
Porosity (%)	10–14	16–21
Al_2O_3 Content (wt %)	26–39	46–69
SiO Content (wt %)	57–62	24–49
Hot Strength (HMOR) at 900 C (N/mm²)*	12–31	8–15
Crushing Strength Cold (N/mm²)	28–76	45–79
Thermal Conductivity [W/(m K)]	1 5–1 6	0 9–1 6

HMOR = Hot modulus of rupture

Table 2 3 Comparison of Brick and Castables [36]

strong transverse fields produce curvature of the aluminium pad surface and this asymmetry in the transverse field produces instability The greatest effort, however, is to minimize the vertical magnetic field because it interacts with horizontal currents and creates swirls and instability in the molten aluminium pad The electromagnetic force (emf) acting within the aluminium cause the motion of the aluminium in horizontal direction which is balanced by

- the inertia of aluminium
- the drag force exerted by the sides of the cell, that is, the ledge, on the aluminium (horizontal transport of the momentum)
- the drag forces exerted by the cell bottom and bath on the aluminium (vertical momentum transport)
- forces arising from pressure gradients

The desire to reduce ACD to cut down energy consumption, requires a flat aluminium pad with a minimum of wave action As it is not economical to make physical changes on operating cells, therefore, computer models capable of accurate simulation of cell operation are needed to investigate various new ideas before testing them in actual operating cell

2 2 CONTROL OVER THE PROCESS

For optimum operation of the Hall cell, a control system is a must which should monitor each and every process parameter and take steps to keep them within a specified range The control systems are incorporated with trend analyzers which give an idea beforehand by detecting the initial trends of the cells The trend analyzers helps in early detection of abnormal events particularly anode effects, over tapping and under tapping, anode replacement etc, allowing more opportunity for man/machine interactive decisions and choice of remedial actions [1,3,8 39]

The main process parameter to be monitored is alumina content of the bath and it is fed from feeder system as and when required [40] This alumina sensor forms a part of the complete resistance based control which is described in this section To sense the concentration of alumina at any time in the bath alumina sensors are being used Most of the

alumina sensors have been based on electroanalytical techniques that provide an electrical signal of magnitude that is directly proportional to dissolved alumina concentration This electrical signal is used in an automatic control loop to adjust the feed rate of alumina The online alumina sensor can provide significant direct savings in electrical power if anode effects are avoided entirely For example, with an aluminium production output of 4 million tonnes per year and an operating cell voltage that decreased by a time-averaged 0 1V from 4 5 to 4 4V, the annual energy savings would be around $1\ 25x10^9$ kWH

Resistance based control are found to be very effective for the control of the cell This type of control consists of following the change in cell voltage or pseudo resistance in response to alumina feeding and changing anode- cathode distance

Pseudo resistance is calculated as

$$R_p = (E_{cell}-K)/I$$

where K is the zero current intercept of volts versus amperes for a small change in operating conditions (a value between 1 6 and 1 7V) and I is the cell current [1]

In various modern plants, a resistance based equipment is being used for better control of operating parameters of the cell [3] It is being used to

- adjust pot voltage automatically
- control noise by noise control routines
- avoid overfeeding through its Search Routines
- minimise number of anode effects
- to avoid overfeeding of the pots during low stub breaking through its Low Stub Routines
- to adjust pot voltage through tapping routines during tapping
- to provide a systematic voltage, required during new anode setting through its Set Routines
- to provide sufficient alumina to the pot through Feed Routines
- to kill anode effects through its AET routines
- to deliver 'AUDIO MESSAGE', in case of failure of any of mentioned routines

The usual technique involved in AET routine to kill anode effect is to increase the alumina feed rate and lower the anode for a short period of time When the cell voltage falls, indicating that the anode effect is extinguished, the computer readjusts the anode-cathode distance to produce the set point resistance or voltage The normal electrolysis can be restored in 40-80 seconds with such systems

Tapping is monitored, either by tracking the weight gain of the tapping crucible or by measuring the amount of anode lowering required to hold the cell resistance constant, the latter being converted to weight of metal tapped

In set routine, spent anodes are being replaced on routine basis It is important that new anodes be set to the proper depth so that when the electrolyte, which freezes on the surface, melts off and the anode starts carrying current, it will be at the correct a-c spacing Anode setting cranes are used to position new anode They sense the position of the anode to be removed and combine this information with the height of new anode and its heat up time to position new anode In absence of the cranes, reference marks placed on the new and old anode support rods permit manual positioning to achieve similar results

So, by these several routines each taking care of different operational problems of the process, the cell could be prevented from going into abnormal condition and could be operated at optimum energy requirements

2 3 MATHEMATICAL MODEL OF THE HALL-HEROULT CELL

In Hall cell several interacting phenomena such as heat transport, fluid flow, mass transport, bubble effects, chemical and electrochemical reactions, charge transport (electric current), and electromagnetic effects are going on Models for cell voltage and current distribution, thermal models, magnetic models and models for flow of the melts, for interface distortion, and for mass transport have been developed and interrelated and regularly improved on for better performance of the cell All these models must be linked to each other as none of them can be used in isolation [41 42,43,44]

One may consider the example of maintaining ledge on the side walls Thermal

models take care of the ledges Its thickness depends on the heat transport in the ledge, walls, and bottom of the cell i e on the balance (imbalance) of heat fluxes at the ledge-bath or ledge-metal interface At steady state, heat convected by the melt to the interface is conducted away into the ledge The convective transfer is affected by flow of the melt adjacent to the ledge as well as by the melt temperature Here, it is seen that a model for fluid flow as well as for ohmic heat generation by dissipation of electrical energy is needed as an input to the thermal model

On the otherhand, the flow is dependent on electromagnetic forces, bubble drag To find out emf, one must know how the magnetic field and the currents interact within each other in the bath The currents within these melts are dependent on the ledge profile and on the (temperature-dependent) electrical conductivity of anodes, carbon lining, and collector bars It is observed that a model for fluid flow that does not embrace heat transport is incomplete

2.3 1 THERMAL MODELS

Thermal models have been developed based on relevant heat transfer equations The solution of the equation requires a knowledge of current distribution within the cell Temperatures (isotherms) throughout the cell, i e in the bath, side walls, bottom, anodes etc are computed and the information in combination with the knowledge of liquidus temperature gives the profile of ledge [45,46,47,48] Predicting the ledge profile is a moving boundary problem Iterative solution is necessary to solve the problem because the equilibrium position of the ledge is not known at the start of the calculation and is dependent on heat input into the ledge/molten bath interface and heat conducted away into the ledge from this interface Through the iterative process, the position of ledge surface is adjusted until this balance is achieved The thickness of the ledge is governed mainly by the amount of ohmic heat produced which depends on amount of current flowing through the cell Increase in current leads to the melting of the ledge and its formation at a new position depending on the balance of the heat flux Effect of changing various operating and design parameters on the temperature profile within the cell could be predicted by the use of these thermal models

2 3 2 FLUID FLOW MODELS

Fluid flow models are used to predict the the flow in the molten bath arising due to emf and bubble effect by solving Navier Stokes equation in conjunction with allowance made for turbulence by k-ϵ model Different regions of the cell have different velocities, depending on force field, which make the bath more turbulent and disturb the flat metal-cryolite interface [49] Aluminium/electrolyte interface is predicted by equating the pressures in both the liquids Various models have been developed based on several assumptions Some consider the magnetic field only due to the current in the bath others take into account the additional field due to currents in the bus bars and neighbouring cells In few of the models [50], effect due to the vertical rise of the bubble has been neglected Despite short of accurately simulating the exact working conditions, these models are found to be very useful in predicting the flow field in the bath, and predicting effect of various design and operating parameters These models have been very successful in reducing the turbulence of the cell and aided in better design and control of the modern cells

Although till date no complete model of aluminium cell has been developed, still they have provided valuable insight into the behaviour of real cells The present existing models are valuable building blocks from which a complete model will eventually be constructed

CHAPTER 3

SCOPE OF THE PRESENT INVESTIGATION

The modern aluminium industry has higher energy consumption rate, 12 9 kWH/kg, against the theoretically possible value of 6 2 kWH/kg The primary reason behind this lower energy efficiency is directly linked with higher voltage drops in different components of the cell and poor magnetohydrodynamic design of the cell which leads to excessive turbulence created at the metal/electrolyte interface These wide oscillations in the melt are induced by large magnetic torques generated by the interaction of magnetic field, generated by the large currents of magnitude 150-250kA flowing through the cell, with the current itself

The primary challenge before the Hall cell operators and technology experts has been to understand the factors which are responsible for metal/electrolyte interface oscillations, and to arrive at conditions which lead to quietened and non turbulent interface Oscillating interface results in fluctuating anode-cathode distance causing unsteady cell operation - one of the main contributing factors for lower energy efficiency in Hall cells

Attempts have been made in the past to investigate the interfacial phenomena in Hall cells using the direct experimental approach as well as the approach of mathematical modelling to measure/predict current, magnetic and fluid flow fields, cell topography and temperature isotherms in various parts of the cell While the experimental approach is essentially based on trial and error methodology involving frequent changes in cell designs, particularly, the bus bar design and other

operating condition incurring heavy expenditures, the approach of mathematical modelling suffers due to lack of experimental data in published literature on current, magnetic fields and fluid velocity distributions, needed to validate any mathematical model

The present investigation is one part of a major DST sponsored research project which aims at studying Magnetohydrodynamics in electrically driven melt flows in general and in Hall-Heroult cells used for aluminium extraction in particular The magnetohydrodynamic studies essentially involve elaborate mathematical modelling of the cell phenomena to predict complete thermal profile of the cell, current distribution within various cell components, magnetic and velocity fields within the electrolyte and the metal layers as a function of various operating conditions with the ultimate objective of predicting the electrolyte/metal interface behaviour To validate the mathematical model developed in this project, it is also planned to carry out elaborate laboratory scale measurements as well as to collect data on operating cells in the commercial aluminium plants

The mandate in the present investigation has been to set up a laboratory scale Hall cell and run it under conditions as close to those normally employed during industrial operations, and to study the effect of process parameters on current efficiency, thermal behaviour of the cell, ledge profile formation and other cell phenomena It was decided to carry out laboratory scale investigations in several stages In the first stage a single anode Hall cell was designed and fabricated to generate magnetic and velocity field distribution in the cell and gain experience on cell operations and become familiar with typical problems encountered in laboratory scale cell operations A bigger multi-anode cell was then to be fabricated for further investigations However, during the course of investigations on single anode cell it became evident that the measurement of magnetic and velocity fields on actual and multi-anode Hall cell will be very difficult in the laboratory particularly due to the limitations on maximum permissible temperature to which the Hall effect probe could be exposed in the corrosive environment of the molten electrolyte Moreover,

laboratory scale single anode Hall cell is not able to exactly simulate the real Hall cell The reasons are discussed in section 1 4 of this thesis It was, hence, decided to carry out the magnetic field measurements in a simulated low temperature model of multi-anode Hall cell using Wood's alloy

Thus, the present investigation can be divided into two parts The first part essentially deals with the design and fabrication of a single anode Hall cell which is then operated under different operating conditions for electrolysis of alumina dissolved in cryolite Effect of process parameters like anode current density, electrolyte composition, anode cathode distance, etc on current efficiency, metal recovery, anode effect, ledge formation and other thermal phenomena is studied The second part involves design and fabrication of a simulated low temperature Hall cell involving six anodes arranged in two rows The cell is run using Woods metal which has a melting point around 75^{o}C Measurements of magnetic fields at several locations are made under different operating conditions of temperature, current density, anode-cathode distance, and anode assembly It is hoped that data generated in these experiments will be useful for validating the mathematical model being developed to predict the cell magnetohydrodynamics

PART 1

STUDIES ON SINGLE ANODE HALL HEROULT CELL

CHAPTER 4

EXPERIMENTAL

4 1 DESIGN AND FABRICATION OF SINGLE ANODE HALL CELL

After about three months of rigorous experimentation with various cell designs it became evident that in the single anode Hall cell the heat generated due to resistance heating of the electrolyte will not be adequate to melt the electrolyte and then maintain it at the operating temperature of about 960^{o}C due to large surface area to volume ratio, resulting in very high heat losses from the cell to the surroundings Therefore, an additional source of heat would be necessary Two alternatives were considered

1 To melt the electrolyte outside the cell in a separate facility and then transfer it to the cell in the molten state

2 To design and fabricate a cell-cum furnace which permits in-situ melting of the electrolyte in the cell cavity

In view of the hazards involved in melting such a corrosive material in large quantities and then transferring it to the Hall cell, the first alternative was not found to be very attractive Nonavailability of a furnace/facility to melt cryolite in kilogram quantities in the laboratory was an additional factor against the first alternative It was, therefore, decided to go for the second alternative In what follows is a design of the furnace-cum cell which has been used for investigating single anode Hall cell

4 1 1 HEATING FURNACE CUM CELL ASSEMBLY

Schematic diagram of the single anode Hall type cell cum electrically heated furnace is shown in Fig 4 1 The top view of the cell assembly is shown in Fig 4 2 As can be seen, the furnace consists of eight silicon carbide heating elements of 1 5cm diameter and 40cm length placed in a fire brick refractory lined muffle which constitutes the outer portion of the cell cum furnace assembly The furnace muffle has external dimensions of

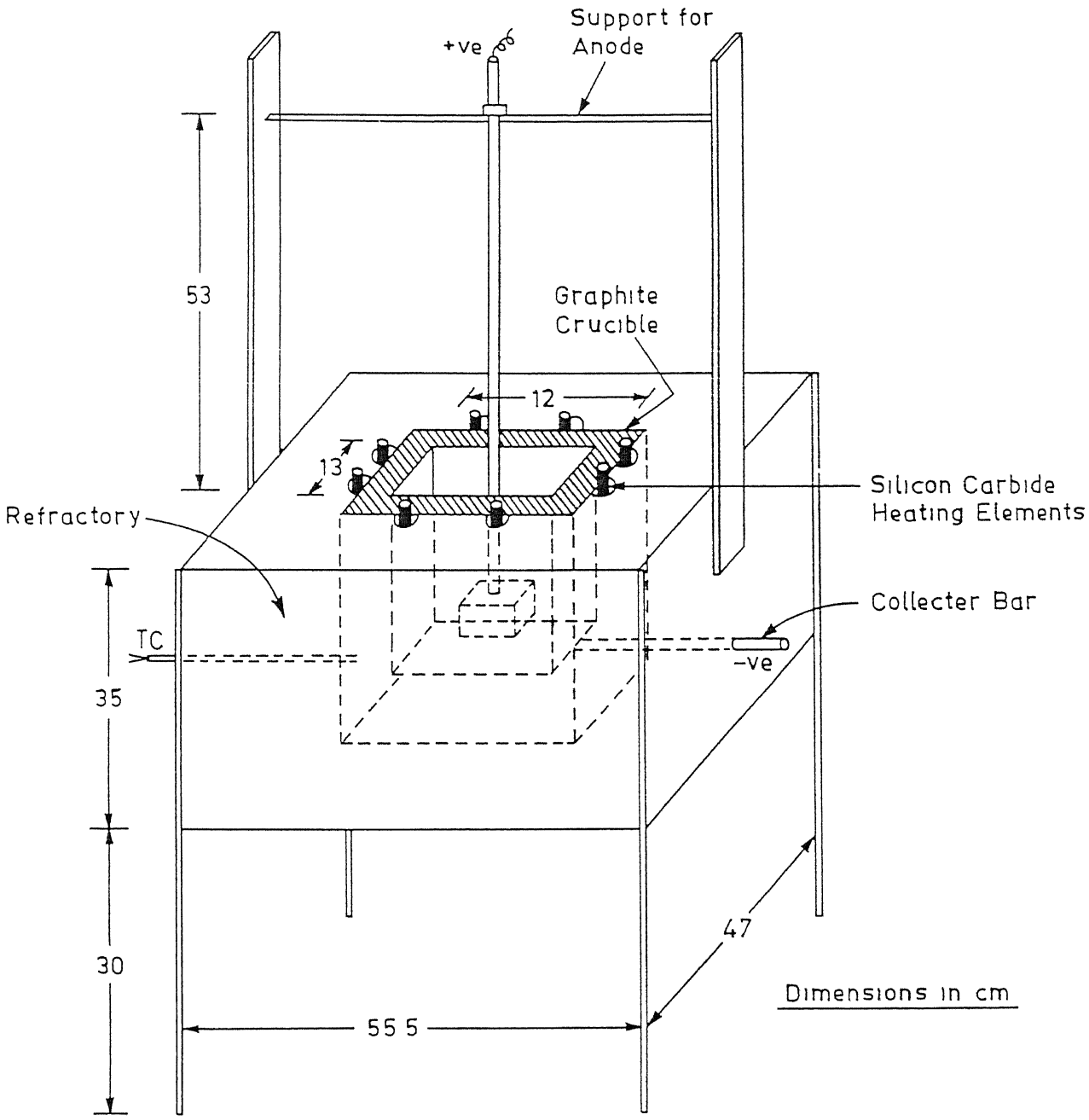

Figure4 1 Schematic drawing of Heating Furnace cum Cell Assembly

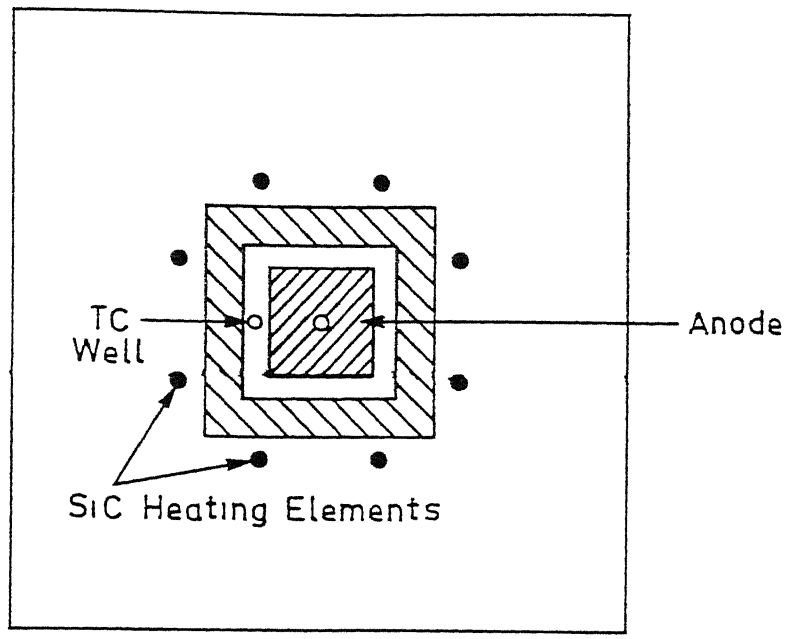

Figure4.2 Top view of furnace cum single anode Hall cell

55 5cmx47cmx35cm and those of the inner cavity 20cmx20cmx22cm The heating elements are placed in the vertical grooves cut on the inner walls of the muffle The entire furnace-cell assembly is placed inside a mild steel rectangular shell of 2mm wall thickness To provide better thermal insulation, a thick layer of ceramic wool is placed between the refractory muffle and the steel shell The power input to the furnace is from the mains through a variable transformer The furnace is designed to attain a maximum temperature of about 1200^{o}C and can hold charge of 2 5kg

In a conventional Hall cell the container walls which are made of electrically conducting carbon lining act as the cathode in the initial stages of the electrolysis After sometime when a thick layer of aluminium is formed at the bottom it starts acting as cathode It is therefore necessary that inner walls of the cell is electrically conducting The cell assembly used in present investigation is also required to have electrically conducting walls of the cell cavity which contains the electrolyte and the molten aluminium during the electrolysis For the inner cell cavity two different designs have been attempted and are described below

4 1 1 1 CELL CAVITY CREATED BY JOINING GRAPHITE PLATES

The cell cavity is created out of different graphite plates with slots cut at the edges and sealed to make it leak proof The internal dimension of the fabricated cavity is 13cmx12cmx15cm, and the thickness of the graphite plates used is 3cm A groove is cut at the base of the crucible to tight fit the SS collector bar A base plate also with the slot is screwed at the outer base of the cell to have better grip of the stainless steel collector bar as shown in Fig 4 3

4 1 1 2 USING A SEPARATE GRAPHITE CRUCIBLE AS THE CELL CAVITY

After about two months of exhaustive efforts to work with the fabricated graphite crucible, it became evident that it would be very difficult to operate with this fabricated system due to rather rapid attack of molten cryolite on the sealant materials used at the joints of the graphite plates The edges and the joints at the graphite plates were sealed with a paste formed out of fine carbon powder and tarcoal Various proportions of carbon

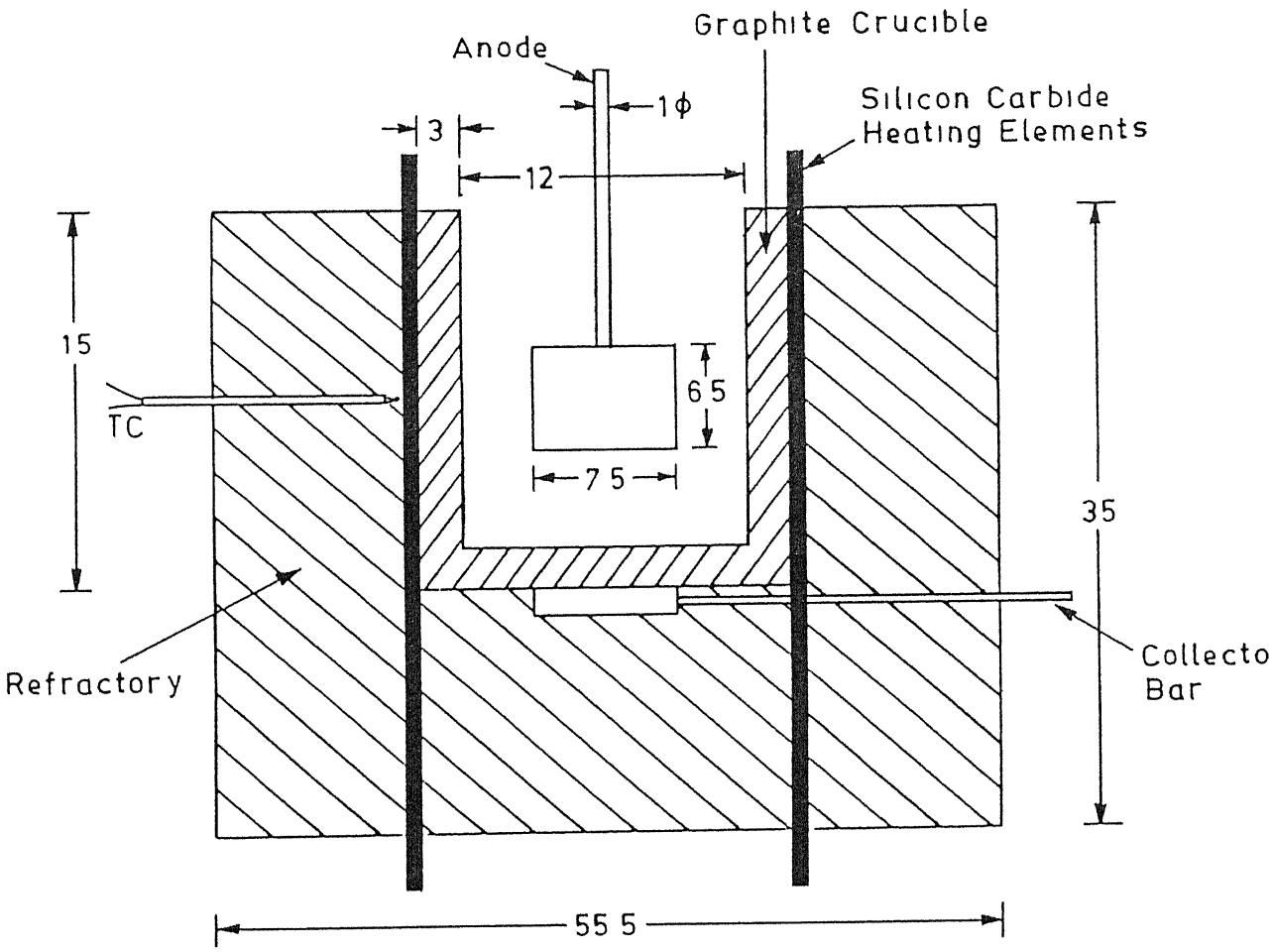

Figure4 3 Open view of heating furnace cum cell assembly with cavity made out of graphite plate

particles and tarcoal were tried out Incidentally this is the sealant which is also used in the commercial Hall cells However, in the commercial cells, the sealant does not come in direct contact with the molten cryolite because of the presence of a frozen layer of cryolite in between the cell cavity walls and the molten cryolite In the present system because of the absence of frozen cryolite layers (reasons are discussed in detail in a later section) there was a direct contact between the molten cryolite and the cell cavity walls Several other sealants including the silicon carbide mortar was also used to seal the gap between the machined plates, but all these sealants failed the moment bath melted and cryolite seeped through the cavity edges damaging refractory lining and shortcircuiting the furnace Due to the nonavailability of high temperature, cryolite resistant sealant, it was decided to go for a single piece cell cavity made out of a graphite block

A single piece graphite crucible (diameter 15 5cm and height 14cm) machined out from cylindrical graphite rod was used Though the electrolysis experiments were very successful with this design, the option was abandoned due to excessively high cost Each crucible lasted for maximum of two runs due to high rate of oxidation To reduce the attack of oxygen on the crucible, graphite pieces were placed between the refractory lining of the furnace and the crucible so that these pieces are preferentially oxidised But this arrangement was also not able to increase the crucible life beyond two runs Furthermore, since there is no provision in the design to siphon out the aluminium formed, the frozen materials (electrolyte and aluminium) are taken out only by chiselling and hammering This factor is also responsible for the reduced life of the graphite crucible As the graphite crucibles machined from graphite blocks/rods were very expensive, a cheaper option was explored

The clay graphite crucibles, available in the local market were found to be reasonable satisfactory and economically viable Hence, in most of the subsequent experiments only clay graphite crucibles were used The typical dimension of these crucibles are given below

Top diameter 17 5cm, Bottom diameter 12cm
Height 19cm, Thickness 1 5cm

Base plate used in this crucible has diameter of 10 7cm In some of the initial experiments,

the base plate fitted at the bottom of the crucible was made of graphite, but later on to have resemblance with the plant conditions, it was made of cathodic carbon used in Hindalco Industries, Renukoot The SS collector bar was attached as explained above Typical crucible assembly used in the experiments is shown in the Fig 4 4

4 1 2 ANODE ASSEMBLY

The current enters the electrolytic cell through the anode stem attached to anode In industrial cells, the anode stem is fitted in the anode cavity Molten cast iron is then poured on to this joint which on solidification provides a permanent joint As this arrangement could not be feasible in the laboratory scale cells, the anode stem was screwed on to the threaded cavity at the top surface of the anode This worked satisfactorily during the experiments

Graphite anodes of various sizes and shapes ranging from cylindrical to cuboidal have been used Cuboidal anode consists of a graphite block (7 5cm by 6 5cm by 6 5cm) with top centre threaded up to 3cm depth, so that copper rod is easily screwed into it Cylindrical anode has cross-sectional area of 22cm^2 with same screwing mechanism to allow the rod of 1cm diameter to be fitted into it

A top cover made of fire bricks is provided to cover the crucible containing the bath to reduce radiation heat losses Anode rod runs through a hole cut at the centre of this cover The cover is provided with three additional openings through which alumina is charged to quench the anode effects These openings are also used for inserting thermocouple in the bath for measuring bath temperature When not in use, these openings are covered with insulating lids

4 1 3 COLLECTOR BAR

In industrial cells, current entering from the top leaves the cell from the bottom through the collector bar fitted into the cathodic carbon blocks constituting the pot Similar arrangement has been incorporated in the cell design - slots are cut on the base plate as well on the outer surface of the bottom through which a SS collector bar of dimension

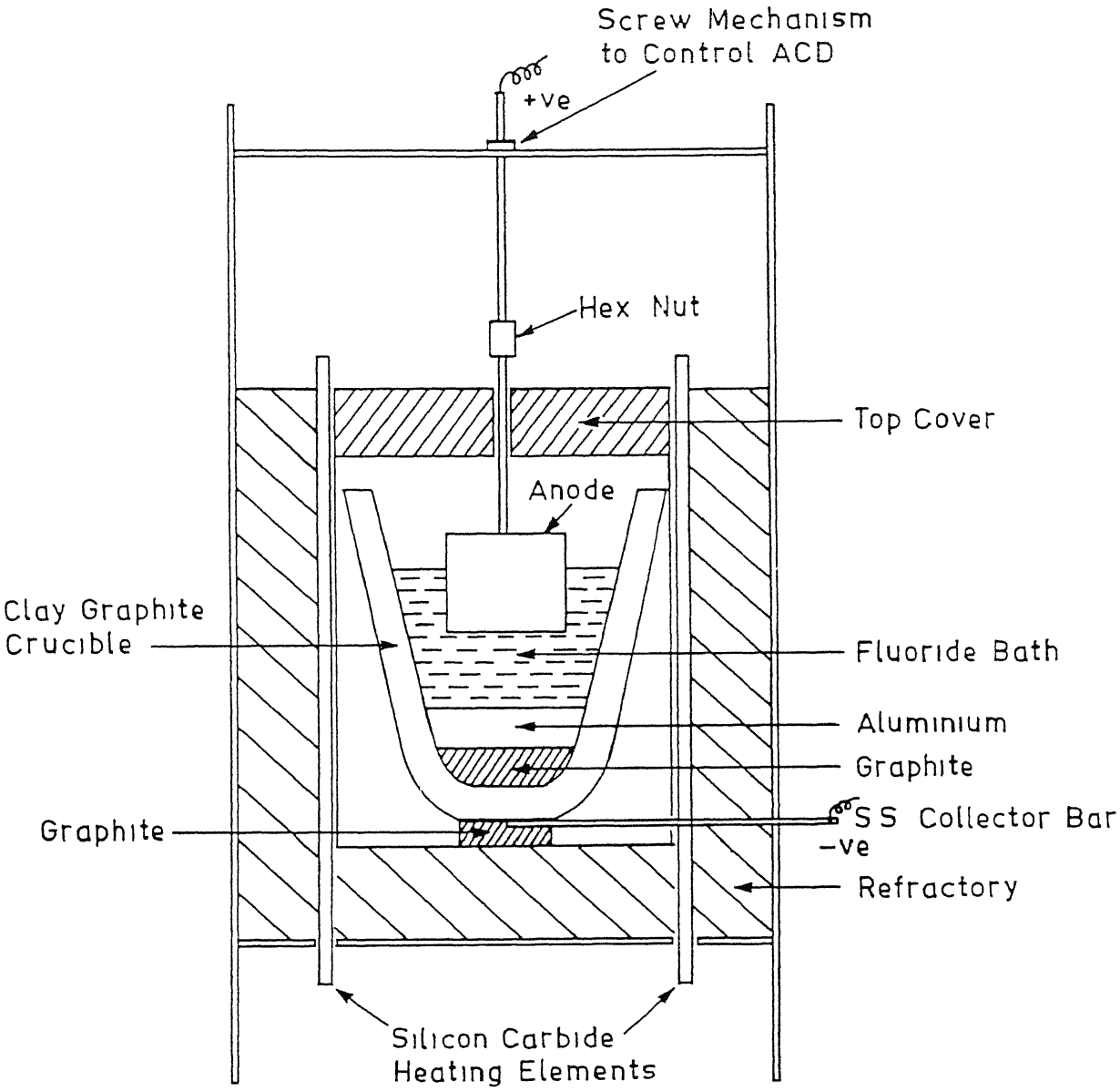

Figure4 4 Typical clay graphite crucible assembly placed in the furnace

33 5cm long, 2 5cm wide and 4mm thick is fitted The collector bar passes all the way through the refractory lining of the furnace and is connected to the negative terminal of the power supply

4 1 4 INTERPOLAR DISTANCE CONTROL

Interpolar distance or anode cathode distance (ACD) is distance measured from the top of the aluminium layer formed at the base plate to the bottom of the anode It is very important to maintain a constant ACD for stable operation of the cell To control the ACD, the anode rod is clamped on one side and depending on the ACD required the rod is moved up or down This mechanism was not able to maintain a constant ACD across the base of the anode because the rod connecting the clamp with its stand used to bend by the weight of anode So, idea of clamping the anode rod from two opposite sides was incorporated into the existing design to give a better grip to the anode rod But the anode rod used to slip due to poor grip So, this design was also abandoned To improve on this an overcell assembly is designed and incorporated into the cell as shown in the Fig 4 4 This structure proved to be very successful in maintaining a constant ACD as it was strong enough to support the weight of the anode In the new mechanism some modifications are done in the anode rod Holes are made in it and height is set by inserting a pin in the proper hole Though height is controlled very accurately by this improved mechanism, but continuous setting of height is not possible, as holes are made at 0 5cm gaps Later, after a lot of efforts, this pinning mechanism is replaced by an improved screwing mechanism In this, the copper rod suspending the anode is made of two pieces, one screwed into the other through a hexagonal nut as shown in the Fig 4 4 The top of the upper rod is threaded and a nut is screwed on to it which rests on the over cell assembly Thus anode is suspended in the bath and desired ACD is set

4 1 5 ARRANGEMENT FOR MUFFLE AND BATH TEMPERATURE MEASUREMENTS

It is very important to monitor the temperature of the bath because performance of the cell is determined to a large extent on the bath temperature The details

have been discussed in chapter on Literature Review Alumel chromel thermocouple is used to measure the temperature

A thermocouple for measuring temperature of the furnace, is inserted through a 5mm diameter hole made in the cell The hole passes all the way through the mild steel shell and the refractories up to the cavity

Moreover, to measure temperature of molten bath, thermocouple sheathed in stainless steel casing is used Details of different arrangements tried for measuring the temperature has been discussed in the next section

4 1 6 POWER SUPPLY

A regulated power supply, model # 7254, APLAB, US Make (output 0-30 V, 0-60 A Max) is used to supply current to the cell for electrolysis Positive terminal of the power supply is connected through copper wire to the copper rod fitted to the anode and negative terminal is connected to the collector bar

4 2 RAW MATERIALS

The basic raw materials used in the Hall-Heroult Cell are cryolite, aluminium fluoride, calcium fluoride and Bayer's alumina These are procured from Hindalco Industries, Renukoot Various physical properties of these materials of analytical grade purity are listed in Table 4 1 [1,51]

Raw Material	Density (g/cm^3)	Melting Point (^oC)
Cryolite	2 97	1009
AlF_3	3 1	2250
CaF_2	3 18	1418
Al_2O_3	3 75	2050

Table 4 1

Since many of the raw materials used in this investigation were not of analytical grade purity, it was decided to characterize them using the conventional techniques of chemical analysis, X-ray diffraction, INEL X-ray, and DTA Results of these characterization studies are summarized below

4.2 1 CHEMICAL ANALYSIS

Ratio of sodium fluoride to aluminium fluoride in the cryolite as well as in the bath has very strong influence on the performance of the cell which has been explained in detail while discussing Bath Chemistry in chapter 3 Chemical analysis is carried out to know the molar ratio of sodium fluoride to aluminium fluoride of both cryolite (raw material) as well as of the bath used in the experiments The molar ratio of cryolite used is determined to be 2 83 Similarly, the ratio in the bath is found to be 2 52

4 2 2 X-RAY ANALYSIS

Cryolite, aluminium fluoride, calcium fluoride and alumina are characterized by X-ray diffraction (XRD) using a Rich Seifert 2000D diffractometer Considering cryolite to be very important for the process, it is further analyzed using INEL X-ray technique XRD pattern of cryolite is shown in Fig 4 5

X-ray analysis has revealed that the alumina supplied by the Hindalco Industries consists of two phases, delta alumina and chi alumina XRD pattern of alumina is shown in Fig 4 6 Other raw materials matched well with the standard theta values of the corresponding materials XRD patterns of CaF_2 and AlF_3 used is shown in Fig 4 7 and Fig 4 8 The standard values of the X-ray 2 theta values and hkl values have been given in Appendix A

The details of the conditions maintained during X-ray diffraction and INEL X-ray analysis have been given below

Copper (K-alpha) target is used for the X-ray diffraction The other conditions for it are

wavelength = 1 541841A
Scanning speed = 3 deg /min in 2theta
Chart speed = 3cm/min
Counts/second = 10K
Time constant = 10 sec
20mA/30kV

For INEL wavelength used is 1 5406 A
Voltage used = 40kV
Current = 30mA

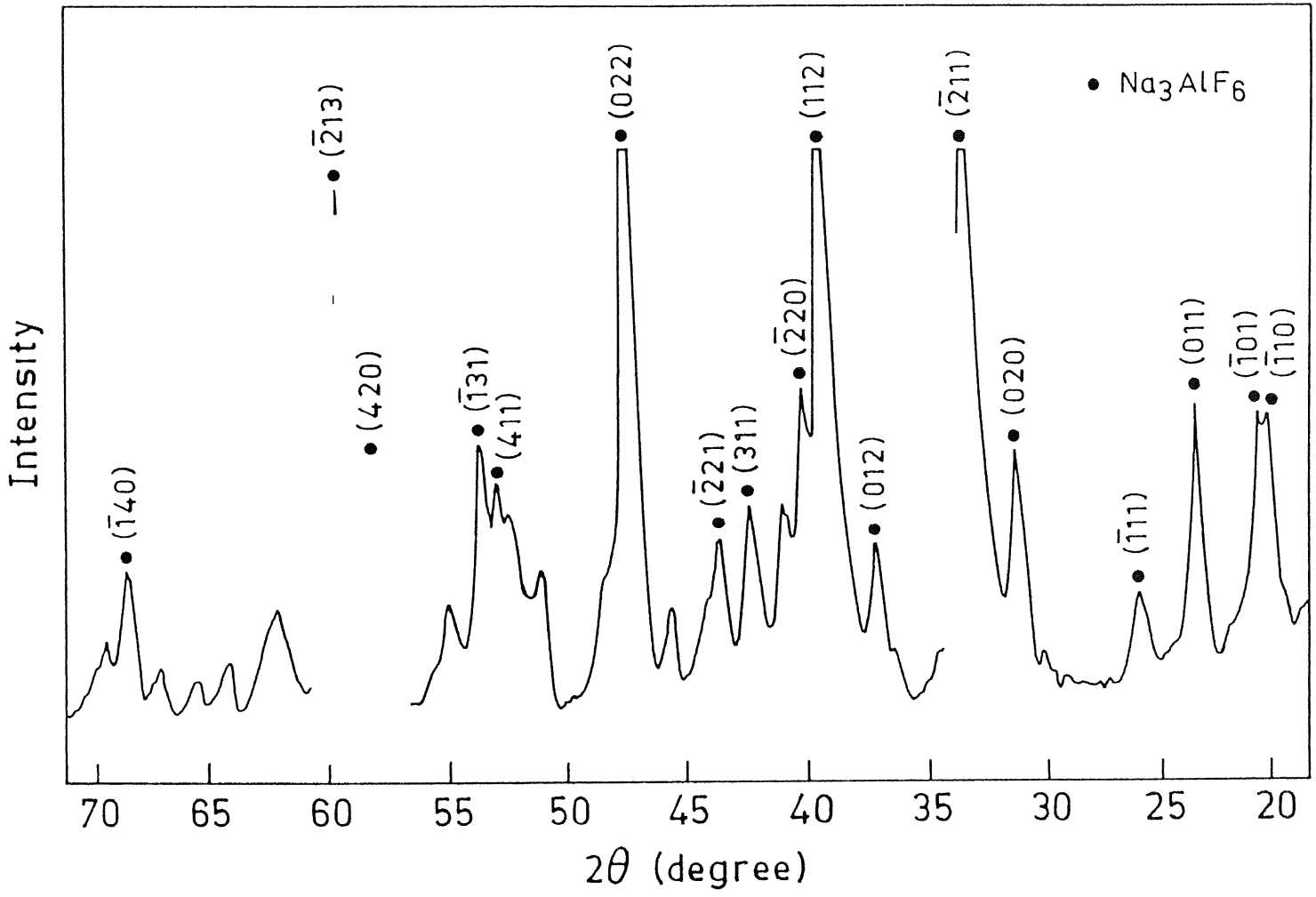

Figure4 5 XRD patteı n of cı yolite used ın experiments

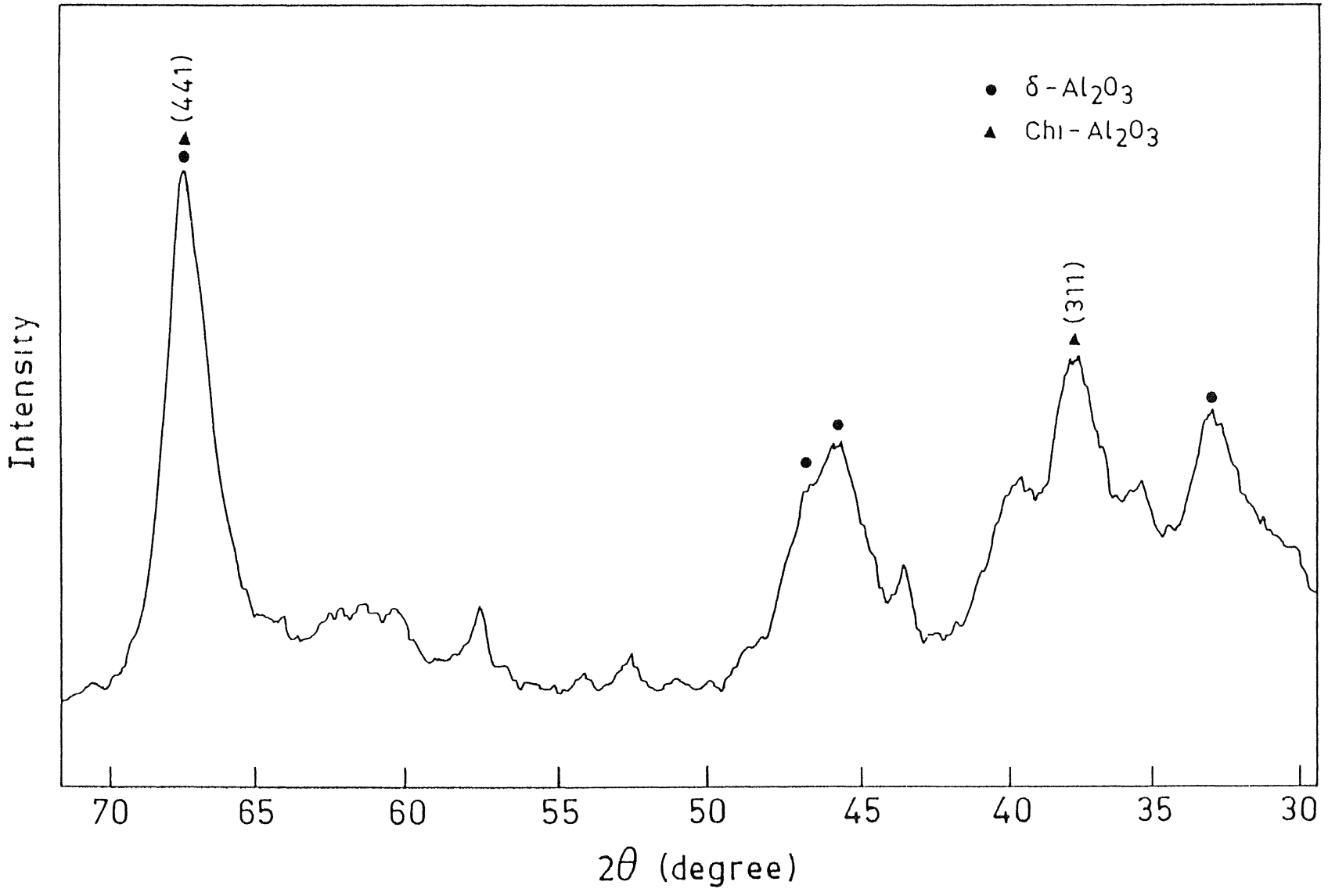

Figure4 6 XRD pattern of alumina used in experiments

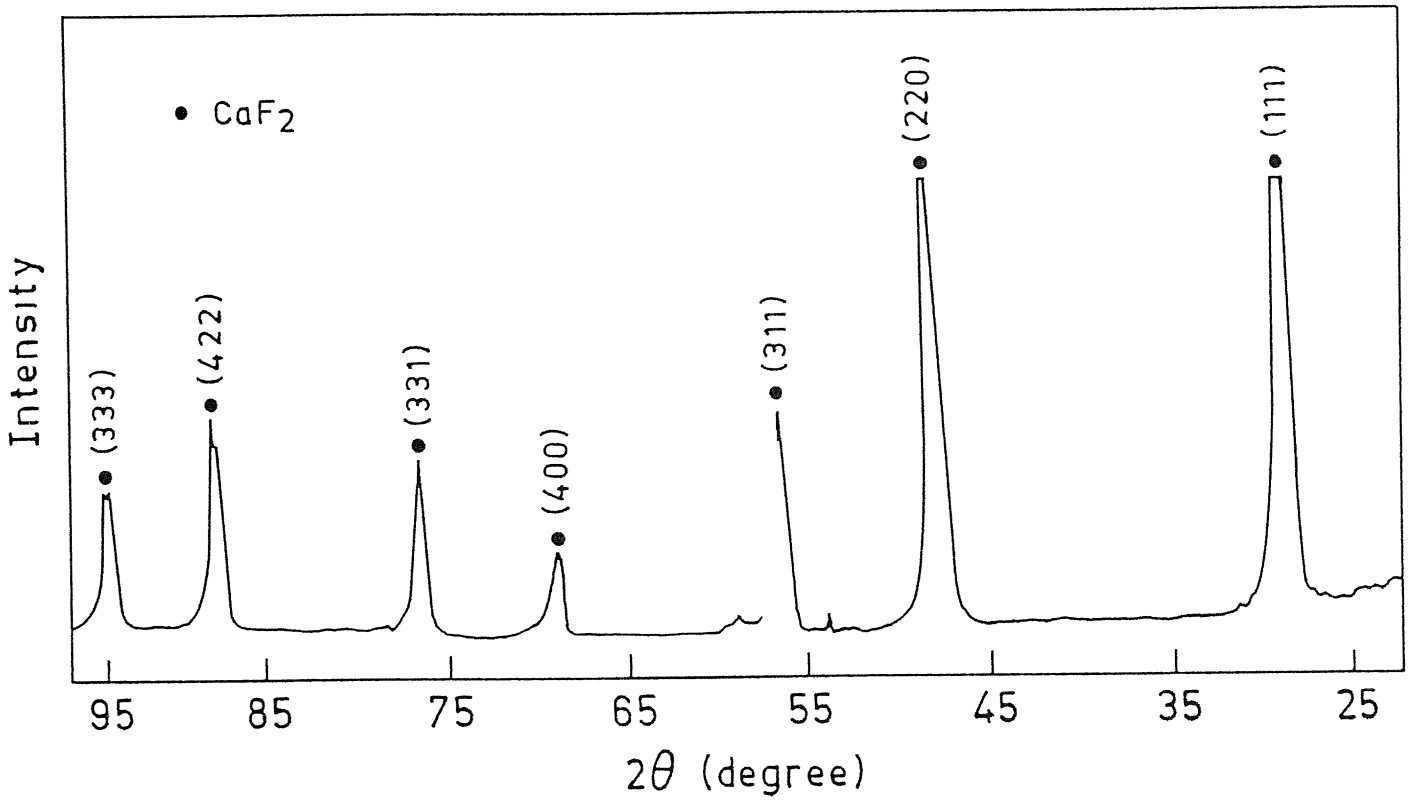

Figure4 7 XRD pattern of calcium fluoride used in experiments

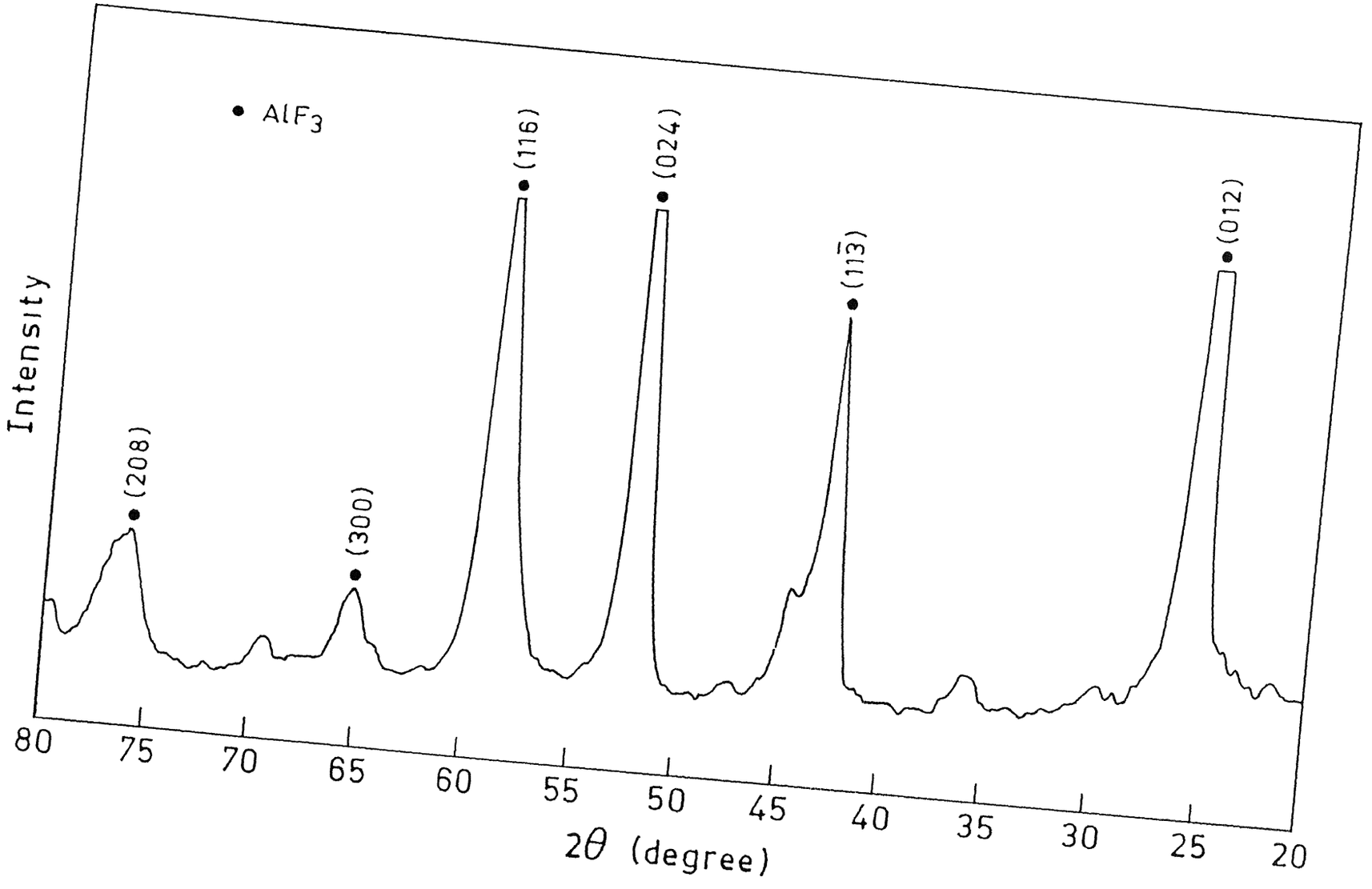

Figure4 8 **XRD pattern of aluminum fluoride used in experiments**

4 2 3 MELTING POINT OF CRYOLITE AND BATH

It is very important to know the melting point of the bath as operating temperature is governed by superheat of the bath which has to be maintained for optimum performance of the cell The details of the effects of the temperature on the cell has been discussed in much detail in chapter 3

Differential Thermal Analysis is carried out primarily to determine the melting point of cryolite The analysis could not be performed up to the melting temperature because spilling of cryolite is observed around 936^{o}C, which may have damaged the instrument During the analysis various temperatures were recorded at which the cryolite undergoes phase changes Major phase changes are observed at 514^{o}C, 682 6^{o}C, 890 1^{o}C and 936 3^{o}C as shown in Fig 4 9

Initial attempts were made to measure the melting point of the bath in the single anode furnace cum cell but due to bulk quantity of material in the crucible around one kg, the temperature is not uniform through out the material and melting point recorded is more prone to error So, a new experiment is designed to measure the melting point of the bath as well as the cryolite About 45g of cryolite is taken in a small graphite crucible and melted in the tubular furnace The readings were recorded in an half a minute interval The melting point of cryolite is measured to be 1001^{o}C Similarly, melting point of bath used is measured to be 960^{o}C

Theoretically, melting point of the bath is given by a correlation as a function of the bath composition [52]

$$T_{liquidus}(^{o}C) = 1009\ 4+4\ 059(CaF_2)-1\ 167(CaF_2)^2+0\ 968(CaF_2)AlF_3- 0\ 105(CaF_2)(AlF_3)^2+0\ 073(CaF_2)^2(AlF_3)+0\ 002(CaF_2)^2(AlF_3)^2- 4\ 165(AlF_3)-0\ 054(AlF_3)^2-5\ 33(Al_2O_3)$$

The melting point of the bath used in various experiments, based on this correlation is calculated to be 971 96^{o}C

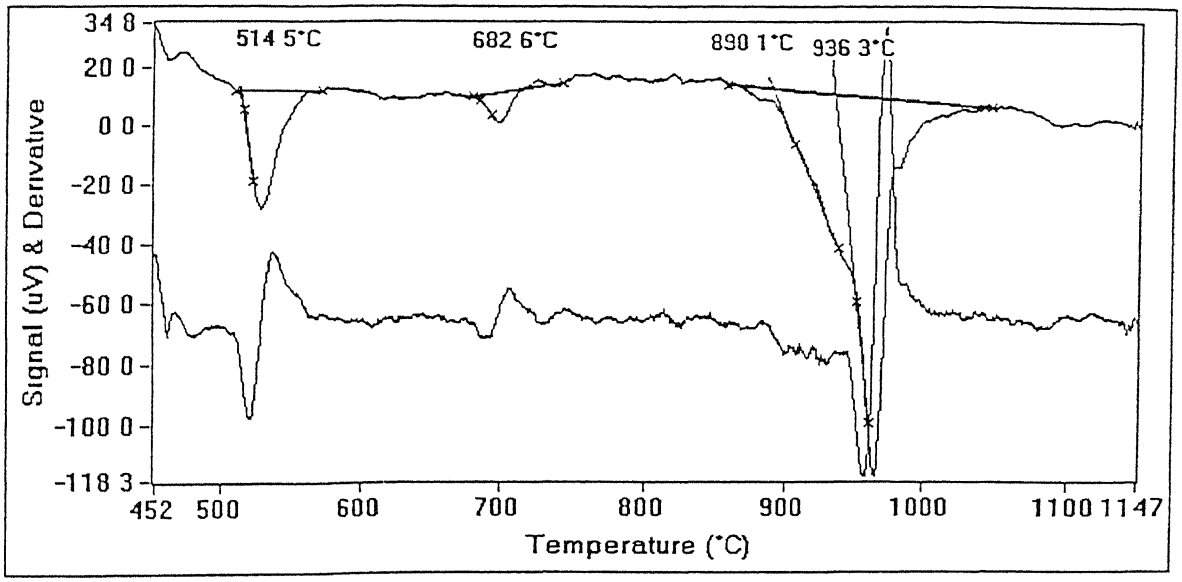

Figure 4.9 A typical DTA plot for the cryolite used in various experiments

4 3 EXPERIMENTAL PROCEDURE

A typical electrolytic experiment involves mixing of raw materials in right proportion, charging the cell cavity with raw mix, operating the cell furnace and adjusting the line voltage to to get the required temperature When the bath is in molten state and the temperature is around 970^{o}C, the power supply is switched on, the interpolar distance is adjusted and the cell current and voltage is recorded as a function of time

4 3 1 MIX PREPARATION

Cryolite as received is in the form of small globular like shape which are reduced to powder form AlF_3, CaF_2 and Al_2O_3 as received are in powder form All the four components to be charged to the crucible are mixed thoroughly The mix comprises of 5% AlF_3, 5% CaF_2 and 4 5% Al_2O_3 and rest cryolite which are mixed thoroughly before charging

4.3 2 CELL CHARGING

In the initial experiments all the raw materials, including solid aluminium were charged when the crucible achieved a temperature of about 960^{o}C-980^{o}C This practice led to the spilling of charge in the furnace, which on melting damaged the furnace In later experiments, they were charged right from the beginning except aluminium which was charged at around 700^{o}C, to prevent its oxidation The charge is varied from 1kg to 2kg Aluminium precharged ranged from 25g to 200g

45g of alumina is charged in two steps, 25g being charged along with the mix and rest 20g on melting to ensure homogeneous distribution of alumina in the bath Initially, alumina charging was done from one side of the cell only, but later holes were made on the top cover and the alumina charging was done through these holes to ensure proper distribution of the alumina

4 3 3 BATH TEMPERATURE MEASUREMENTS AND TEMPERATURE CONTROL

Temperatures of the furnace as well as of the bath have been recorded with chromel alumel thermocouple (TC) Temperature outside the cavity i e of the furnace is monitored continuously and recorded in 15 mins interval The temperature of the bath is measured with the thermocouple enclosed in a stainless steel (SS) sheath to protect the tip of it from being damaged by the corrosive behaviour of cryolite

To find the best method of measuring the temperature of the bath, several trials were taken by putting alumina, cement and silica up to different heights in the tube sheathing thermocouple and comparing it with the simultaneous recording of temperature by the bare tip in solid bath, at temperature around 850^{o}C The attempt was to place both the TCs as close as possible so that they are exposed to similar temperature zone But these designs were not found to be acceptable because even after ten minutes of insertion in the bath the temperature differences between the two TCs ranged from 50^{o}C-60^{o}C Moreover, thermocouple in the tube often used to break due to the formation of clumps because of some kind of sintering of materials present in the tube So, further measurements were done in absence of the powder To improve on this further, the diameter of the tube sheathing the TC was reduced and after 5mins of insertion in the bath, a difference of around 25^{o}C was recorded with this design This design was accepted for further temperature measurement

To check the uniformity of the temperature along the height of the crucible, experiments simulating the bath by an alumina bed of 10cm is performed A temperature difference of around 100^{o}C is observed between the top and base of the alumina bed To counter this the base of the furnace is lowered so that the bath comes infront of the heating zone of the silicon carbide elements This improved the result and the temperature difference decreased to 40^{o}C The difference was further cut down to 10^{o}C by raising the height of heating elements so that the heating zone of the elements almost coincides with the bed height

4 3 4 ACD CONTROL

The anode has to be maintained at a proper height for stable operation of the

cell With 100g of precharged aluminium, 4mm thick layer of molten aluminium forms over the base plate This metal layer acts as cathode ACD is measured from the top of the aluminium layer to the bottom surface of the anode The ACD is varied from 1 5cm-4 5cm with the help of screwing mechanism discussed in the earlier section

4 3 5 ELECTROLYSIS

At approxmately 960^{o}C, the whole bath melts and is ready for electrolysis With the help of regulated power supply, the cell is run at 55A and 4 5V The cell is run for 6-8 hours continuously and three to four successive anode effects are observed in each of the experiments

4 3 5 1 VOLTAGE AND CURRENT MEASUREMENTS

On switching on the power supply, regular monitoring of voltage and current flowing in the cell is done Apart from the panel readings on the power supply, readings have also been recorded from a voltmeter connected in parallel to the circuit and an ammeter connected in series with the circuit A slight difference of around 4A and 0 3V have been observed between the panel readings and ammeter and voltmeter attached

4 3 5 2 ADDITION OF ALUMINA TO QUENCH ANODE EFFECTS

Anode effects are detected when current falls from 55A to 5A and voltage shoots upto 15-20V This abnormality is quenched by adding 36g of alumina to the bath, to maintain its alumina content at 5% For quicker recovery of the cell from the anode effect, turbulence is created in the bath by providing vertical movement to the anode or by stirring the bath by a graphitic or stainless steel rod In one set of experiments, the bath is frozen just after an anode effect and samples are taken out from a region just below the anode and chemically analyzed to know the alumina content of the bath at the anode effect

4 3 5 3 LEDGE FORMATION

In industrial Hall cell, often a ledge is desirable at the sides of the cell (i) to protect the carbon lining from the attack of cryolite and (ii) to maintain thermal balance of the cell Initial efforts to form ledge in the single anode cell by gradually decreasing the furnace temperature were not successful The furnace temperature is reduced by decreasing the current supply to the heating elements On reducing the temperature, bath starts freezing partially from all the sides including from top A crust which forms over the bath grips the anode In some of the initial experiments it was observed that along with the top crust, bath starts freezing at the base also, thus indicating a higher voltage on the panel In an attempt to maintain the voltage in the cell, ACD is decreased and in the process many a times anode got detached from the anode rod and the experiment had to be terminated at that point itself To counter this, temperature of the furnace was again raised to melt the solidified bath at the base In later experiments, the heating zone of the heating elements was aligned with the bath height which prevented the bottom freezing in the cell After several trials, the behaviour of the cell at reduced furnace temperature was closely observed and this knowledge in combination with the improvements made in the cell, like using poker to break the crust before changing ACD, aligning the charge in the crucible with the heating zone of the heating elements made possible to run the cell for about one and half hour with the ledge and crust before it was frozen completely

4 3 6 TERMINATION OF THE EXPERIMENT

After operating the cell for 6-8 hours and observing 3-4 anode effects, the power supply both to the cell and the furnace is switched off The anode is removed from the cell when the bath is still in the molten state so that it doesn't get stuck in the bath After several hours, when the bath cools down, collector bar is removed from the base of the crucible and the crucible taken out The electrolytic product were taken out from the crucible by chiselling and hammering Many a times, in the process the crucible has to be broken to take out the fluoride bath and metal formed The electrolytic products of the bath were then analyzed either chemically or by X-ray technique

4 4 CHARACTERIZATION OF ELECTROLYTIC PRODUCTS

4 4 1 X-RAYS ANALYSIS

The content of the crucible is removed by chiselling and discrete aluminium chunks were physically separated from the bath X-ray analysis is then conducted to determine the constituents of the bath and confirm the formation of aluminium Samples of bath from various locations viz sidewalls, on and below the base plate were analyzed Analysis showed that constituents of the charge has changed to chiolite and $NaAlF_4$ During the electrolysis, the molar ratio of sodium fluoride to aluminium fluoride has changed to 5 3 and 1 1 In addition, samples present on the base plate below the aluminium chunks revealed the presence of aluminium carbide The aluminum formed is also analyzed using this technique Fig 4 10-Fig 4 14 shows the corresponding XRD patterns

4 4 2 CHEMICAL ANALYSIS OF THE BATH AT ANODE EFFECT

In one set of experiments, cell was freezed just after anode effect and sample was collected from just below the anode Chemical analysis of it is done to know the alumina content of the bath during anode effect

Analysis report of 0 5g cryolite and 0 5g bath is given in Table 4 2

Constituents	Cryolite	Bath
Si	0 03%	0 03%
Fe	0 2%	0 2%
Al	14 84%	17 55%

Table 4 2

From simple stoichiometric calculations, alumina content of the bath during anode effect is calculated to be 1 97 wt% The value lies well within the range of 1-2 wt%, reported in the literature

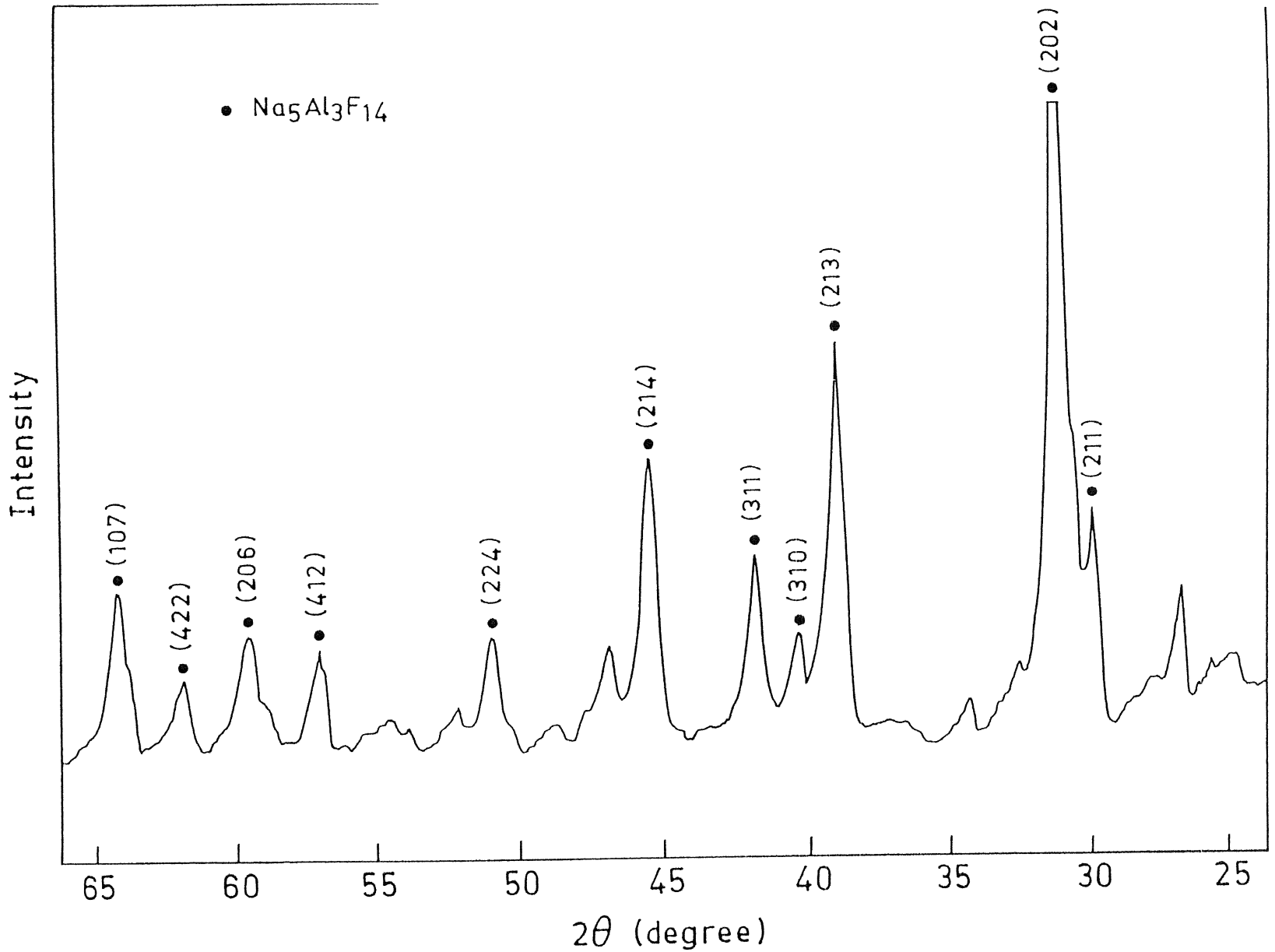

Figure4 10 XRD pattern of the material adhering to the side walls of clay graphite crucible

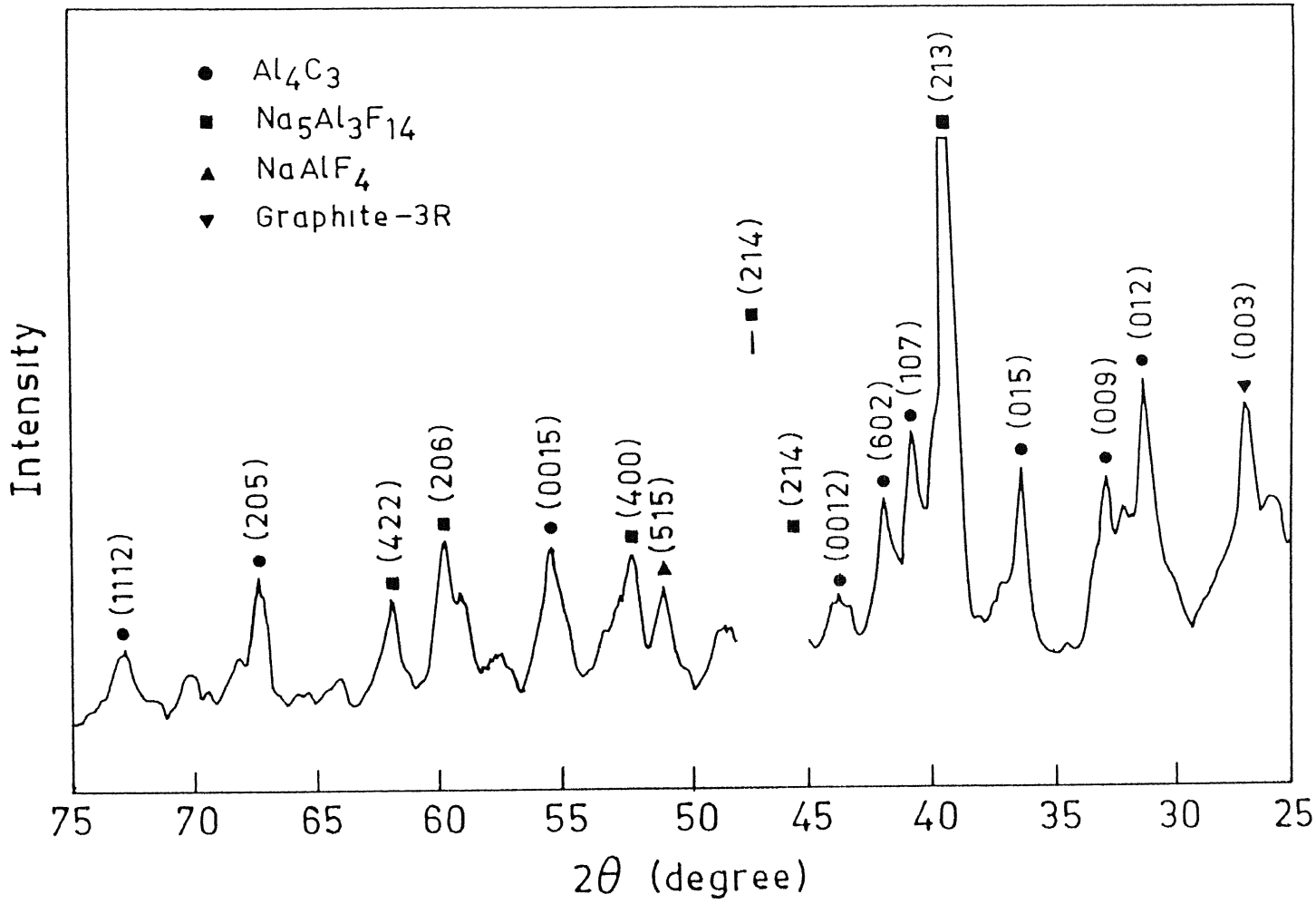

Figure4 11 XRD pattern of the material formed on the base plate of crucible

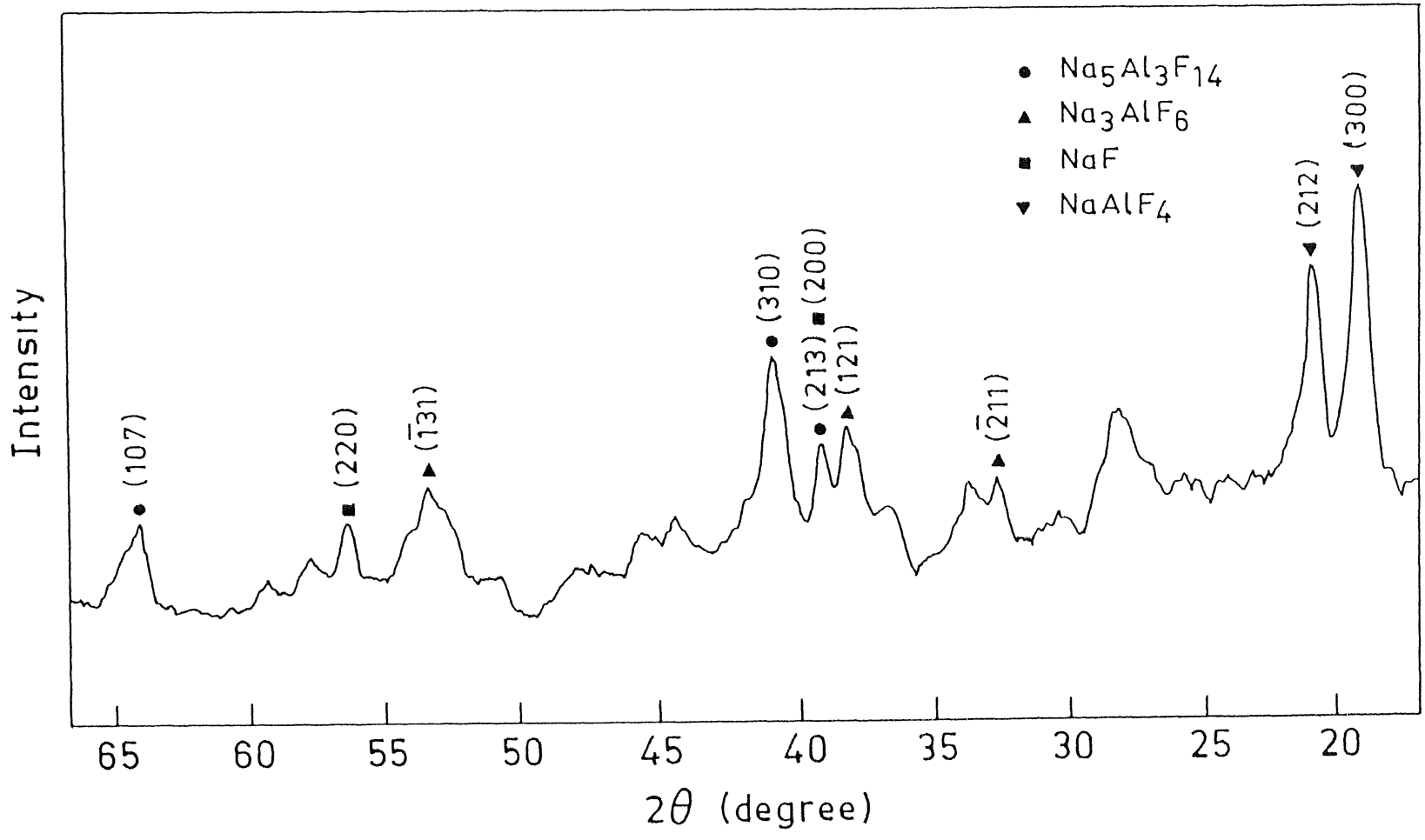

Figure4 12 XRD Pattern of material below the base plate of crucible

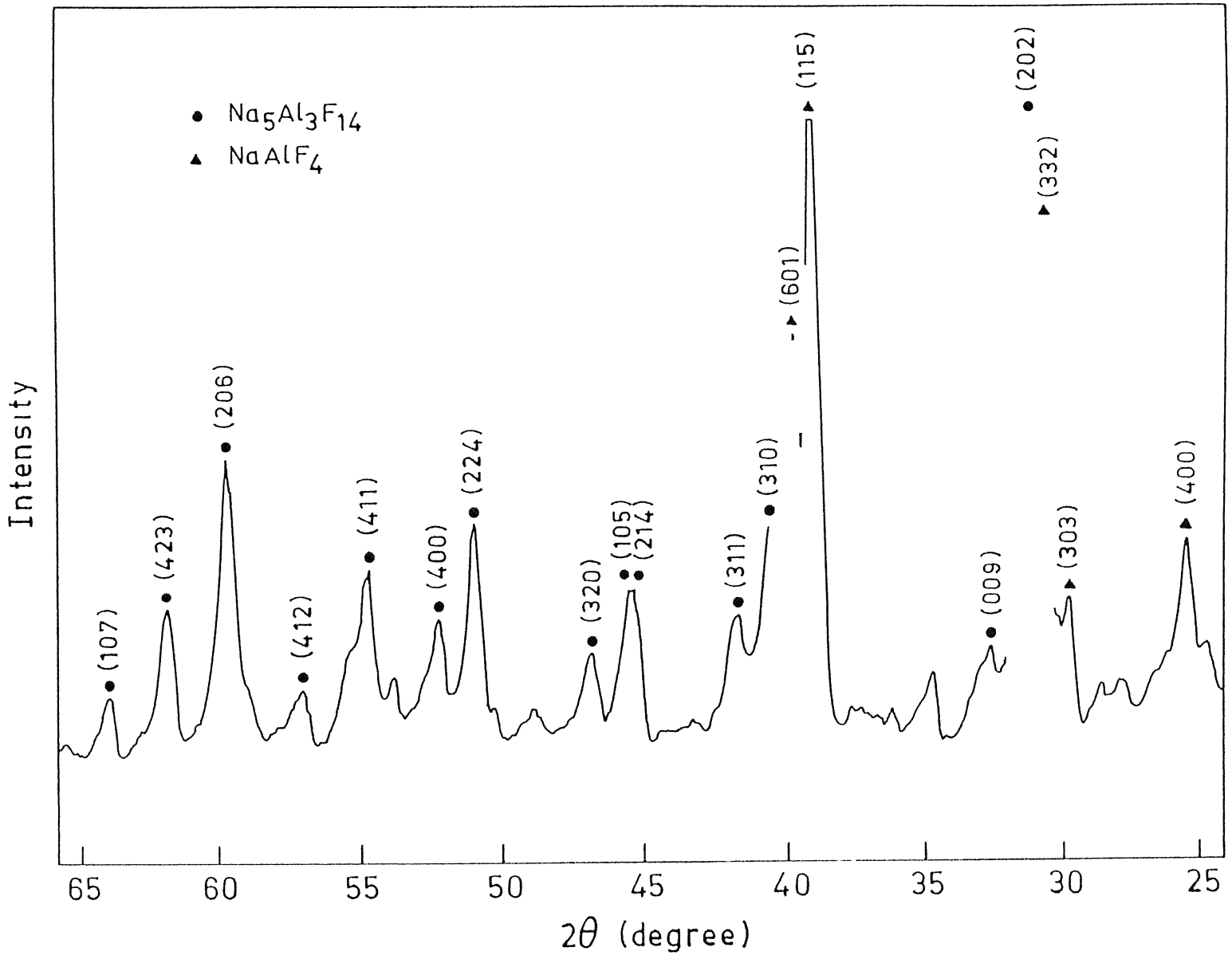

Figure4 13 XRD pattern of material between the base plate and anode

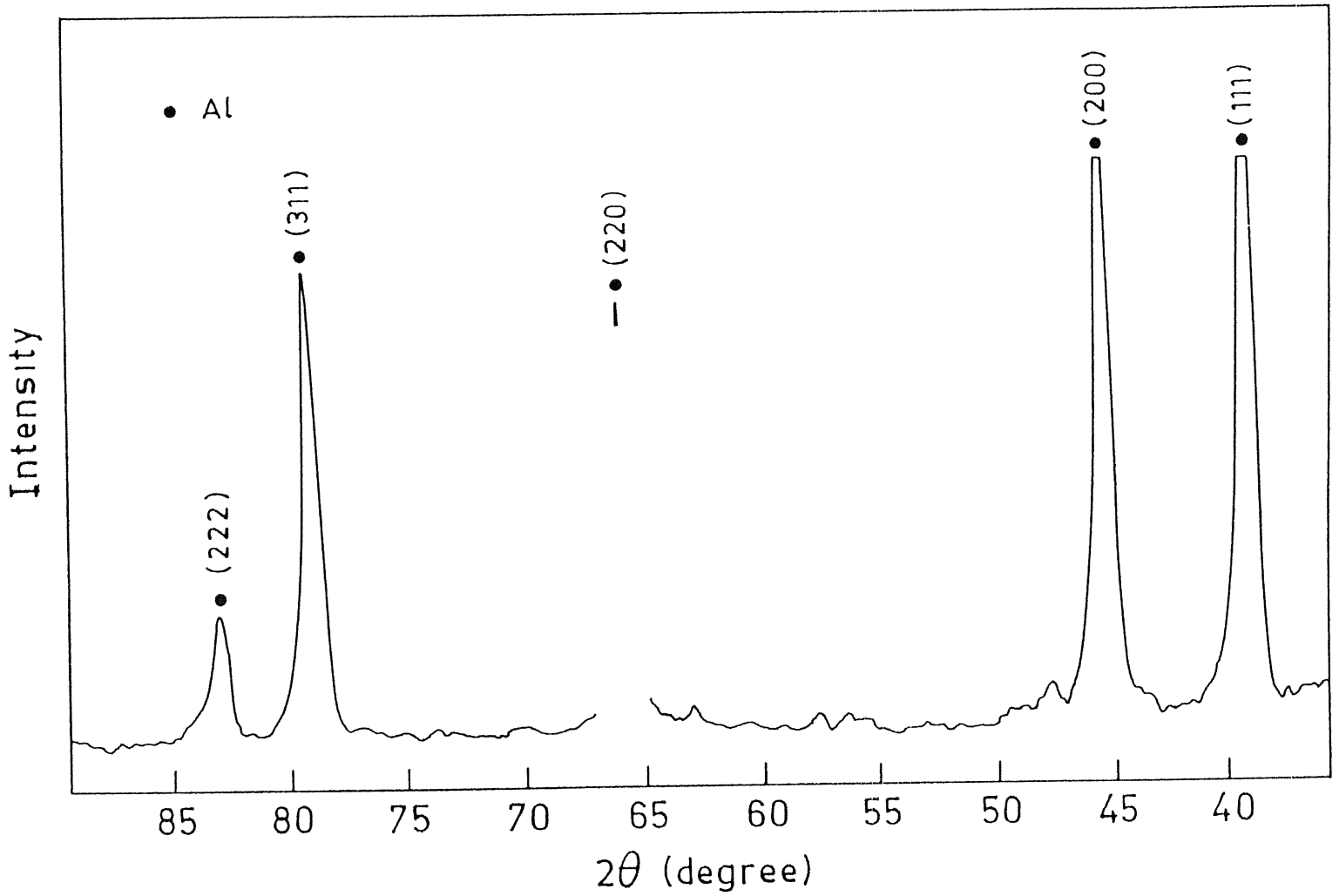

Figure4 14 XRD pattern of aluminum formed during the electrolysis

CHAPTER 5

RESULTS AND DISCUSSION OF SINGLE ANODE HALL CELL

Primary objective of the initial experiments was to establish the conditions under which the single anode Hall type cell could be operated successfully to produce aluminium As described in one of the following sections, some of the initial experiments failed due to various design and materials problems which were amended in a stepwise manner leading to successful cell operation

A typical electrolysis experiment involved

1 continuous monitoring of cell current and voltage as a function of time
2 monitoring the occurrence of anode effect
3 quenching anode effect by adding more alumina to the cell

Each experiment lasted for six to eight hours Three to four anode effects were observed in each of the experiments, after which the experiment was stopped and the electrolytic products were analyzed as described in the previous chapter

Several experiments were planned to study the effect of various process parameters on cell performance The process parameters and their ranges planned in this investigation are given in Table 5 1

SI #	Parameter	Ranges
1	Anode shape	Rectangular, Cylindrical
2	Anode cross sectional area	$22cm^2$ - $56cm^2$
3	Current density	1 03A/cm^2 - 2 63 A/cm^2
4	Interpolar distance	1 2cm - 4 5cm
5	Bath weight	1kg - 2kg
6	Weight of aluminium precharged	25g - 200g
7	Bath temperature	970°C - 1010°C

Table 5 1 Process variables and their ranges examined in various experiments

One of the objectives of this part of the study was to systematically examine the effect of these variables on the performance of single anode Hall cell However, sudden power failures in the laboratory, breakdown of crucibles due to inconsistent quality, leakage of electrolyte and sometime due to anode assembly failure, this objective could not be completely fulfilled However, these experiments have been very useful in terms of gaining valuable experience on operating a laboratory Hall cell, and become familiar with some of the typical problems arising due to anode effects, density difference, and changes in bath chemistry Various observations along with the methodology taken up to tackle these problems are discussed in some detail in this chapter

5.1 PRELIMINARY EXPERIMENTS

Several experiments were performed without external heating of the cell Two options of dry start up and wet start up was to be tried, out of which the latter was abandoned due to danger involved in transporting the molten corrosive bath of about a kg from a furnace to the cell So, dry start up was attempted in all the initial experiments The procedure employed in industries, during dry start up is to produce arcing by shorting anode and cathode in the pot charged with the raw mix The heat generated melts the bath around the arcing area and slowly as the melt quantity increases, the anode is gradually lifted A similar attempt was made in the laboratory Current of the order of 55-58 A was passed through the cell at 5V, which could not produce arcing in the bath despite several efforts So, the idea of operating the cell with its own ohmic heat generation was abandoned

Later experiments were carried out with an external heating source The charge was heated in the graphite cavity fabricated from graphite plates The main problem with this design was poor sealing of the machined edges and joints of the plates On melting, the bath starts seeping through the joints and flows down to the furnace, "eating" up the refractories and short circuiting the furnace It takes about five days to again make the whole set up ready for the next experiment Several sealants were used in an attempt to make the pot leak proof Initially, consistent with industrial practice, pastes made out of carbon powder and tarcoal was tried After filling the gap with this paste, the pot was baked for a few hours to allow the paste to set properly Many a times, during baking itself, the carbon particles of the paste came out of the edges Later different ratios of carbon powder to tarcoal were

attempted with and ultimately, by trial and error a paste was developed which remained intact during baking, but unfortunately failed as the bath melted The failure of the carbon paste was probably due to poor ramming practice employed in the laboratory

Silicon carbide mortar, a promising binder was tried in the next set of experiments It was applied over the edges and filled into the gaps through a thin strip For two to three days the mortar was allowed to dry on its own The bath was charged and melted in the sealed pot But this sealant also could not resist the corrosive nature of the fluoride bath

As shown in the previous paragraphs, it is not possible to plug the leaks of the fabricated cavity in the laboratory Therefore the next set of experiments were performed in a graphite crucible machined out of a graphite block/rod The raw mix was charged into the crucible and melted As expected the crucible "resisted" the corrosive cryolitic bath An experiment was carried out for one hour, and the electrolytic products were taken out of the crucible Unfortunately, it did not contain any aluminium metal Experiments were then carried out for one and half, two, and three hours, but with the same result Therefore, in consonance with industrial practice, solid aluminium was added to the crucible along with the cryolite charge, prior to the experiments Initially, 25g of aluminium was fed into the crucible along with the raw mix and after about four hours of electrolysis, the weight of aluminium in the crucible increased to 41g Hence, this strategy of precharging aluminium was followed in all subsequent experiments Because of the need to break the crucible after each experiment to analyze the electrolytic products, more expensive graphite crucible was replaced with relatively cheaper clay graphite crucible

5.1 1 TEMPERATURE MEASUREMENTS OF THE BATH

Experiments were performed with temperatures ranging from 960^{o}C - 1010^{o}C The temperature was maintained on the higher side to ensure that the bath remains in a molten state Three to four anode effects were allowed to occur in each of the experiments During each of the anode effects the bath temperature shoots to 1100^{o}C and by the time the bath cools down to 1000^{o}C, the next anode effect is ready to overheat the cell At temperatures around 1000^{o}C a lot of fumes come out of the cell mainly comprising of fluorides

Apart from regular recording of temperature of the cell, close monitoring was done during the onset of the anode effect as well as during the anode effect On the onset of an anode effect, the temperature of the bath starts increasing and temperatures in the range of 1020-1030^{o}C is recorded A sudden increase in temperature of the bath is observed as soon as the panel voltage reading shoots up to a higher value The temperature of the bath even touches a peak value of about 1100^{o}C The furnace temperature which is maintained at around 965^{o}C, also shows a sudden rise in temperature of up to 1020^{o}C Along with the excessive overheating of the cell, a strong corrosive environment is also created in the cell because many a times the sheath enclosing the TC gets damaged

5 1 2 WETTABILITY OF ALUMINIUM ON CARBON SUBSTRATE

The aluminium formed during the electrolysis is not making a flat pool over the base plate This phenomenon is confirmed when the aluminium formed in the process is recovered in the form of discrete convex chunks sitting on the base plate In order to investigate whether aluminium chunks are formed during solidification or it exists in the molten state, wettability tests were conducted on the carbon substrate, the material which forms the base plate of the crucible When molten aluminium is poured on to the carbon plate it was observed that metal did not cover the entire plate Instead it formed discrete convex globules, with unoccupied space between them The experiment confirms that the convex chunks existed in the molten state and did not form during solidification In the centre, the height is more, thus giving nonuniform ACD across the anode surface during electrolysis Due to the bulge at the centre, there is more chances of short circuiting between metal and anode, thus reducing the current efficiency

Later, it was thought that increasing the amount of aluminum precharged might improve the wettability of aluminium on the carbon substrate So, the amount of aluminium precharged in the cell is increased from 25g to 150g during start up of the cell in subsequent experiments, but this practice also gave no improved results

5 1 3 OXIDATION OF MOLTEN ALUMINIUM

To check the extent of oxidation molten aluminium in the single anode cell due to openness of the process, the following experiment was carried out 100g of aluminium was charged along with 900g cryolite, 50g AlF_3, 50g CaF_2, and 45g Al_2O_3 and kept at 970^oC for 6hrs , without passing current i e with no electrolysis Around 63g of aluminium could be recovered after the experiment Rest 37g was oxidised as well as reacted with the carbon substrate to form aluminium carbide which was clearly evident from the yellow deposit seen on the base plate

5 2 ELECTROLYTIC EXPERIMENTS

A detailed table summarising the performance of the cell at different operating conditions is given in Table 5 2 Detailed readings of Run4 has been given in Table 5 3

In most of the electrolytic experiments, current efficiency, recovery and energy consumption of the process has been calculated using eqs (1), (2) and (3), given below

$$\textbf{Current Eff (CE)} = \frac{\textit{Aluminium formed assuming alumina content of the bath at anode effect to be 1 97wt\%}}{\textit{Aluminium produced by Faraday Law assuming 100\% CE}} \qquad \text{[Eq 1]}$$

$$\textbf{Recovery} = \frac{\textit{Actual aluminium produced}}{\textit{Aluminium formed assuming alumina content of the bath at anode effect to be 1 97wt\%}} \qquad \text{[Eq 2]}$$

$$\textbf{Energy consumption (kWH/kg)} = \frac{2\ 98xV}{CE} \qquad \text{[Eq 3]}$$

Run	Anode* type & Dimension	ACD (cm)	Cd ($A/cm^{2)}$	Precharged Al (g)	Bath Temp (^{O}C)	(CE) %	Metal recovery %	Energy Con (kWH/kg)
1	1	1 5	2 63	25	1000	41 3	53	36 07
2	1	1 5	2 63	25	1005	40	61 6	37 25
3	2	2 5	2 32	50	1000	55 68	76 32	26 76
4	3	2	1 18	100	1000	45 9	60 1	32 46
5	4	2 3	1 03	100	990	40 18	62	37 08

*** ANODE TYPE & DIMENSION**

1 Cylindrical, diameter 5 3 cm, height 8 2 cm, cross sectional area 22 cm^2
2 Rectangular, 5cm x 5cm x 5cm, cross sectional area 25 cm^2
3 Rectangular, 7 5cm x 6 5cm x 6 5cm, cross sectional area 48 75 cm2
4 Rectangular, 7cm x 8cm x 6cm cross sectional area 56 cm^2

Table 5 2 Summary of the performance data of the cell

Time (mins)	Current (Amps)	Volts (V)	Comments
0	58	4	
60	58	4	
120	58	4	
150	58	4 5	
180	58	9	
195	15	11	First anode effect
210	58	5	
240	58	5	
290	20	9	Second anode effect
320	58	5	
350	58	5	
375	40	9 5	Third anode effect
376	58	5 5	Stirring
377	40	9 5	Stirring ceased
378	36	9 5	
379	34	9 5	
381	58	6	
383	32	9 5	
386	58	6	
388	25	9 5	
389-	25	9 5	Stirring resumed
389+	58	6	
450	58	5 5	
479	20	12	Forth anode effect

Table 5 3 Detailed readings of fourth run at T = 1000^{o}C, ACD = 2cm, Cd = 1 18

A typical calculation of current efficiency, metal recovery and energy consumption during fourth run has been given below

Total time for electrolysis	= 479 min
Total alumina added in to the bath	= 153g
Alumina electrolyzed assuming 1 97wt% alumina in the bath at anode effect	= 135g
Theoretical yield of aluminium on electrolysis of 135g of alumina	= 71 47g
From Faraday Law amount of aluminium produced by passing 58A for 479mins	= 155 46g
Current efficiency = 71 47/155 46	= 45 9%
Amount of aluminium actually produced	= 43g
Metal recovery	= 60 1%
Energy consumption	= 32 46 kWH/kg

The energy consumption during the experiments is found to be very high primarily due to large voltage drops across several components of the cell esp across clay graphite crucible which has a large resistance The CE calculated for various experiments carried out is around 40-45% on an average Various reasons behind the lower CE have been discussed below along with the results of various experiments carried out to substantiate them

1) SHORT CIRCUITING

An examination of the bath after the electrolysis revealed the presence of discrete convex chunks of aluminium This implied that molten aluminium was not present as a horizontal pool but as convex globules on the base plate Hence a nonuniform ACD existed across the anode surface The convex shape of the aluminium globules increased the probability of shortcircuiting On short circuiting the current would pass through the cell

without electrolysing the bath, thus cutting down the current efficiency drastically

2) REOXIDATION

Apart from being at the base plate, aluminium is also found to be distributed all over the bath This is confirmed on taking out the solidified electrolytic products There is very strong chances of these distributed aluminium coming in contact with the anode, which may lead to its reoxidation Apart from this, it has been confirmed by several experiments conducted that large amounts of aluminum gets oxidised due to openness of the process

3) POOR CONTROL OVER THE PROCESS, PARTICULARLY, TEMPERATURE AND BATH CHEMISTRY

a) On reusing the bath as well as during the operation of the cell, the bath chemistry is not exactly known During the operation of the cell fluorides are constantly being lost and in industries by constantly monitoring the bath chemistry, aluminium fluoride is being added on a routine basis to make up the deficit On regular loss of fluoride, bath density exceeds that of aluminium and probability of aluminium touching the anode surface increases This leads to shortcircuiting, which decreases the current efficiency of the cell In the laboratory, due to nonavailabity of such control system, bath chemistry could not be controlled as required for optimum performance

b) From the temperature measurements made during the anode effect, it is known that during anode effect temperature rises upto 1100^{o}C In each of the experiments conducted, three to four anode effects were allowed to occur and each time the bath is raised to such high temperatures This high temperature leads to increased solubility of aluminium in the bath and enhanced side reactions which affect the CE very badly Though temperature after anode effect falls down from 1100^{o}C but it never goes below 1010^{o}C According to a widely used thumb rule CE falls by 1% with every four degrees rise in temperature above 960 C If this general rule is considered then, CE straight away falls by approximately 20%

5 3 EFFECT OF ADDING ALUMINIUM FLUORIDE ON BATH DENSITY

In most of the experiments performed, it was observed that aluminium floats on the surface, though it should be present at the base of the cell owing to its higher density This phenomenon of aluminium floatation on the surface is because of the increase in bath density In a typical bath, a very slight difference in density of about 0 2-0 3g/cm^3 is maintained The moment the densities of both liquids equalises or the bath density exceeds that of aluminum such floating of metal over fluoride bath is observed From the literature, it is known that aluminium fluoride decreases the bath density The idea was employed and 10g of aluminium fluoride was fed to the bath at that moment After few minutes, aluminium was no longer visible on the surface

5 4 OCCURRENCE AND QUENCHING OF ANODE EFFECTS

A general trend has been observed with respect to anode effects in the each of the electrolytic experiments carried out in the laboratory First anode effect took about two to two and half hours which is roughly double the time taken by subsequent anode effects In few experiments, the time for first anode effect is not necessarily double but is certainly more than that taken by subsequent anode effects This perhaps may be because when cell starts, it takes time to get stabilised The power supply also takes time to stabilise The first half an hour after the start up in the single anode cell could therefore be considered as stabilising time

Each time the anode effect was killed by adding alumina into the cell and simultaneously stirring the bath In one set of experiments, the time for quenching of anode effect without stirring was noted It was observed that system took around 15 minutes on an average to kill the anode effect on its own, after the addition of alumina into the cell The current and voltage recorded during the experiment have been given in Table 5 3 On stirring the melt the time required to quench an anode effect was reduced to a minute or two

5 5 LEDGE FORMATION

Ledge is maintained in the commercial cells to protect the cathode lining from

the corrosive fluoride melt and also to maintain thermal balance of the cell Similar, protective layer of solidified bath called ledge was formed in the laboratory cell This could only be possible when the zone near the crucible wall has temperature below the liquidus temperature of the bath Such a temperature profile near the walls could be maintained only by reducing the external heat source

On reducing the external heat, bath starts solidifying from the sides and from the top The upper crust is punctured from time to time to get the sight of the molten bath Initially, bath also used to solidify at the bottom, which hindered the flow of current through the cell, thus terminating the electrolytic process Later by thickening the insulation at the bottom, this phenomenon was prevented

The bath froze because the ohmic heat generated in the cell is not sufficient to maintain the bath in molten state This made it very difficult to run the cell without external heating But still the cell was run for about two hours with reduced external heat source

In this set of experiments, floating of aluminium on the surface was a common feature The reason behind this has been discussed earlier

During ledge formation, amount of liquid bath decreases sharply To make up the deficit, further additions of bath in solid form were made Additions of about 1kg bath is further made to increase the total amount of charge in the crucible to 2kg

PART II

STUDIES ON SIMULATED LOW TEMPERATURE HALL CELL

CHAPTER 6

EXPERIMENTAL

6 1 DESIGN AND FABRICATION OF SIMULATED LOW TEMPERATURE HALL-HEROULT CELL

As elaborately discussed in previous chapters, the mandate of this investigation has been to experimentally measure the magnetic and velocity fields in laboratory scale multi-anode Hall cells The experiences and problems faced during the operation of the single anode Hall cell have been discussed in some detail in the previous chapters From these experiences it became evident that the operation of a multi-anode Hall Heroult cell in the laboratory environment would not be a trivial exercise and that even if the cell was satisfactorily running the measurements of magnetic and velocity fields in such highly corrosive environment, as it exists in a conventional Hall cell, at about 1000^{o}C would be an extremely challenging task It would require design and fabrication of an elaborate cooling system to protect the measuring probes from the corrosive environment and to maintain them at temperatures below 100^{o}C (the upper limit of temperature to which the Gauss probe can be exposed is 75^{o}C) Since the magnetic and velocity fields data are essentially needed to validate the mathematical model predicting magnetohydrodynamics, it was decided, as a first step, to generate these data on a simulated low temperature Hall cell which employs molten Wood's metal as the fluid medium The design and fabrication aspects of a multi-anode (6 Nos) cell are described in this chapter This investigation is restricted only to the magnetic field measurements

6 1 1 BASIC STRUCTURE OF THE SIMULATED CELL

Schematic representation of low temperature simulated multi - anode Hall cell has been shown in the Fig 6 1 The cell could be divided into four parts

1) Inner SS tank
2) Anode Assembly And Bus Bars

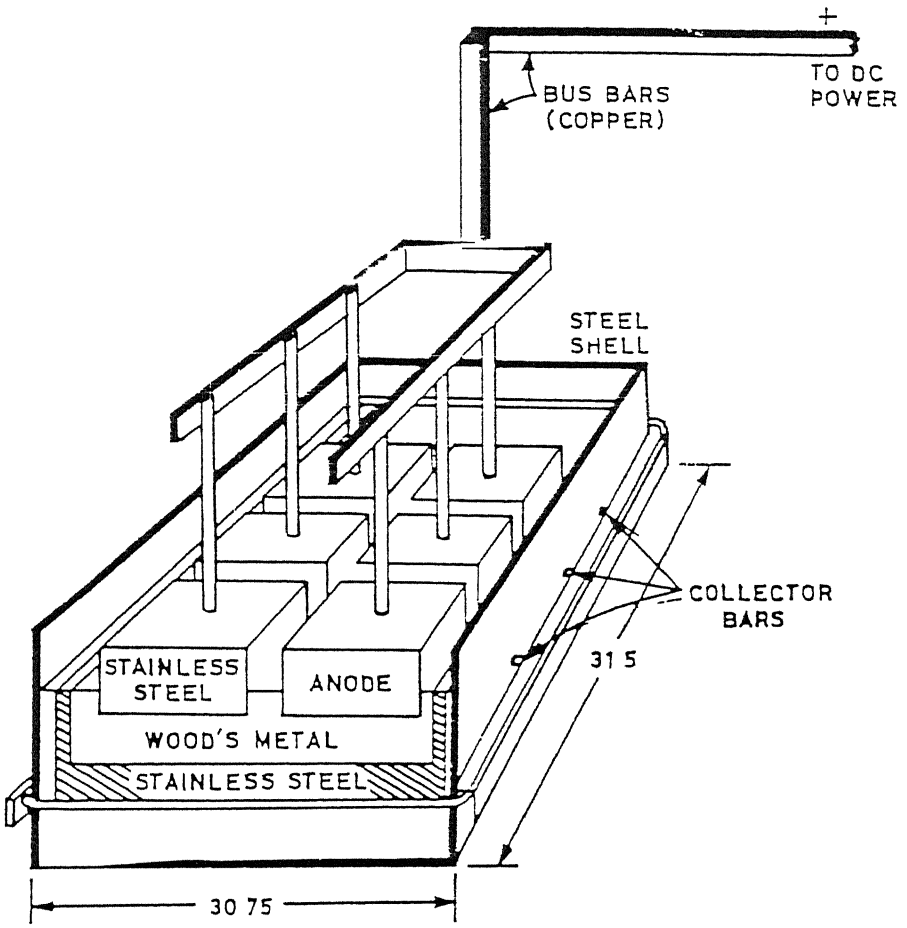

Figure6 1 Schematic diagram of low temperature simulated Hall-Heroult Cell

3) Cathode Collector Bars

4) Heating System

6 1 1 1 INNER SS TANK

The inner SS tank simulates the cavity of the Hall cell It can hold up to 50kg of simulating liquid, Wood's metal Reasons for selecting Wood's metal to simulate the electrolyte has been discussed elsewhere [53] The tank (31cmx31cmx10cm) has been made out of 1 5mm thick SS sheet The sheets are welded and made leak proof by high temperature sealant which can go upto 250^{o}C without failing Slots (6 Nos) have been cut on the opposite sides of the tank so that the collector bars welded on to the base of the tank can pass through them

6 1 1 2 ANODE ASSEMBLY AND BUSBARS

Six stainless steel blocks (12cmx8cmx6cm), representing anodes are suspended from the overcell assembly as shown in Fig 6 2 Each of the SS blocks have a centrally threaded cavity in which a copper rod, simulating the anode rod, of diameter 1cm is tightened Fig 6 3 is showing top view of bus-bars attached to be anode Copper busbars running across the top of the cell also have slots made at proper positions so that the top threaded portion of the copper rod is made to pass through it and tightened by brass nuts which rest on the MS strips Schematic drawing of the major current flows in the bus-bars of the cell is shown in Fig 6 4 Positive terminal of the power supply is connected to the anode bus and negative terminal is connected to the collector bars The connection of the cell to power supply is made through 0 5cm thick copper strips

6 1 1 3 CATHODE COLLECTOR BARS

Copper strips of thickness 0 5cm serve as cathode collector bars Six copper strips, three on each side have been welded on to the upper base of the inner tank which pass through the slots (2 5cmx0 5cm) cut as explained in the previous section

The collector bars carrying away the current from the cell are welded such that they are lying below the anodes suspended into the cavity

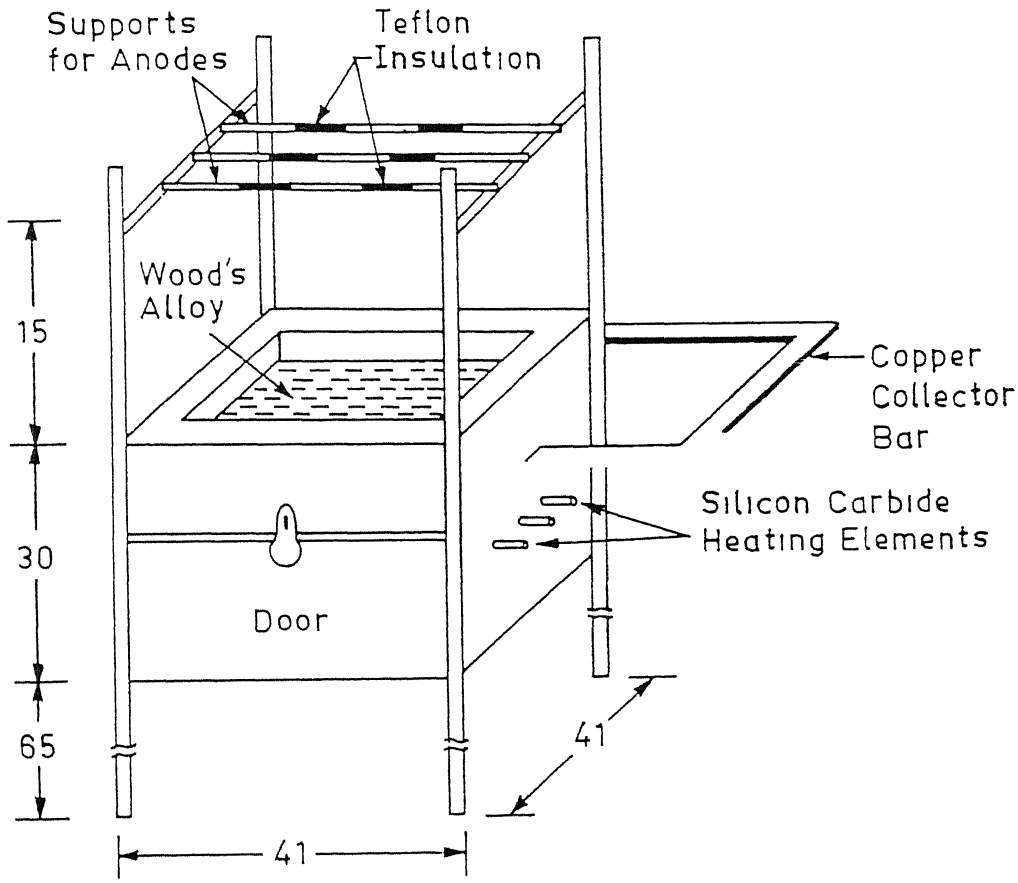

Figure6 2 Diagram showing molten Wood's alloy in the cavity, overcell assembly collector bar and door fitted to the cell

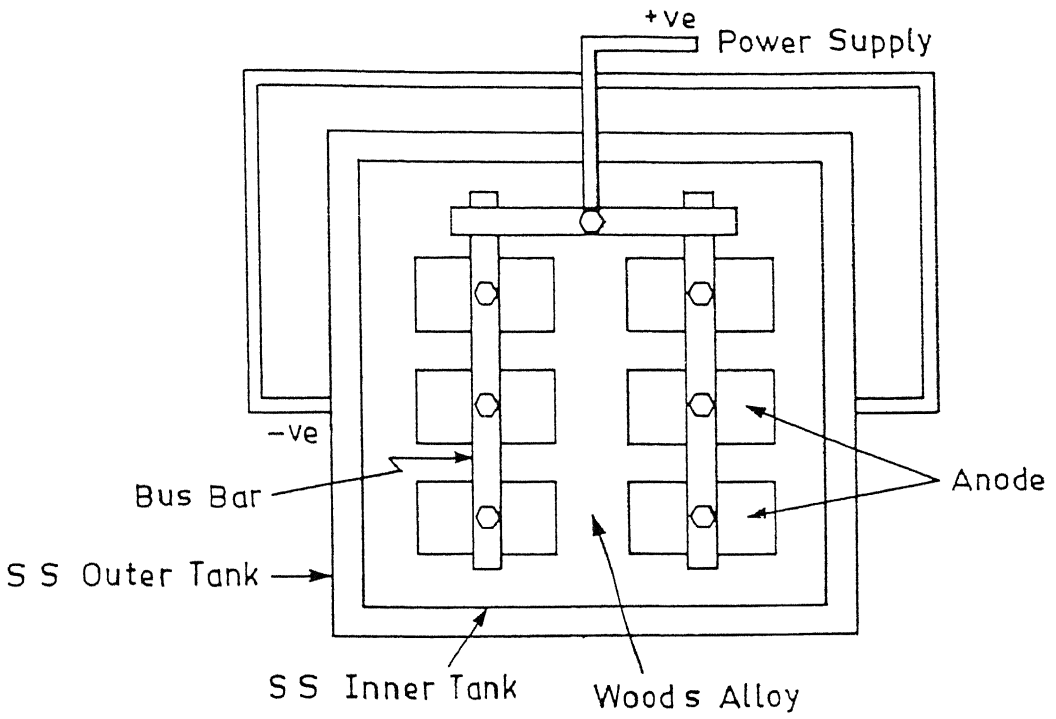

Figure6 3 Top view of bus-bar attached to anodes

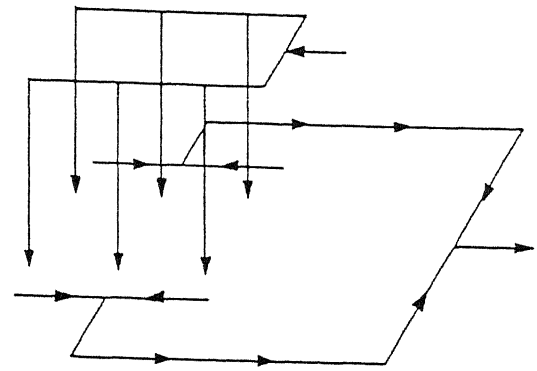

Figure6 4 Schematic drawing of the major current flows in the bus-bar and other conductors of the cell

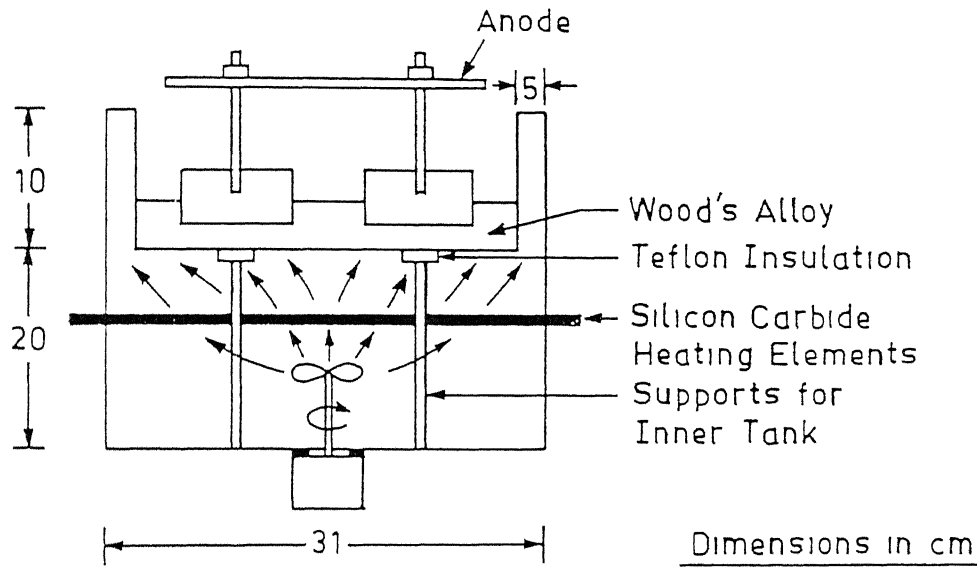

Figure6 5 The heating system based on circulation of hot air

6 1 1 4 HEATING ARRANGEMENT TO MELT THE BATH

Bannerjee and Evans [54] used a hot water system to keep Wood's metal in a molten state The inner cavity of their cell is put in a hot water bath This is electrically insulated from all sides so that current do not leak from it This insulation retards the heat transfer from water bath to Wood's metal to be melted in the cavity It took several hours to melt the Wood's metal The heating system designed in the laboratory based on hot air for multi-anode cell is very efficient in melting the Wood's metal It takes one and half hour to completely melt the Wood's metal Moreover, in the present design, there is no need for such insulating layer to be fitted on outer walls of the cavity

The heating system consists of a tank (41cmx41cmx30cm) as shown in the Fig 6 5 Three silicon carbide heating elements, spanning the width of the tank, are fitted in it through the three holes made across the sides of the outer tank They are placed 10cm below the cell (inner tank) An air circulating fan is also fitted at the bottom of the outer tank to provide a uniform temperature around the inner tank as shown in the Fig 6 5

The multi-anode cell is placed inside the heating chamber, supported by four rods (diameter 2cm) welded at their base as shown in the Fig 6 5 Rectangular mild steel pieces of 3cmx4cm are also welded on the top of the rods to give better support to the inner tank which can sustain load of the order of 50kg Rectangular teflon pieces, 4cmx5cm, are fitted on to the mild steel pieces at all the four contacts between the two tanks to prevent leakage of current from the inner tank to the outer tank

An over cell assembly running across the width of the cell has been designed and incorporated into the cell It consists of three mild steel strips overlaid with wood as shown in Fig 6 2 Rectangular pieces of teflon has been further fitted on to the wooden strips to reduce the chances of electrical contact between the busbar and overcell assembly Each of the strips has slots cut in it to adjust the inter anode gap and anode to wall gap

In case of any breakdown components fitted in the hot air chamber is accessed through a door as shown in Fig 6 2

Thermal insulation have been provided by wrapping asbestos cloth around the side walls The gap between the two tanks at the top, is covered by putting asbestos sheets on it

6 1 2 POWER SUPPLY

Current is passed through the cell by a DC power supply Model# 6681A (0-8V/0-580A), of Hewlett Packard, US Make The power supply is operated in a constant current mode

6 1 3 MAGNETIC PROBE

Magnetic field is measured using a Gaussmeter model# 9640 (0 1G-30kG), FW Bell, Orlando, Florida, USA Make The Gaussmeter is attached with a three axis probe Accuracy of the system claimed by the manufacturer is 0 275G

6 2 RAW MATERIALS

Wood's metal is being used as simulating liquid for the bath The physical properties of Wood's metal are listed below

Chemical composition

Sn 13 3%
Pb 26 7%
Bi 50%
Cd 10%

Density	9 38g/cm3
Resistivity	52 microohm cm
Temperature Coeff	0 002 (0-100 C)
Electrical Cond	4 17 (% compared with Cu)
Melting Point	72^{o}C

6 3 TEMPERATURE CONTROL AND MEASUREMENT

Temperature is maintained manually by controlling variac of external heating source Two alumel-chromel thermocouples (TC) are used to monitor the temperature of the tanks To protect the TC tip from being damaged, TC monitoring the temperature of Wood's alloy is kept in an SS tube

6 4 EXPERIMENTAL PROCEDURE

20kg of Wood's alloy is charged in the cell and is melted in one and a half hour On melting, the bath height is 2 2cm In each of the experiments, interpolar distance is maintained at 1cm and inter anode gap is maintained at 1 5cm

6 4 1 START UP

After about one and half hours of switching on the external heat source, the whole bath melts down and it has uniform temperature Though the melting point of the bath is $72^{o}C$, but at around $80^{o}C$, it is possible to maintain the whole bath in molten condition Side by side Gaussmeter is also put on and allowed to stabilize The probe to be used is inserted into the model and allowed to stabilize, after which the Gaussmeter to which it is connected is zeroed Now the power supply is turned on and current is set depending on the current density (cd) at which experiment has to be conducted The power supply is allowed to stabilize for 10 minutes before readings are taken

6 4 2 MAGNETIC FIELD MEASUREMENT

Magnetic field measurements were made in the Wood's metal in all the three directions at two horizontal planes, one at z=0 and other at z=1 1cm To protect the probe against heat or any corrosive damage, the probe is put into an aluminium tube

6 5 REPRODUCIBILITY EXPERIMENTS

Reproducibility experiments were carried out at $84^{o}C$ temperature, cd of 0 9 A/cm^2 and z = 0 The corresponding readings are given in Table 6 1

30/6/98			
Points	Bx(G)	By(G)	Bz(G)
A	0 45	4 6	3 43
B	-1 53	0 83	-1 13
C	-0 68	-2 56	-4 53
D	1 4	-3 76	-2 46
E	2 7	-0 35	-0 06
F	4 56	3 86	-0 16
G	3 76	3 43	-2 46
H	4 4	-0 53	1 66
I	2 36	-5 93	4 7
J	4	-2 76	7 43
K	5 13	-0 06	1 67
L	3 6	1 03	-3 87

2/7/98			
Points	Bx(G)	By(G)	Bz(G)
A	0 47	4 6	3 37
B	-1 6	0 73	-1 4
C	-0 67	-2 17	-4 27
D	1 37	-3 93	-1 97
E	3 06	-0 23	0 23
F	4 5	4 17	- 18
G	3 7	3 93	-2 27
H	3 4	-0 43	1 4
I	2 37	-5 8	5 67
J	4 17	-2 1	7 97
K	5 83	-0 87	1 63
L	4 27	1 13	-3 87

Table 6 1 Measured magnetic fields at Cd = 0 9 A/cm^2, T = 84^{0}C & Z=0

CHAPTER 7

RESULTS AND DISCUSSION OF SIMULATED LOW TEMPERATURE HALL CELL

7 1 MAGNETIC FIELD MEASUREMENTS

In each set of the experiments, magnetic field is measured at positions marked A to L in the Fig 7 1 Effects of changing temperature, current density and unbalanced anode system has been observed on the magnetic field distribution in the cell at two horizontal planes (Z=0 and Z=1 1cm) Fig 7 2 shows the points A to L in the cell with an anode removed from the anode assembly

Interpolar distance maintained in each of the experiments is 1cm The wall to anode distance maintained in each of the experiments is shown in Fig 7 1 Process variables and their ranges examined in the experiments conducted are given in Table 7 1

Sr No	Variables	Ranges
1	Temperature	$84^{o}C$, $95^{o}C$
2	Current Denisity	0 7, 0 8, 0 9 A/cm^2
3	Anode	One anode removed from the middle row

Table 7 1 Process variables and their ranges investigated in various experiments

Recorded datas of magnetic fields at different operating conditions have been presented in tabular form in Appendix B Fig 7 3-7 10, represent the measured magnetic fields in vectorial form The rectangular blocks shown in in the figures are representing anodes and vectors indicate magnetic fields, with broken lines being the vertical component and solid arrows are horizontal field The convention followed in drawing vertical magnetic field is

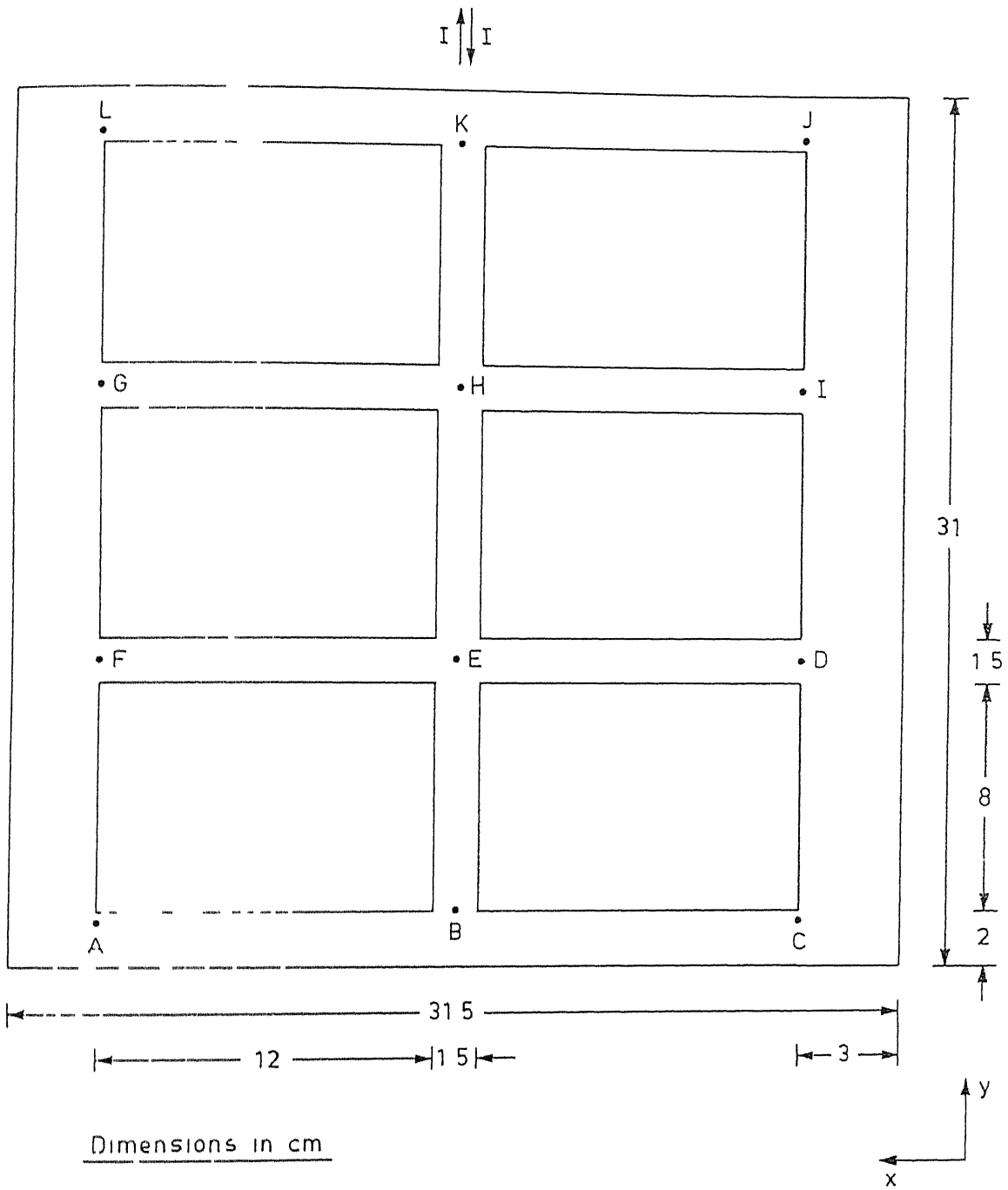

Fig 7 1 **Points being investigated with all anodes intact**

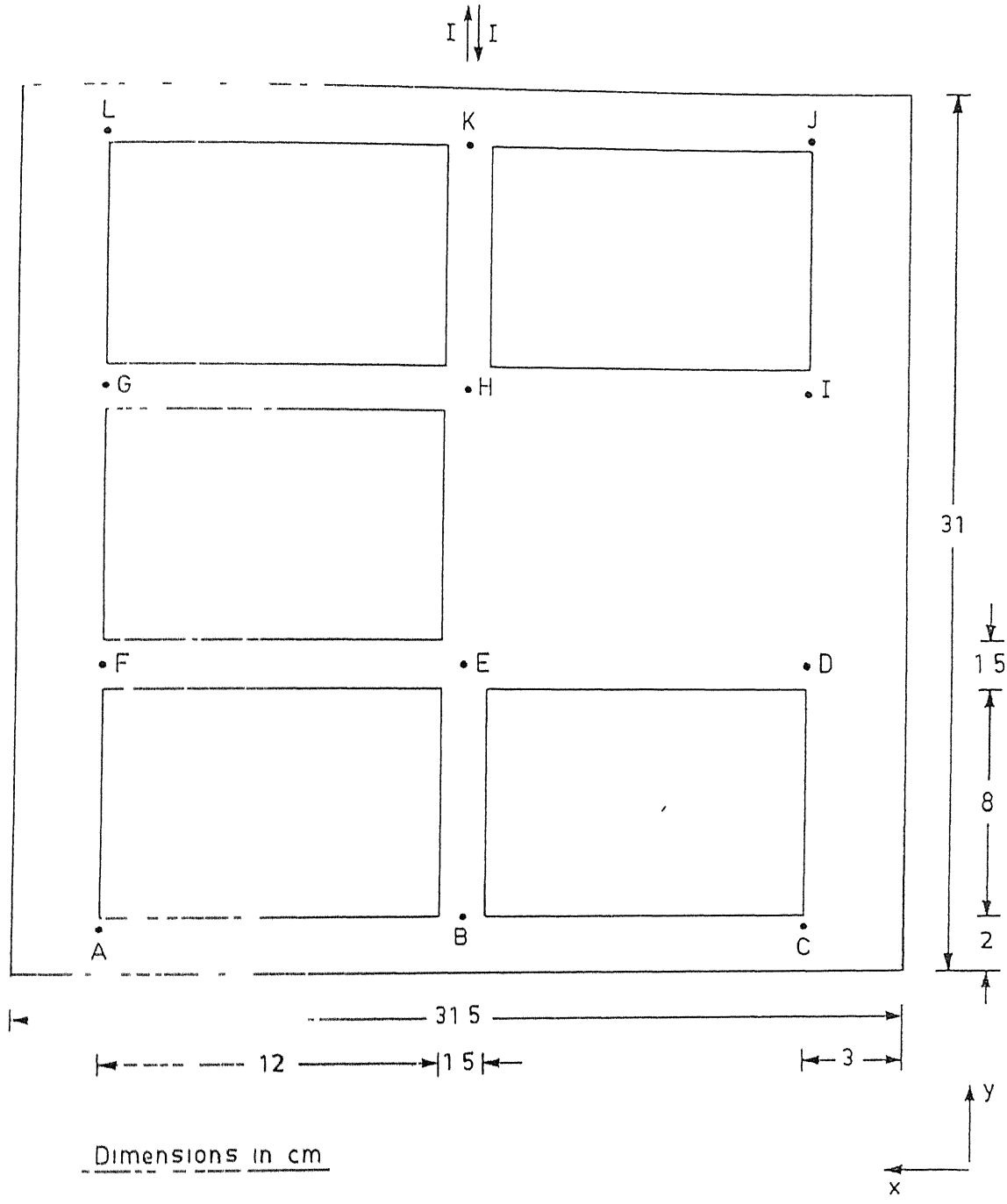

Fig 7 2 Points being investigated with an anode removed

that if the broken arrow is clockwise from the solid arrow, the field is downward, if anticlockwise, it is upward The operating conditions existing in Fig 7 3 (cd=0 9, T =84C,z=1 1cm) is assumed to be " base" case, so that results obtained at other operating conditions could be compared with

As expected, the overall horizontal component (B_x and By) of the magnetic field is approximately clockwise barring a few exceptions, because they are due to predominantly downward vertical current flowing through the anode rods Even the magnitude and direction of the vertical magnetic field (B_z) is consistent with the horizontal current flowing in anode bus-bar, collector bar as governed by the right hand rule A general trend in all the investigations carried out is that the vertical component of the magnetic fields at points B,E,H, and K have very small magnitude (< 1G) This is because the magnetic fields produced by segments PQ and RS (Fig 6) are in opposite direction, cancelling each other One more interesting trend observed in all the investigations conducted is that, directionwise, the diagonally opposite regions have similar vertical component of the field Points L, G, C, and D experiences downward vertical field where as A, F, J, and I have it in upward direction

7 1.1 EFFECT OF TEMPERATURE

On observing the trend in Fig 7 3 and Fig 7 4, it is found that roughly same magnetic field distribution is maintained at 84°C and 95°C, with cd of 0 9A/cm^2 From this observation it is concluded that temperature has no effect on the magnetic field distribution in the cell

7.1.2 EFFECT OF CURRENT DENSITY

Fig 7 4, Fig 7 5 and Fig 7 6, represent the distribution of magnetic field at current density of 0 7, 0 8, and 0 9A/cm^2 with temperature of 95°C The clockwise trend is maintained at each current densities and magnitude of horizontal as well as vertical magnetic field is more at higher cd (0 9A/cm^2) as compared to lower current density, owing to large currents flowing through the cell at higher current densities

On observing Fig 7 10 with the base case, it is concluded that the magnitude of the horizontal magnetic field at the base of the cell (z=0) is less than horizontal field at midplane of the bath (z=1 1cm) The vertical component of the field exhibits a reverse trend It is recorded to be more at the base than at the midplane of the bath

7 1 3 COLD ANODE

Anodes in Hall cells are replaced every 10 to 20 days, typically, one anode would be replaced each day On placing a new anode at room temperature into a cell, it is usual for this "cold" anode to carry little current until it heats up Electrolyte freezes onto the anode and, the frozen electrolyte being a poor conductor, it must melt off before passage of significant current The maldistribution of current caused by introducing a cold anode has long been thought to disturb a cell

The upset was simulated in the cell by removing an anode from the anode assembly Fig 7 7 and Fig 7 8 shows the magnetic fields with an anode removed On comparing the trend of these two figures with that of base case, it is concluded that cold anode will have a small effect on the magnetic field of a Hall cell, except in their immediate vicinity

7 2 CONCLUDING REMARKS

Even though the magnetic field displays the expected trend, there are some differences with the measurements of Banerjee and Evans [54], whose results have been shown in the Fig 7 11 The difference stems from the fact that cell configuration of Banerjee and Evans was different They operated with fourteen anodes and with a different bus-bar design as shown in Fig 7 12 The bus-bar shown in Fig 7 12 is forming a closed loop where as the bus-bar design used in this investigation as shown in Fig 6 is not forming such loop Moreover, the connecting strips running from the anode assembly and collector bar to the power supply is not straight, it is inclined for convenience in making connections In their configuration, current enters from one side and exits from the opposite side (right to left) where as the cell investigated has such a design that current entry as well as the exit is from the same side

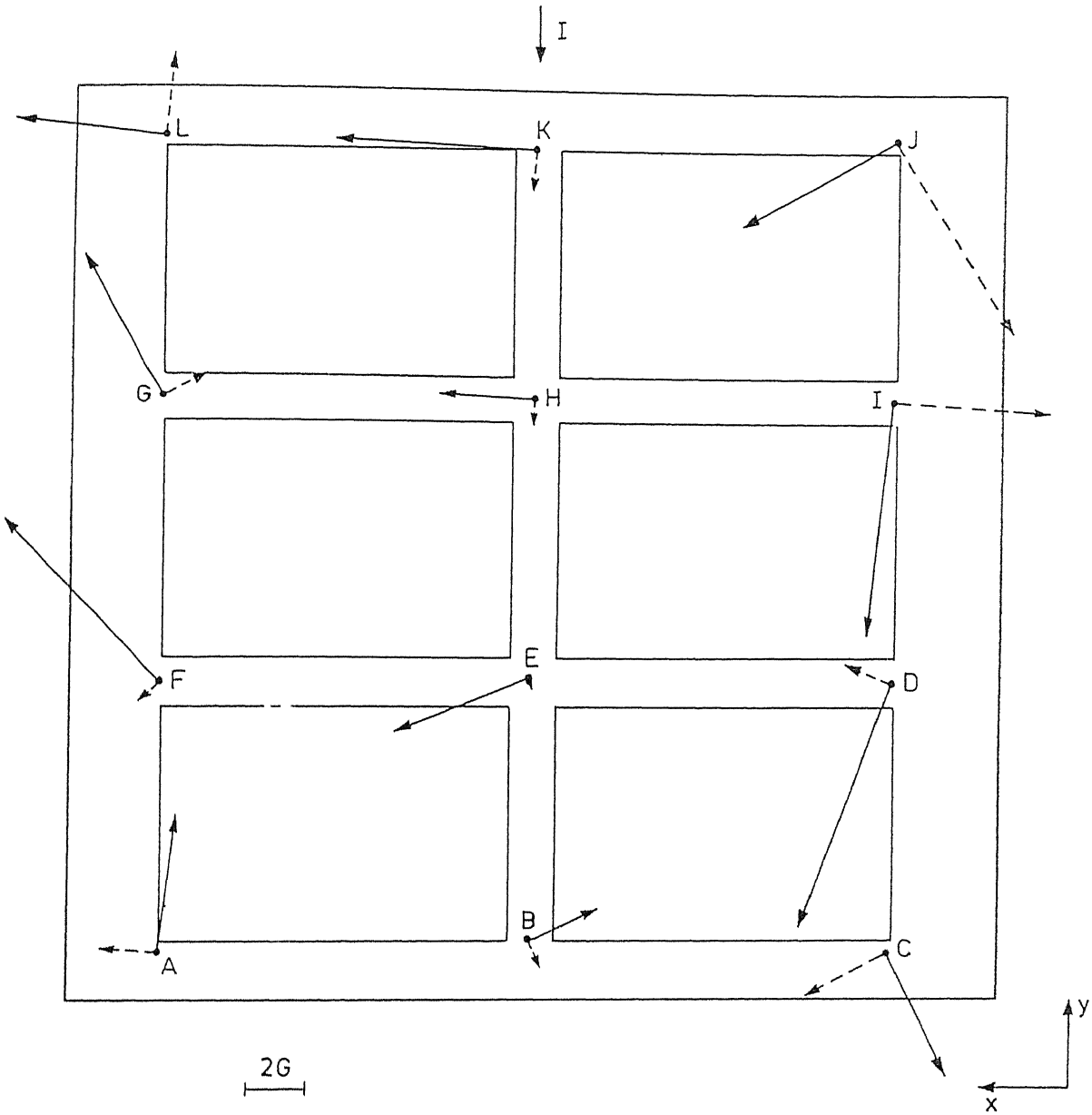

Fig 7 3 Measured magnetic fields in the cell at Cd=0 9A/cm^2, T=84°C, and Z=1 1cm

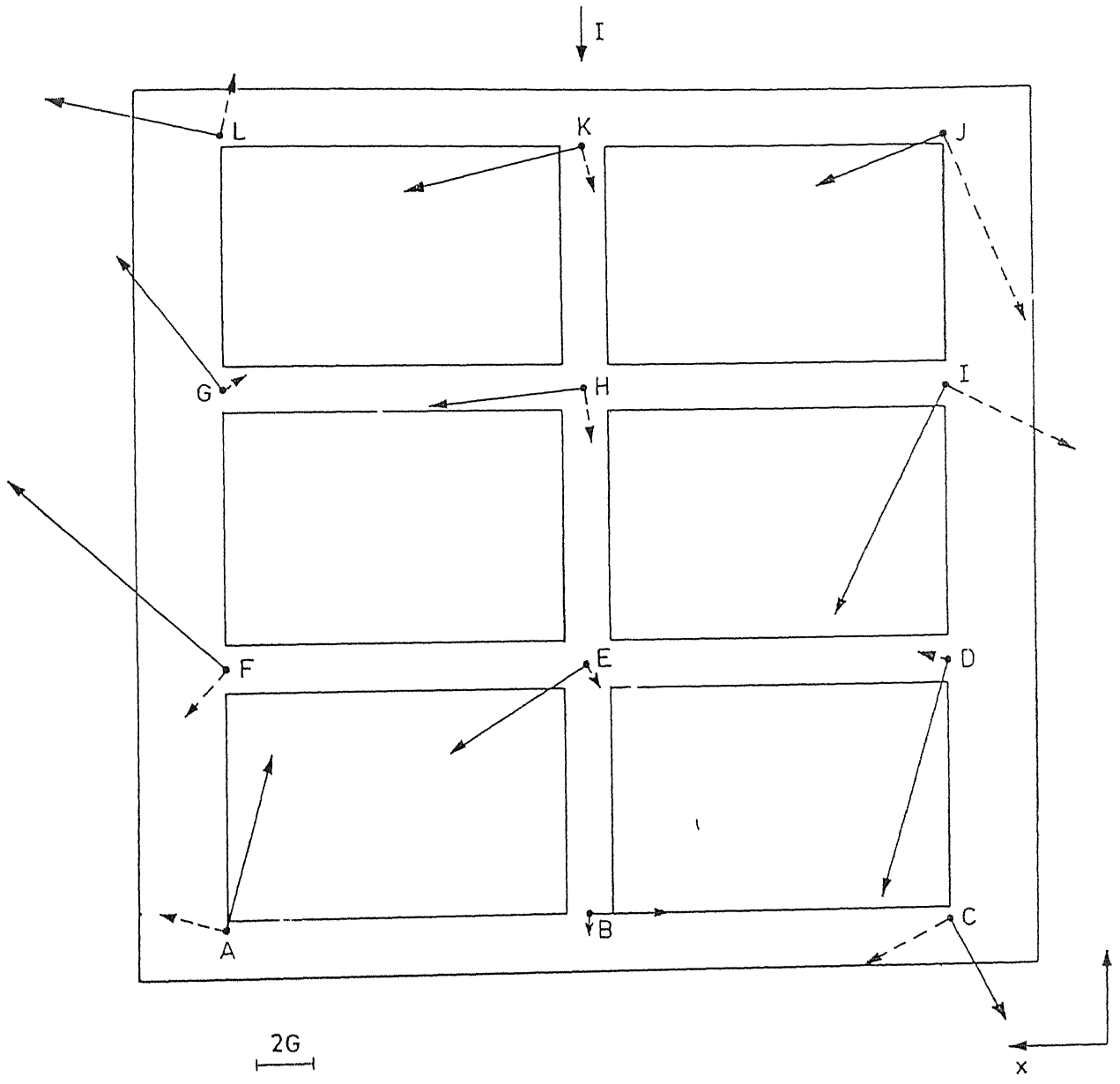

Fig 7 4 Measured magnetic fields in the cell at Cd=0 9A/cm^2, T=95°C, and Z=1 1cm

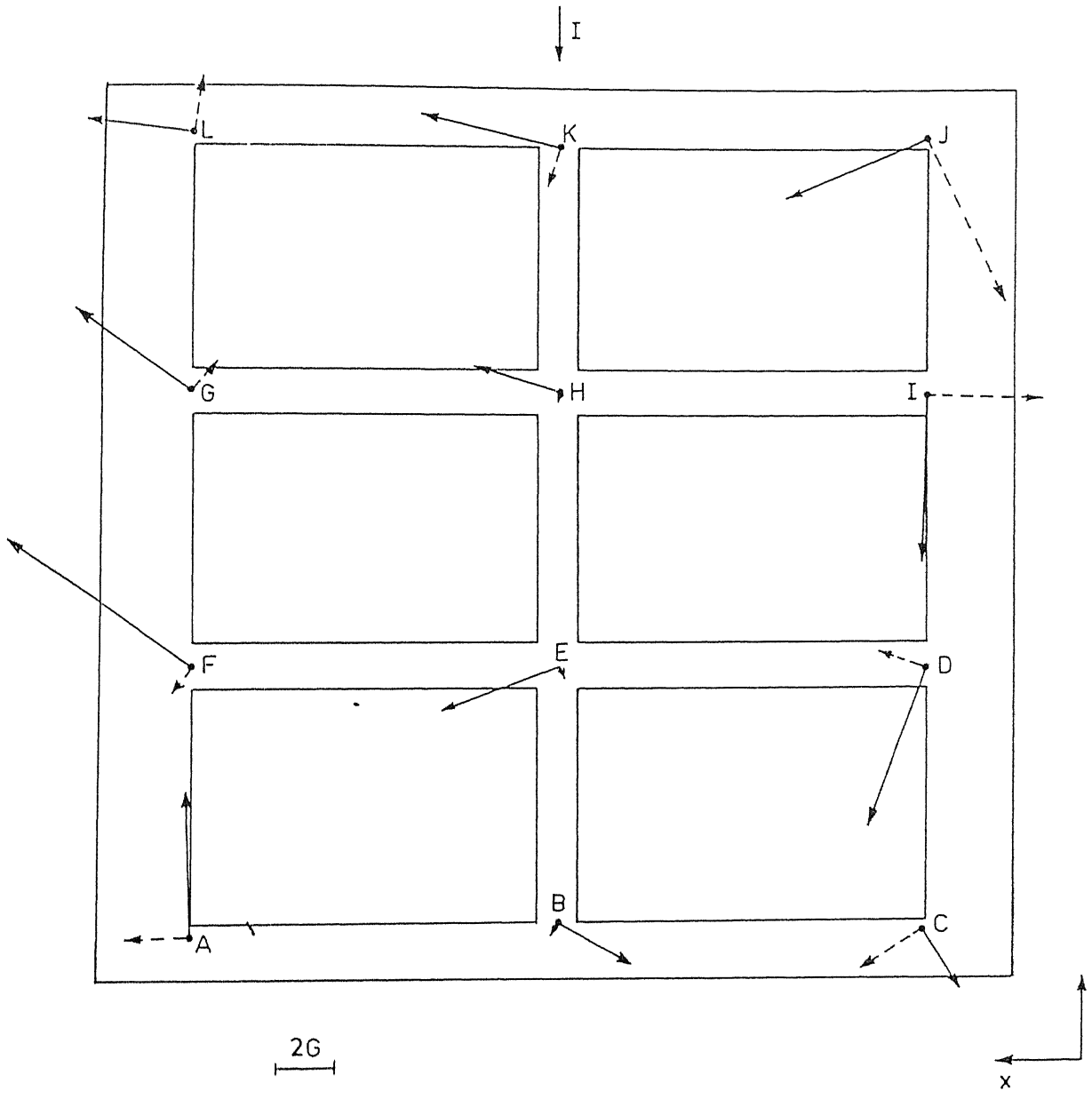

Fig 7 5 Measured magnetic fields in the cell at Cd=0 7A/cm^2, T=95°C, and Z=1 1cm

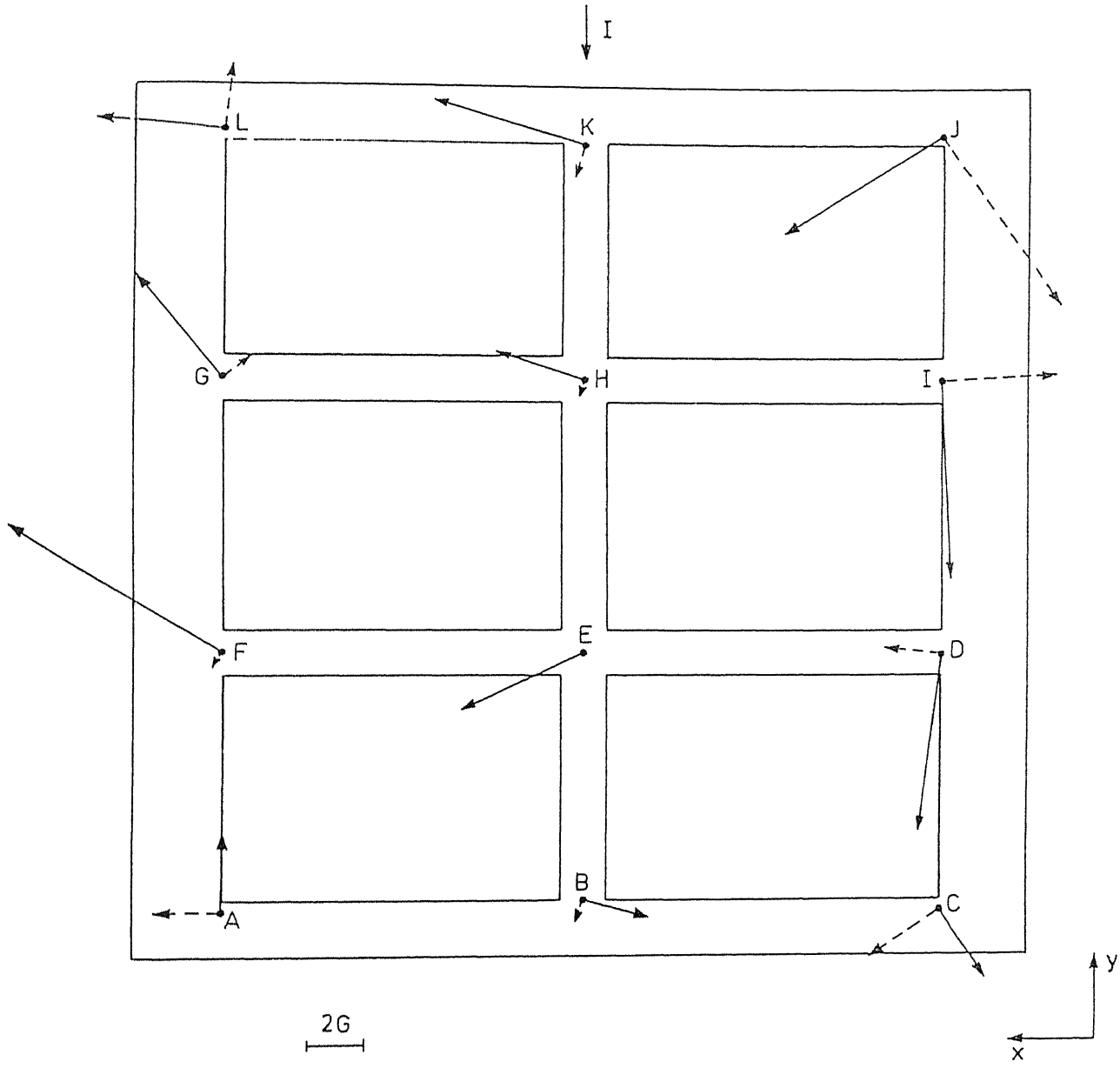

Figure 7 6 Measured magnetic fields at Cd = 0 9, T = 95^{0}C and Z = 1 1cm

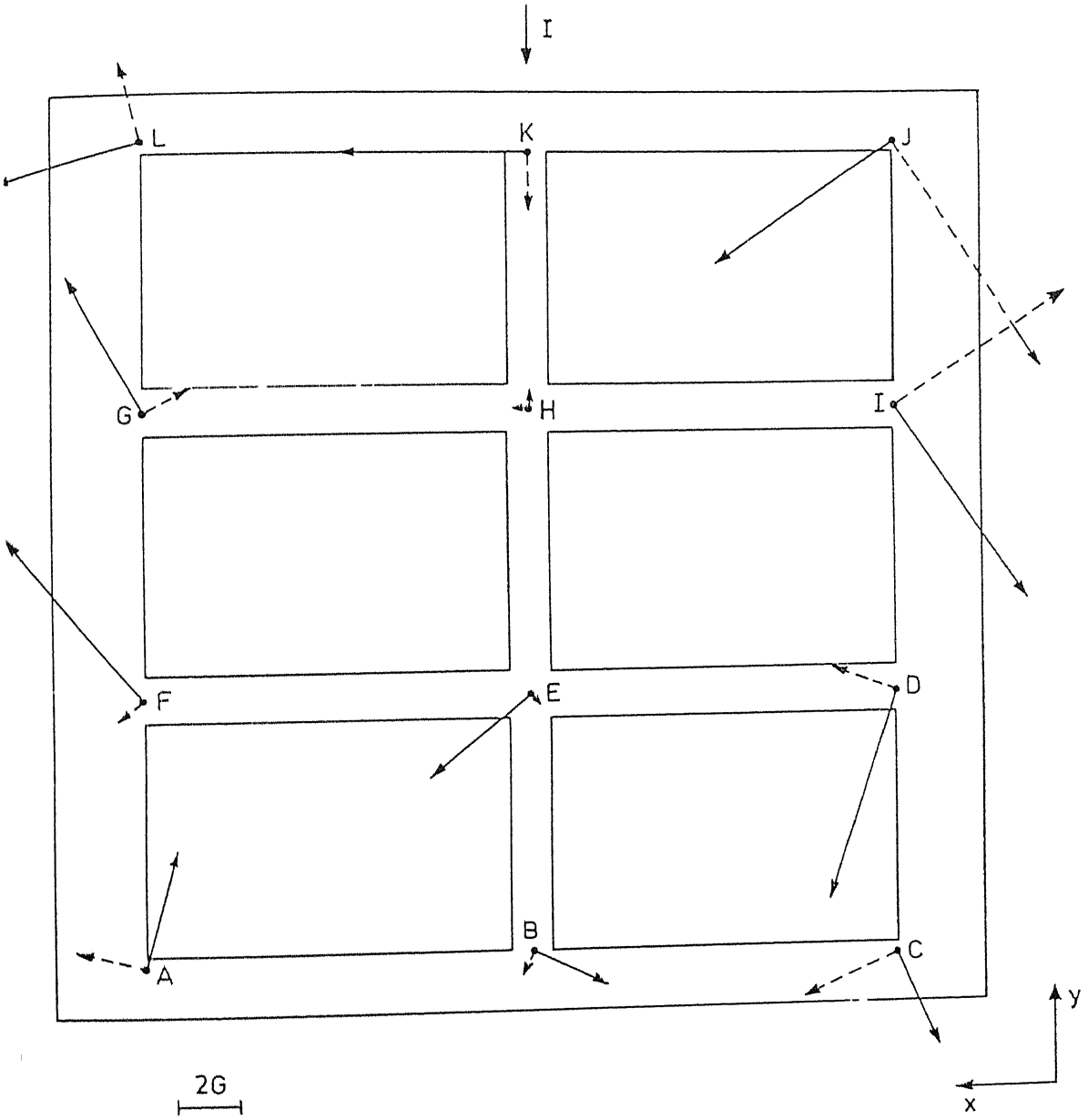

Fig 7 7 Measured magnetic fields in the cell with an anode removed at Cd=0 9A/cm^2, T=84°C, and Z=1 1cm

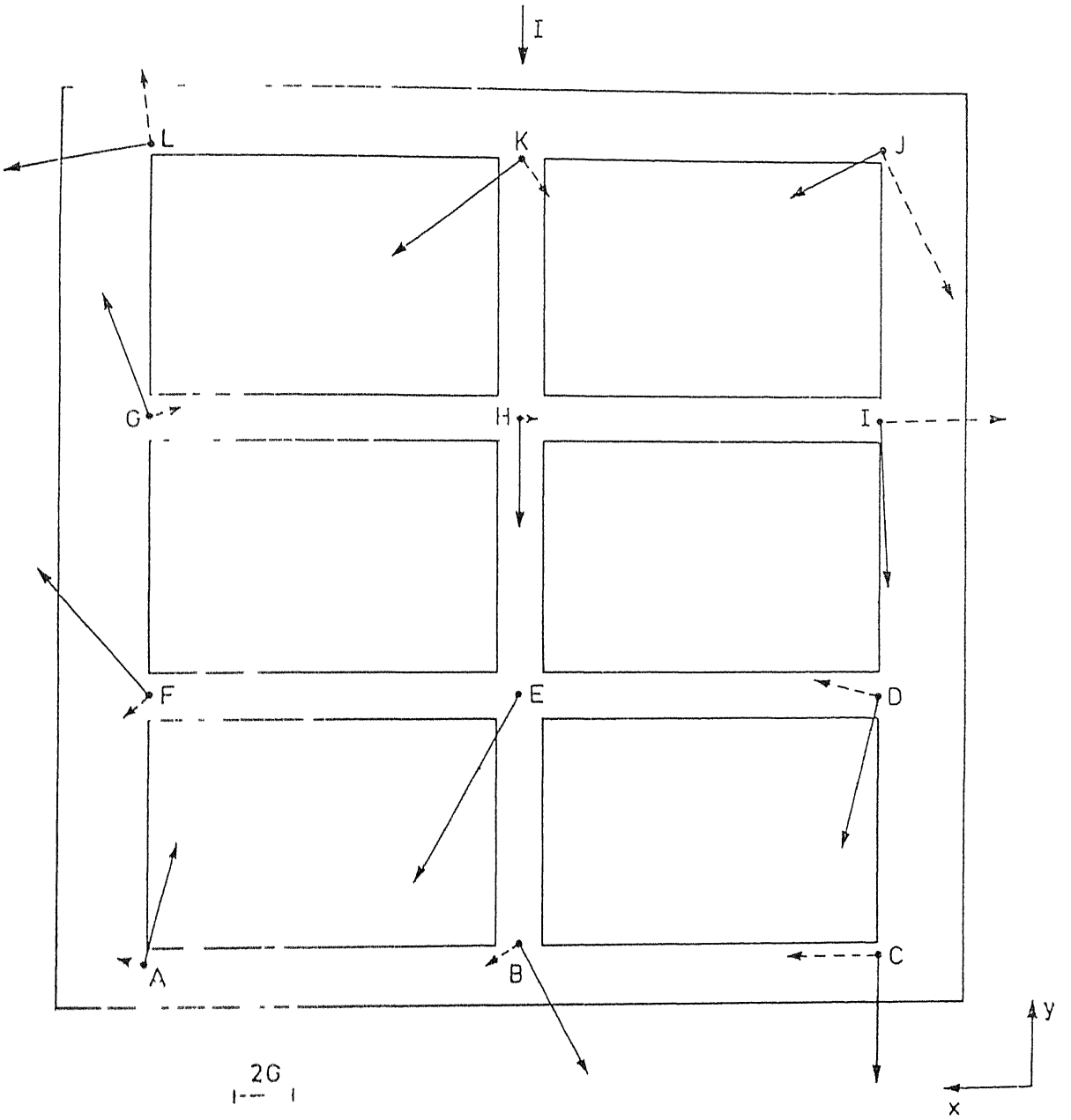

Fig 7 8 Measured magnetic fields in the cell with an anode removed at Cd=0 7A/cm^2, T=84°C, and Z=1 1cm

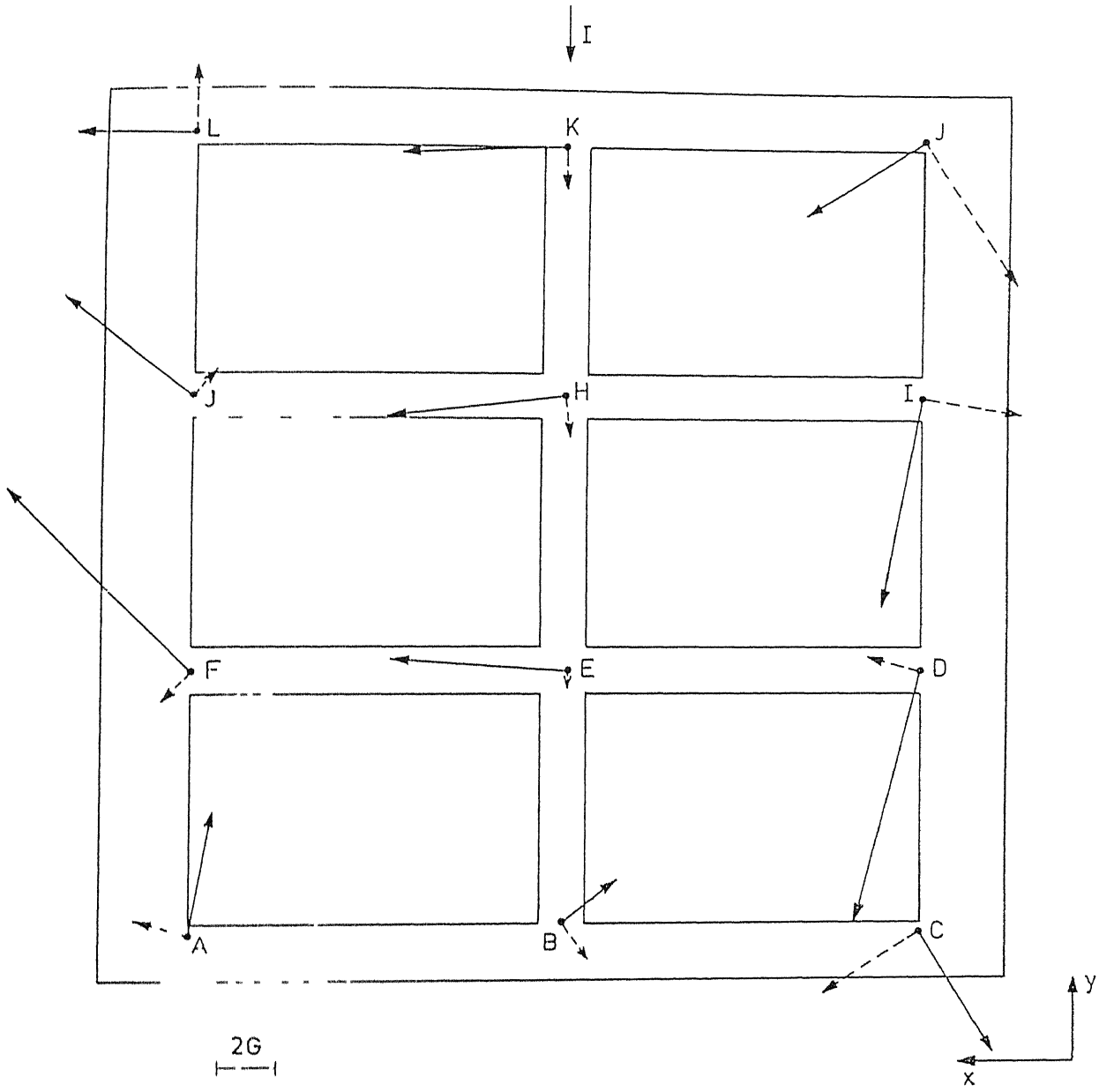

Fig 7 9 Measured magnetic fields in the cell at Cd=0 8A/cm^2, T=84°C, and Z=1 1cm

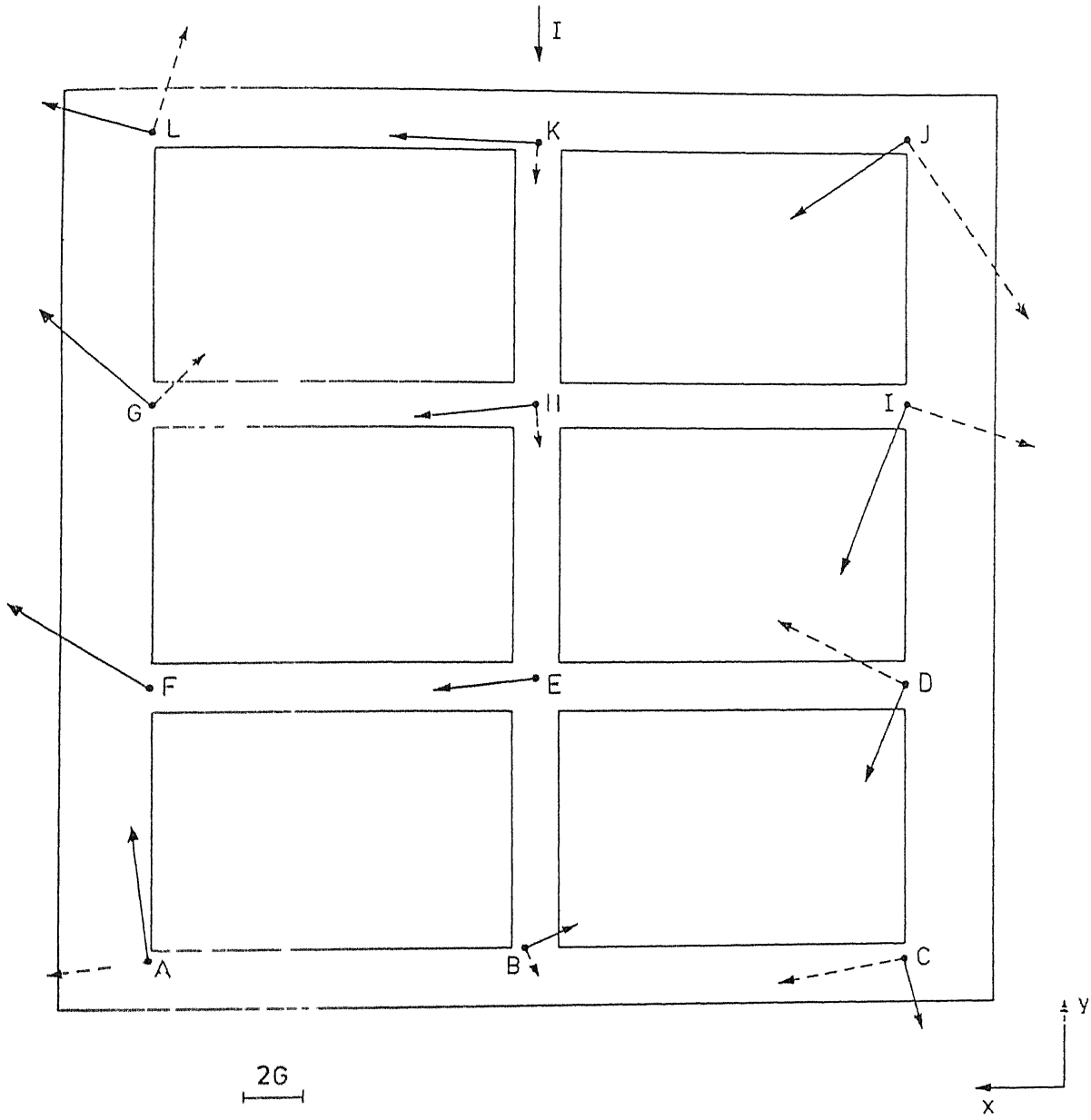

Fig 7 10 Measured magnetic fields in the cell at Cd=0 9A/cm^2, T=84°C, and Z=0

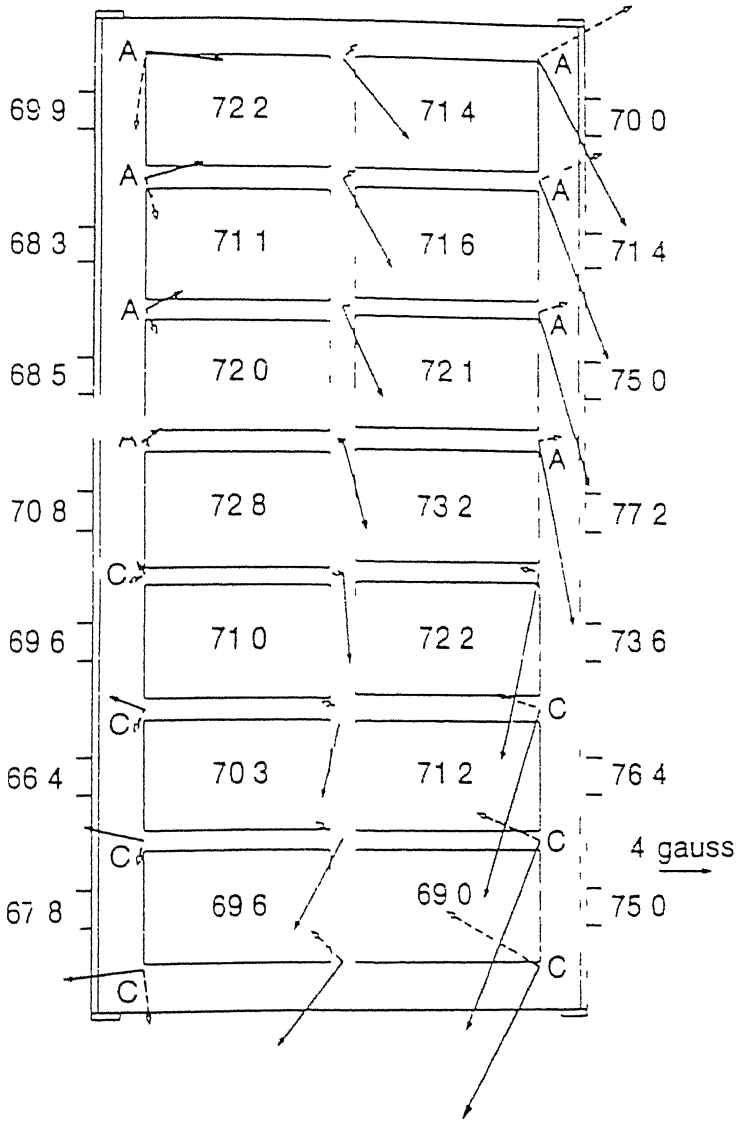

Fig 7 11 **Measured current and magnetic fields [54]**

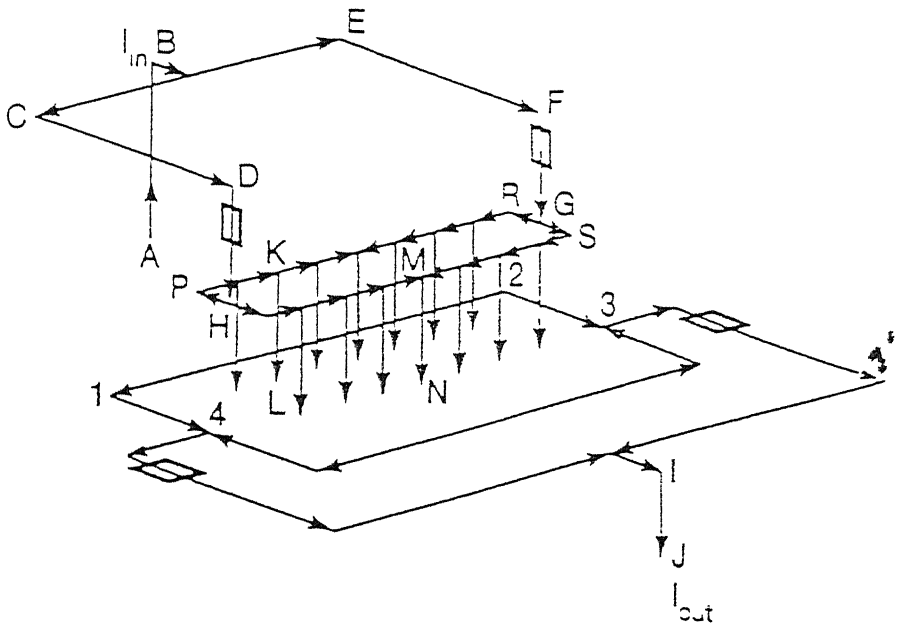

Fig 7.12 **Schematic drawing of the major current flows in the bus-bar and other conductors**

CHAPTER 8

SUMMARY AND CONCLUSION

The present investigation is carried out with the prime objective of generating laboratory scale data of magnetic and velocity fields in Hall cells for validating the mathematical model being developed The mathematical model being developed is aimed at improving the present knowledge of magnetohydrodynamics of the cell, which controls the oscillations at the metal/electrolyte interface These oscillations prevent the operation of the cell at reduced interpolar distance, thus operating at higher energy consumption It was decided to carry out the investigations in several stages In the first stage, a single anode Hall cell is designed, fabricated and operated at conditions existing in real Hall cells with the aim of studying the behaviour of cell and to get familiar with the various operating problems Later, based on the operating experiences on this cell, a multi-anode Hall cell was then to be developed for generating laboratory scale data of magnetic and velocity field distribution in the cell

This idea of carrying out measurements at actual conditions was given up because of (a) the corrosive nature of electrolyte, (b) high level of heat losses and (c) nonavailability of good and reliable cooling system required for Hall effect probe

As discussed above, the magnetic field measurements in Hall cell could not be carried out, but the aim of familiarising oneself with the operation of a Hall cell was very well achieved Typical operational problems of Hall cells were encountered and measures were taken up to control them In the experiments conducted current efficiency is found to be approximately 45% on an average The fact that current efficiency is on the lower side (as compared to current efficiency of industrial cells - 95%) could be attributed to several reasons, particularly, shortcircuiting, higher temperature, openness of the system and reoxidation Higher energy consumption is due to large voltage drops in various parts of the cell esp in the clay graphite crucible being used for economical reasons Interesting findings were made on analysing the electrolytic products of the cell Cryolite undergoes phase change

and converts to chiolite and $NaAlF_4$ X-Ray analysis confirmed the presence of aluminium carbide, on the base plate of the crucible

After familiarising with the operation as well as with the typical problems of the single anode laboratory scale Hall cell, it was decided to design and fabricate a low temperature simulated multi-anode Hall cell for recording magnetic field distribution in it Wood's metal was found to be a suitable simulating liquid for the electrolyte Magnetic field measurements were conducted using a Hall effect probe at different temperatures and current densities A special case of unbalanced anode assembly was also investigated by removing an anode from the middle row of the assembly The trend of horizontal magnetic field in each of the experiments is clockwise as expected These investigations match well with the findings of other investigators Effect of temperature, current density, and unbalanced anode assembly on the magnetic field distribution of the cell has been discussed in some detail It is hoped that magnetic field measurement carried out in low temperature simulated Hall cell would help in validating the mathematical models being developed for the design and optimization of industrial Hall-Heroult cell

8 1 SUGGESTION FOR FUTURE WORK

In the present investigation, experiments were carried out in a laboratory scale single anode Hall cell Its current efficiency is found to be 45% on an average The current efficiency can be increased to higher value by incorporating changes in operating and design conditions such as improving the anode and cathode material, carrying out the experiment for 5-6 hours with the ledge, and incorporating a control system into the cell which can monitor the alumina content and temperature of the bath The performance of the cell can also be improved by pursuing the earlier idea of carrying out experiments in a laboratory scale bigger multi-anode Hall cell There is lesser probability of short circuiting in the multi-anode Hall cell and reduced heat losses due to higher volume to surface area than the single anode cell

Magnetic field measurements could not be recorded at operating conditions existing in real Hall cell due to nonavailability of Hall effect probe equipped with a good cooling system and protective sheath On acquiring a compatible cooling system, magnetic

field measurements can be recorded in laboratory scale Hall cell

Studies made on low temperature Hall cell is limited to magnetic field measurements only It is necessary to carry out velocity measurements for exact knowledge of fluid flow within the cell Current distribution in each of the anode is important to be known for the study of magnetohydrodynamics being carried out Though effects of temperature, current density, and unbalanced anode assembly have been conducted at two horizontal planes, yet there is lot of scope of investigations to be carried out Effects of increasing bath level by increasing the amount of Wood's metal, varying interpolar distance, inter anode distance, wall to anode distance, varying bus-bar design, simulating ledge by placing a nonconducting material along the walls etc on the magnetic and velocity distribution can be recorded

APPENDIX A

44-231 JCPDS-ICDD Copyright (c) 1994 PDF-2 Sets 1-44 database Rad = 1 54060 Quality *

AlF
3

Aluminum Fluoride

Rad CuKa1 Lambda 1 54060 Filter Mono d-sp Diff
Cutoff 2 1 Int Diffractometer I/Icor 7 06
Ref Hoffmann C Auernhammer F Lengauer Ch , Tillmanns E , Univ Vienna
Vienna, Austria, ICDD Grant-in-Aid, (1992)

Sys Rhombohedral (Hex) S G R-3 (148)
a 4 9278(1) b c 12 444o(4) A C 2 5254
A B C Z 6 mp
Ref Ibid

Dx 3 197 Dm 3 130 SS/FOM F30=94(007 49)

ea nwB ey Sign 2V
Fer

Color Colorless
Pattern taken at room temperature Sample was provided by Hoppe, R , Institute of Inorganic and Analytical Chemistry, Justus-Liebig-University, Giessen Germany and Zemann, J Institute of Mineralogy and Crystallography, University of Vienna, Vienna, Austria CAS no 7784-18-1 First (NH4)3[AlF6] was synthesized from Al(OH)3 and a saturated solution of NH4F then decomposed under a FE-flow at 450-700 C for 48 hours to get a colorless powder of AlF3 Lattice parameters were refined by least squares treatment of the powder data Si used as internal standard PSC Pf8 To replace 9-138 Structure reference Hoppe, R , Kissel, D , J Fluorine Chem 24 327 (1984) Mwt 83 98 Volume[CD] 261 71

2-theta	In	h k l	2-theta	In	h k l	2-theta	In	h k l
94 185	<	0 4 2	115 915	1	1 4 3			
95 935		0 0 12	122 205	1	0 4 8			
98 520		4 0 4	124 535	1	0			
102 855	2	2 1 10 3	127 830	2	1 3 10			
103 600		3 2 -2	130 115	1				
107 385	<	1 1 12	133 620	1	3 0 12			
109 720	<	1 3 -8	136 780		2			
111 145		2 2 -4	138 760	1	0			
112 585	<	4 1 0						
113 555	<	1 2 11						

Strong lines 3 52/X 1 70/3 2 2 2 1 59/1 1 56/1 1 20/1 1 19 1 2 51/1

NaF

Sodium Fluoride

Villiaumite, syn

Rad CuKa1 Lambda 1 540598 Filter Mono d-sp Diff
Cutoff [illegible] Int Diffractometer I/Icor
Ref McMurdie H et al , Powder Diffraction, 1 74 (1986)

Sys Cubic S G Fm3m (225)
a 4 6332(12) b c A C
A B C Z 4 mp
Ref Ibid

Dx 2 80 Dm 2 79 SS/FOM F11=154(007,11)

ea nωB 1 3246 ey Sign 2V
Ref Winchell, A Winchell, H Microscopic Character c Artificial Inorg Solid
Sub , 16 (1964)

Color Colorless
Peak height intensity The mean temperature of data collection was 25 6 C
The sample was obtained from Mallinckrodt Chemical Works St Louis Missouri,
USA CAS no 7681-49-4 References to other early patterns and structures
will be found in Swanson Tatge [illegible] Optical data for synthetic material
sigma(Iobs)=+ -1 Barth Lunde (1) studied the structure of NaF Halite -
group halite subgroup W used a internal standard PSC cF8 To replace
4-793 Structure reference 1 Barth T Lunde, G Cen Mineral Abt A,
1927 57 (1927) Additional powder data references Swanson, H Tatge
Natl Bur Stand (U S) Circ 539 1 63 (1953) Debye, P Scherrer P
Phys Z , 19 474 (1918) Davey W Phys Rev , 2 140 (1918) Wyckoff R
Hedstrom [illegible] Kristallogr [illegible] alloeon Kristallin [illegible] , Kristallchem , [illegible]
400 (19[illegible] Hanawalt [illegible] Rinn [illegible] Frevel L Ind Eng Chem Anal Ed , 10
457 (1938) [illegible] Volume [illegible]

2-theta	Int	h k l
35 4[illegible]8	2	[illegible] [illegible] 1
38 642	100	[illegible] [illegible] 0
56 1[illegible]0	44	[illegible] 2 0
[illegible] [illegible]22	2	[illegible] 1 1
70 [illegible]	10	[illegible] [illegible] 2
82 [illegible]54	3	4 [illegible] 0
92 [illegible]76	<1	[illegible] [illegible] 1
96 [illegible]74	7	4 [illegible] 0
10[illegible] 078	4	4 2 2
1[illegible] [illegible]97	<1	5 1 1
14[illegible] 267	1	4 [illegible] 0

Strong lines 2 32/X 1 64/4 [illegible] 1 C4/1 0 95/1 [illegible] 10/1 2 68 1 1 40/1

Na AlF
3 6

Sodium Aluminum Fluoride

Cryolite, syn

Rad CuKa1 Lambda 1 54050 Filter Mono d-sp Guinier
Cutoff 50 0 Int Densitometer I/Icor 0 37
Ref Technisch Physische Dienst, Delf , The Netherlands, ICDD Grant-in-Aid

Sys Monoclinic S G P21/n (14)
a 7 769 b 5 593 c 5 404 A 1 3891 C 0 9662
A B 90 18 C Z 2 mp 1020 C
Ref Ibid

Dx 2 97 Dm 2 97 SS/FOM F30=51(012,49)

ea 1 3376 nwb 1 3377 ey 1 3387 Sign + 2V 43 deg
Ref Dana's System of Mineralogy, 7th Ed

Color Colorless
CAS no 15096-52-3 PSC mP20 To replace 12-257 Mwt 209 94 VolumeCCD
234 81

2-theta	Int	h k l
19 537	55	-1 1 0
19 982	40	-1 0 1
22 866	65	0 1 1
25 584	12	-1 1 1
31 972	25	0 2 0
33 558	100	-2 1
33 115	16	0 0 2
36 116	6	0 2
36 900	25	0 2
38 017	25	-1 0 1
39 490	30	-3 0 1
39 559	6	3 0 1
39 766	25	1 2
39 891	25	-2 2 0
40 568	8	-2 0 2
40 682	8	2 2 2
41 928	20	3 1 1
42 167	20	-3 1 1
42 805	4	-1 2 2
43 894	2	2 2 2
46 713	95	0 3 0
47 862	6	3 2 0
48 240	6	1 3 0
49 642	2	-4 1 0
50 947	4	3 2 1

2-theta	Int	h k l	2-theta	Int	h k l	2-theta	Int	h k l
51 409	4	-3 1 2	52 724	35	-2 1 3	71 528	2	-5 2 1
51 847	8	0 3 1	61 076	2	4 1 2	73 352	2	4 3 1
52 026	2	-1 0 3	61 526	2	-1 3 2	73 000	2	6 0 0
52 521	14	-4 1 1	62 167	2	5 0 1	74 135	2	2 4 1
52 659	10	4 1 1	62 834	4	3 3 1	76 590	2	2 1 4
53 245	20	-1 3 1	65 289	4	-5 3 2	77 699	10	2 3 3
54 582	2	2 3 0	66 817	4	0 4 0	78 613	2	0 2 4
54 794	6	1 1 3	66 085	12	-1 4 0			
57 324	14	-3 3 1	69 407	4	0 4 1			
57 756	14	4 2 0	70 541	2	-1 4 1			

Strong lines 2 75/X 1 94/X 3 89/7 4 54/6 4 44/4 1 57/4 2 34/3 2 80/3

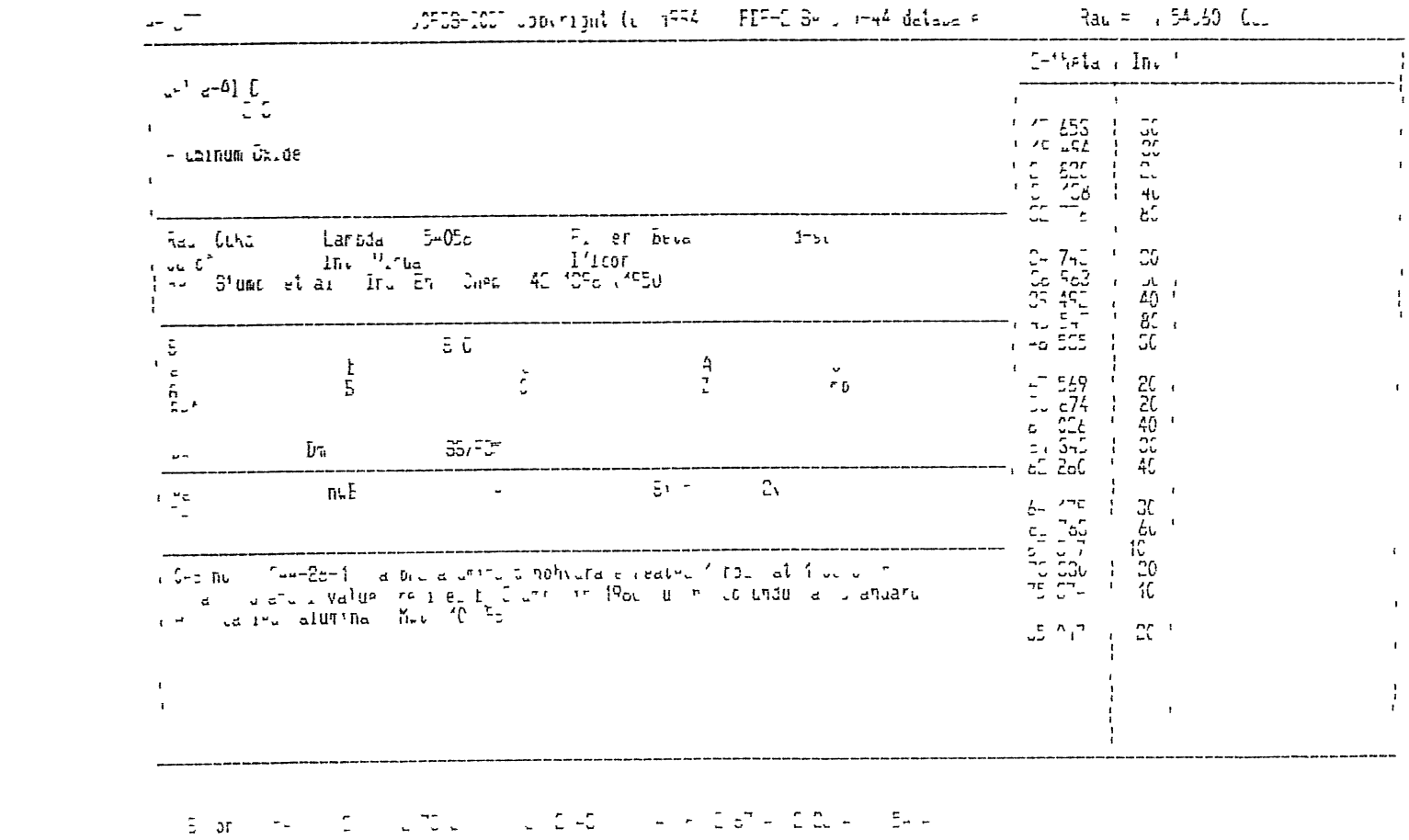

4- ... JCPDS-ICDD Copyright (c) 1994 PDF-2 Se ...-44 database Rad = 1 5-060 Qual

chi-Al_2O_3

Aluminum Oxide

Rad CuKa Lambda 1 5418 Filter Beta d-sp
Cutoff Int I/Icor
Ref Stumpf e al Ind Eng Chem 42 1396 (1950

Sys Cubic S G
a 7 95 b c A C
A B C Z mp
Ref Ibid

Dx Dm SS/FOM F6=1(022,27

ea nwB ey Sign 2V
Ref

CAS no 1344-28-1 alpha alumina trihydrate heated 1 hour at 80 ... moving dry air d and I values revised ... Stumpf in 1950 using corundum standard Al reflections are diffuse Also called alumina Mwt 101 96 Volume[CD] 502 40

2-theta	Int	h k l
37 4..	40	[illegible]
39 6..	20	[illegible]
40 224	30	[illegible]
45 75.	20	[illegible]
60 45.	10	[illegible]
67 30.	100	4 .

5 strong lines 397 ... 40/4 ... 27 ... 50 ... 0 ... 60/

CaF
2

Calcium Fluoride

Fluorite, syn

Rad CuKa1 Lambda 1 540598 Filter Mono d-sp Diff
Cutoff 17 7 Int Diffractometer I/Icor
Ref Natl Bur Stand (U S) Monoo 25 21 52 (1985)

Sys Cubic S G Fm3m (225)
a 5 46305(8) b c A C
A B C Z 4 mp
Ref Ibid

Dx 3 18 Dm SS/FOM F16=214(005 16)

ea nwB 1 433 ev Sign 2V
Ref Swanson, Tatge, Natl Bur Stand (U S) Circ 539 1 69 (1953)

Color Colorless
Peak height intensities The mean temperature of data collection was 24 5 C
The sample was obtained from the U S Geological Survey CAS no 7789-75-5
These data were recollected to add weak peaks missing in the earlier pattern
sigma(Iobs)=+/-2 CaF2 type Fluorite group fluorite subgroup W used
as internal standard PSC cF12 To replace 4-864 Structure reference
Bragg, W , Proc R Soc London, Ser A, 89 468 (1914) Additional powder
pattern reference Hanawalt J et al , Ind Eng Chem Anal Ed 10 457
(1938) Mwt 78 08 Volume[CDD] 163 04

2-theta	Int	h k l
28 267	92	1 1 1
32 761	<1	2 0 0
47 005	100	2 2 0
55 765	33	3 1 1
58 476	1	2 2 2
68 674	10	4 0 0
75 850	9	3 3 1
78 184	1	4 2 0
87 373	17	4 2 2
94 217	7	3 3 3
105 804	4	4 4 0
113 064	6	5 3 1
115 570	1	6 0 0
126 202	8	6 2 0
135 208	3	5 3 3
138 556	2	6 2 2

Strong lines 1 93/X 3 15/9 2 65/3 1 12/2 1 37/1 1 25/1 0 86/4 05/1

Na A F
5 3 14

Sodium Aluminum Fluoride

Chiolite syn

Rad CuKa1 Lambda 1 54056 Filter Mono d-sp
Cutoff Int Diffractometer I/Icor 1 15
Ref Natl Bur Stand (U S) Monogr 25, 16 63 (1979)

Sys Tetragonal S G P4/mnc (128)
a 7 0142(8) b c 10 400(3) A C 1 4827
A B C Z 2 mp
Ref Brosset, C , Z Anorg Allg Chem , 238 201 (1938)

Dx 3 00 Dm 3 00 SS/FOM F30=62(013,36)

ea nwb 1 3486 ey 1 3424 Sign - 2V
Ref Dana's System of Mineralogy, 7th Ed II 123

Color Colorless
Pattern taken a 25 C CAS no 1302-84-7 Made by treating NaHCO3 and Al powder with HF solution The precipitate was dried and heated to 450 C for 10 minutes Optical data on specimen from Miask Ilmen Mountains, Urals USSR Si used as internal standard PSC tP44 To replace 2-749 Mwt 461 87
Volume[CD] 511 67

2-theta	Int	h k l
15 238	20	1 0 1
17 031	30	0 0 2
17 661	10	1 1 0
24 787	6	1 1 2
25 391	18	2 0 0
28 706	3	1 0 3
29 716	18	2 1 1
30 710	100	2 0 2
34 454	7	0 0 4
36 176	8	2 2 0
36 697	50	2 1 3
39 081	6	1 1 4
39 456	8	3 0 1
40 246	8	2 2 2
40 625	12	3 1 0
41 584	20	3 1 1
43 276	2	2 0 4
44 370	2	3 1 2
45 258	25	2 1 4
45 402	20	1 0 5
46 636	12	3 2 0
46 789	7	3 0 3
50 859	25	2 2 4
52 111	23	4 0 0
52 749	5	3 1 5

2-theta	Int	h k l	2-theta	Int	h k l	2-theta	Int	h k l
52 819	2	4 1 0	55 521	3	3 3 0	64 [illegible]	[illegible]	1 0 [illegible]
53 897	2	3 2 3	56 909	6	4 1 2	65 [illegible]	1	4 [illegible] 3
54 330	6	3 1 4	56 837	[illegible]	4 2 0	65 [illegible]	1	3 2 [illegible]
54 838	[illegible]	4 1 1	59 439	[illegible]	2 0 6	66 [illegible]	[illegible]	4 3 0
55 [illegible]	[illegible]	4 0 2	61 740	28	4 2 2	67 [illegible]	4	3 3 4

Strong lines 2 91/X 2 33/5 5 20/3 2 00/3 1 79/3 1 55/3 1 75/2 5 81/2

Na F
4

Sodium Aluminum Fluoride

Rad CuKa Lambda 1 5418 Filter Ni d-sp D S -114 6
Cu off Int Visual I/Icor
Ref Carton Wanklyn, J Inorg Nuc Chem , 27 2461 (1965

Sys Tetragonal S G
a 4 00 b c 12 00 A C 8571
A B C Z mp
Ref Ibid

Dx Dm SS/FOM F30=1(107 220)

ea nwB ev Sign 2V
Ref

Data on unit cell agree with Howard J Am Chem Soc , 76 2041 (1954)] but not Mashovets et al , Dokl Akad Nauk USSR 113 1290 (1957) Probably due to coincidence and the presence o Na5Al3F14 (chiolite) and AlF3 reflections the Soviet authors' report unit cell a=3 48, c=6 29, S C =P4/mmm (isomorphous with Rb Tl, and K compounds) Chiolite is tetragonal with cell a=7 00 (half possible cell dimension of NaAlF4) AlF4 is pseudocubic cell a=3 51, alpha=88 deg 40' "The closely-related cell dimensions would account for the fac that these compounds appear to have many reflections in common with NaAlF4 Mwt 125 96 Volume[CD] 2352 00

2-theta	Int	h k l
11 932	30	1 1 1
15 185	30	0 0 2
17 005	50	1 0 2
17 725	20	2 2 0
18 547	10	2 0 0
20 639	80	2 1 2
22 902	20	3 2 0
25 901	30	1 1 3
25 354	100	4 0 0
29 256	100	3 0 3
29 757	30	0 0 4
30 699	80	3 3 2
36 131	30	3 1 4
38 628	50	1 1 5
39 312	10	2 0 1
40 078	10	2 1 4
40 625	10	3 0 4
41 544	50	0 0 6
43 016	60	4 1 2
45 378	50	0 1 6
46 459	60	7 1 1
48 763	30	5 0 4
49 584	30	3 1 6
50 614	100	5 1 5
52 006	40	6 0 2

2-theta	In	h k l	2-theta	Int	h k l	2-theta	Int	h k l
55 913	80	2 0 1	61 706	40	7 4 4			
[illegible]	[illegible]	0 1 5						
[illegible]	[illegible]	0 2 6						
[illegible]	[illegible]	0 0 1						
[illegible]	[illegible]	0 1 7						

Strong lines 3 51/X 3 04/1 1 80/2 4 30/8 2 91/6 1 73/8 1 55/8 2 10/6

Al C
- 3

Aluminum Carbide

Rad CuKa1 Lambda 1.540598 Filter Mono d-sp Diff
Cuto 17.7 Int Diffractometer I/Icor
Ref Natl Bur Stand (U.S.) Monogr 25, 21 7 (1984)

Sys Rhombohedral (Hex) S.G. R-3m (166)
a 3.3388(3) b c 24.996(3) A C 7.4865
A B C Z 3 mp
Ref Ibid

Dx 2.972 Dm SS/FOM F29=61(.012,39)

ea nwB e Sign 2V
Ref

Color Dark greenish yellow-brown
Peak height intensities. The mean temperature of data collection was 23.9 C.
The sample was obtained from Materials Research Corp., Orangeburg, New York, USA. CAS no. 12069-85-1. Rhombohedral cell: a=8.552, alpha=22.51.
Sigma(lobs)=+/-.5. A 403 type. Ag FP used as internal standards. PSC: hR. To replace 11-625. Structure reference: Jeffrey, G., Wu, V., Acta Crystallogr., 20, 538 (1966). Mwt: 143.96. Volume[CD]: 241.31.

2-theta	Int	h k l
10.604	2	0 0 3
21.305	10	0 0 6
31.113	54	1 0 1
31.740	100	0 1 2
35.222	13	0 0 9
38.850	54	0 1 5
40.085	83	1 0 7
42.575	10	0 1 8
43.431	49	0 0 12
48.075	23	1 0 10
51.057	13	0 1 11
55.043	86	2 0 10
57.532	<1	1 0 13
59.624	<1	1 1 6
60.921	18	0 1 14
64.525	4	0 2 1
64.875	10	2 0 2
65.166	6	1 1 9
67.362	9	2 0 5
68.163	<1	1 0 16
70.164	11	2 2 7
71.979	10	0 1 17
72.477	28	1 1 12
75.980	3	0 2 10
78.342	2	2 0 11

2-theta	Int	h k l	2-theta	Int	h k l	2-theta	Int	h k l
8.324	5	1 0 19						
88.555	5	2 0 14						
89.745	5	1 1 1						
90.047	7	1 2 2						

Strong lines: 2.82/X 1.07/9 2.25/6 2.87/5 2.50/5 2.08/5 .30/3 1.89/2

4- 87 JCPDS-ICDD Copyright (c) 1994 PDF-2 Set 1-44 database Rad = 1 54060 Quality *

Al

Aluminum

Aluminum, syn [NR]

Rad CuKa1 Lambda 1 54056 Filter Ni d-sp
Cutoff Int Diffractometer I/Icor 3 61
Ref Swanson Tatge, Natl Bur Stand (U S) Circ 539, 4 11 (1955

Sys Cubic S G Fm3m (225)
a 4 0494 b c A C
α B β Z 4 γ
Ref Ibid

D 2 70 Dm SS/FOM F9=53(014 9)

ε nωb ηr Sign 2V
Ref

Color Light gray metallic
Pattern at 25 C CAS no 7429-90-5 The material used for the NBS sample wa
a melting point standard sample of aluminum prepared at NBS Gaithersburg
Maryland USA The chemical analysis (/) Si 0 011 Cu 0 006 Fe 0 00, Ti-
0 C001, Zr 0 C03, Ga 0 C04 Mn 0 0000, S 0 0001 Al 99 9+ (by di erence)
Mineral species of doubtful validity Am Mineral 65 205 (1980)
Cu type Gold group gold subgroup PSC cF4 Mwt 26 98 Volume [CD]
mp 40

2-theta	Int	h k l
38 473	100	1 1 1
44 740	47	2 0 0
65 135	22	2 2 0
78 230	24	3 1 1
82 438	7	2 2 2
99 081	2	4 0 0
112 046	8	3 3 1
116 574	8	4 2 0
137 463	8	4 2 2

Strong lines 2 34/X 2 02/5 1 22 C 1 43/2 0 93/1 0 8,/1 0 82/1 1 17/1

26-1079 JCPDS-ICDD Copyright (c) 1994 PDF-2 Sets 1-44 database Rad = 1 54060 Quality C

C

Carbon

Graphite-3P, syn [NR]

Rad CuKa Lambda 1 54178 Filter d-sp Calculated
Cutoff Int Calculated I/Icor
Ref Holcombe, Private Communication (1974)

Sys Rhombohedral (Hex) S G P3 (146)
a 2 456 b c 10 044 A C 4 0896
A B C mp
Ref Holcombe, U S AEC Oak Ridge Y-12 Plant Report [illegible] (1973)

Dx 2 28 Dm SS/FOM F16=72(009 24)

ea nwb ev Sign 2V
Pef

Peak height intensities CAS no 7440-44-0 C type PSC hR2 Mwt 12 01
Volume[CD] 52 47

2-theta	Int	h k l
26 603	100	0 0 3
43 451	11	1 0 1
46 334	9	0 1 2
54 794	6	0 0 6
56 669	4	1 0 4
63 687	2	0 1 5
77 699	4	1 1 0
80 678	1	1 0 7
83 839	6	1 1 3
87 297	1	0 0 9
93 891	1	0 1 8
102 142	4	1 1 6
103 943	1	0 0 12
107 713	4	1 1 9
147 971	1	2 1 1
152 047	1	1 2 2

Strong lines 3 35/X 2 08/1 1 56/1 1 67/1 1 15/1 0 82/1 1 23/1 0 99/1

APPENDIX B

Z = 0			
Points	Bx(G)	By(G)	Bz(G)
A	0 45	4 6	3 43
B	-1 53	0 83	-1 13
C	-0 68	-2 56	-4 53
D	1 4	-3 76	-2 46
E	2 7	-0 35	-0 06
F	4 56	3 86	-0 16
G	3 76	3 43	-2 46
H	4 4	-0 53	1 66
I	2 36	-5 93	4 7
J	4	-2 76	7 43
K	5 13	-0 06	1 67
L	3 6	1 03	-3 87

Z = 1 1cm			
Points	Bx(G)	By(G)	Bz(G)
A	-0 53	4 67	2 07
B	-2 33	1	-1 07
C	-1 97	-4 17	-3 27
D	3 33	-8 53	-1 9
E	4 73	-1 87	0 27
F	5 13	5 73	0 93
G	2 7	4 87	-1 7
H	3 47	0 1	0 97
I	1 07	-8	5 17
J	5 2	-2 9	7 7
K	7 03	0 3	1 4
L	5 03	0 73	-3 1

Measured magnetic fields in the cell at Cd = 0 9 A/cm^2, T=84^{0}C and Z=0,1 1cm

Z = 0			
Points	Bx(G)	By(G)	Bz(G)
A	-0 4	3 03	3 23
B	-1 73	1	0
C	-0 47	0 33	-3
D	-0 8	-3	-2 43
E	0 9	1 6	0 87
F	2 87	3 9	1 77
G	3 07	2 57	-1 5
H	3 57	1 87	0 47
I	2 27	-4 23	4 97
J	3 97	-0 8	6 2
K	4 6	0 6	0 67
L	2 83	1 63	-2 4

Z = 1 1cm			
Points	Bx(G)	By(G)	Bz(G)
A	0	3 87	2 2
B	-1 97	1	-0 67
C	-1 6	-3 67	-2 9
D	3 27	-7 07	-1 73
E	5 13	-0 73	0 17
F	5 13	5 1	1
G	4	3 07	-1 2
H	4 47	0 63	0 53
I	1 57	-6 17	3 37
J	4 17	-1 67	5
K	5 23	0 3	0 77
L	3 9	0 93	-2 13

Measured magnetic fields in the cell at Cd = 0 7 A/cm^2, T=84^{0}C and Z=0,1 1cm

Z = 0			
Points	Bx(G)	By(G)	Bz(G)
A	0 57	3 2	2 9
B	-1 2	-0 75	-0 6
C	-0 2	-1 25	-2 9
D	0 4	-3	-1 6
E	2 9	-0 95	0 45
F	4 15	2 95	0 5
G	2 95	2 1	-0 5
H	2 6	0 55	1
I	0 6	-4 2	4 45
J	4 1	-2 2	8 05
K	4 6	0 1	1 55
L	3	0 2	-1 9

Z = 1 1cm			
Points	Bx(G)	By(G)	Bz(G)
A	0 1	4 9	2 15
B	-2 6	-1 55	-0 65
C	-1 3	-2 1	-2 65
D	2	-5 5	-1 85
E	4 2	-1 6	0 4
F	6 2	4 5	0 95
G	3 9	2 9	-1 4
H	3 1	0 9	0 5
I	0 1	-6 1	3 8
J	5 05	-2 15	6 2
K	5 05	1 1	1 15
L	3 6	0 45	-1 9

B 4 Measured magnetic fields in the cell at Cd = 0 7 A/cm^2, T=95^{o}C and Z=0,1 1cm

Z = 0			
Points	Bx(G)	By(G)	Bz(G)
A	-0 37	3 47	3 13
B	-1 53	-0 5	-0 53
C	-0 57	-1 57	-3 43
D	0 13	-3 57	-2 03
E	3 17	-1	0 43
F	4 3	3 77	1 1
G	3 03	2 17	-1 2
H	3 03	0 87	1 13
I	0 03	-5 07	4 9
J	5 47	-2 2	8 7
K	5 2	0 37	1 77
L	3 53	0 27	2 57

Z = 1 1cm			
Points	Bx(G)	By(G)	Bz(G)
A	0	4 87	2 13
B	-2 47	-0 63	-0 87
C	-1 53	-2 33	-2 93
D	0 77	-6 33	-2 03
E	4 33	-2	0 13
F	7 47	4 53	0 57
G	3 03	3 8	-1 06
H	3 3	0 96	0 7
I	-0 33	-7 03	4 13
J	5 7	-3 67	7 33
K	5 5	1 5	1 2
L	4 3	0 43	-2 37

Measured magnetic fields in the cell at Cd = 0 8 A/cm^2, T=95^{0}C and Z=0,1 1cm

Z = 0			
Points	Bx(G)	By(G)	Bz(G)
A	0	4 4	3 03
B	-1 9	-0 53	-1 17
C	-0 83	-2 06	-3 93
D	0 4	-4 37	-2 17
E	3 93	-1 93	0 7
F	5 33	3 53	0 53
G	4 1	2 03	-1 67
H	4 07	-0 43	2 57
I	0 8	-3 93	6 03
J	5 83	-2 23	9 3
K	6 13	-0 73	1 57
L	4	-0 2	-3 17

Z = 1 1cm			
Points	Bx(G)	By(G)	Bz(G)
A	-0 73	6 13	2 47
B	-3	0	-0 67
C	-1 93	-3 53	-3 4
D	2 43	-8 43	-1 03
E	5 03	-3 03	0 7
F	7 43	6 67	1 97
G	3 5	4 6	-0 93
H	5 6	-0 6	2
I	4	-8	5 1
J	4 5	-1 83	7 2
K	6 4	-1 67	1 8
L	5 97	1 4	-2 3

Measured magnetic fields in the cell at Cd = 0 9 A/cm^2, T=95^{0}C and Z=0,1 1cm

Z = 0			
Points	Bx(G)	By(G)	Bz(G)
A	0	2 63	2
B	-0 87	-1 9	-1 33
C	-0 33	-1 47	-3 4
D	1 23	-3 2	-2 3
E	2 43	-1 2	0 23
F	3 3	3 13	1 13
G	2 3	2 73	-1 27
H	0 63	2 8	1 67
I	-0 17	-4 73	5 9
J	3 37	-2 2	6 97
K	4 6	-1 77	1 2
L	4 4	0 63	2 53

Z = 1 1cm			
Points	Bx(G)	By(G)	Bz(G)
A	-1	4 13	0 83
B	-2 5	-4 4	-1 37
C	0	-2 4	-3 2
D	1 3	-5 33	-2 4
E	3 7	-6 53	0
F	3 73	4 53	1 03
G	1 6	4 2	-1 17
H	0	-1 9	0 6
I	-0 33	-5 77	4 37
J	3 2	-1 8	5 77
K	4 63	-3 5	1 67
L	5 1	0 83	-2 6

Measured magnetic fields in the cell with a missing anode, at Cd = 0 7 A/cm^2, T=84^{0}C and Z=0,1 1cm

Z = 0			
Points	Bx(G)	By(G)	Bz(G)
A	-0 4	3 9	2 5
B	-1 17	-1 77	-1 2
C	-0 3	-1 83	-4
D	1 3	-3 73	-2 2
E	2 67	-2 37	0 7
F	4 83	3 77	1 13
G	2 93	2 9	-1 33
H	2 97	-1 1	1 23
I	1 13	-5 2	6 83
J	4 1	-2 2	7 7
K	5 4	-1 37	1 37
L	4 1	-0 1	-3 17

Z = 1 1cm			
Points	Bx(G)	By(G)	Bz(G)
A	-0 6	5 73	1 6
B	-2 8	-2 9	-1 6
C	-1 2	-3 83	-3 93
D	3 9	-7 1	-2
E	5 1	-6 53	0 37
F	6 2	5 8	1 53
G	4 7	3 73	-1 2
H	3 73	-3 66	1 43
I	1 4	-6 3	4 9
J	3 8	-1 93	6 53
K	5 6	-2 53	1 73
L	5 03	0	-2 43

Measured magnetic fields in the cell with a missing anode, atCd = 0 8 A/cm^2, T=84^{0}C and Z=0,1 1cm

Z = 0			
Points	Bx(G)	By(G)	Bz(G)
A	-0 53	3 03	2 67
B	-1 43	-0 73	-0 5
C	-1 23	-1 83	-3 9
D	1 43	-4 23	-2 77
E	2 3	-1 23	0 6
F	1 93	4 77	1 23
G	2 83	3 53	-1 4
II	1 2	0 4	0 63
I	-1 6	-6 1	8 3
J	5 67	-2 7	10
K	6 5	0 4	2 3
L	4 23	0 4	-3 0

Z = 1 1cm			
Points	Bx(G)	By(G)	Bz(G)
A	-0 97	4 1	2 13
B	-2 5	-1 2	-0 83
C	-1 4	-3 17	-3 6
D	2 47	-7 2	-2 4
E	3 63	-2 93	0 3
F	4 7	5 6	1 13
G	2 5	4 6	-1 57
H	0 00	0 6	0 53
I	-4 5	-6 67	6 97
J	6 23	-4 17	9 1
K	6 47	0 03	2 03
L	4 97	1 3	-2 83

Measured magnetic fields in the cell with a missing anode, at Cd = 0 9 A/cm^2, T=84^{0}C and Z=0,1 1cm

REFERENCES

1) A R Burkin, Production of Aluminium and Alumina Published by John Wiley & Sons, 20(1987)
2) T A Utigard, Light Metals, (1993)239
3) R A Mohr, Light Metals, (1982)595
4) Halvor Kvande, JOM, Feb (1997)21
5) H Kvande, J J J Chen and W E Haupin, Light Metals, (1994)429
6) M Segartz and C Droste, Light Metals, (1994)313
7) Frach D Tarapore, Light Metals, (19)541
8) P Verstreken, JOM, Nov (1997)43
9) E W Dewing, Met Trans B , 22B Apr (1991)177
10) Q Zhuxian, L Jingjiang, C Xiaoli, K Grjotheim, H Kvande and H Oye, Ligl Metals(1994)463
11) Xiaoling Liu, Simon P George and Valerie A Wills, Light Metals, (1994)359
12) Neal Wai-Poi and Barry J Welch, Light Metals, (1994)345
13) S Roselth, R Hovland, and O Kobbeltvedt, Light Metals (1994)351
14) E H Howard, J Am Chem Soc , 76(1954)2041
15) Halvor Kvande, NTH-Trykk Publication, Univ of Trondheim, Norway (1979)
16) W Haupin, JOM, 11(1991)28
17) G T Homes, D C Fisher and W D Ludwig, Light Metals, (1980),401
18) J Bouteillon, J C Poignet, and J J Rameau, JOM, Feb (1993)28
19) A T Tabereaux, T R Alcom and Luke Trembley, Light Metals (1993)221
20) A J Calandra, C M Ferro and C E Castellano, Electrochemical Acta, 25(1980)2(
21) A J Calandra, C E Castellano, C M Ferro and O Lobo, Light Metal, (1982)345
22) J D Edwards and T A Moormann, Chem Met Engg, 24(1921)61
23) J Thonstad and Y-X Liu, Light Metal, (1981)303
24) R Schadinger, Alumino, 22(1953)691
25) J H Kent, JOM, 22(1970)30
26) J Szekely, J W Evans, J K Brimacombe, The Mathematical And Physical Modelli of Primary Metals Processing Operation, John Wiley and Sons, (1988)229

27) David Belitskus and Daniel J Danka JOM Nov (1988)28
28) M B Dell, JOM, Mar (1967)14
29) M B Dell, R W Peterson, and J N Rumble, JOM, Sep (1968)55
30) M B Dell, JOM, Jun (1971)18
31) M Benjamin Dell, Met TransB, 15B Jun (1984)277
32) J Waddington, Extractive Metallurgy of Aluminium Aluminium, 2(1962)435
33) Barry J Welch, JOM, Nov (1988)19
34) O S Chaudhary and R N Prasad, JOM, Nov (1992)9
35) W R Hale, JOM, 41(11)(1989)20
36) Alton T Tabereaux, JOM, Nov (1992)20
37) Jilai Xue and Harald A Oye, Light Metal, (1994)211
38) O Fujishima, M Takasawa and K Wakaizumi, Y Arita and H Ikeuchi, Light Met (1982)559
39) J E Oxley and R J Smialek, JOM, Aug (1997)22
40) W Capitaine, Light Metal, (1982)409
41) A R Johnson, JOM, Oct (1988)11
42) S D Lympany and J W Evans, Met Trans B, 14B Mar (1983)63
43) K J Fraser, D Billinghurst, K L Chen and J T Kenny, Light Metal, (1989) 219
44) Donald P Ziegler, Light Metal, (1991)363
45) J N Bruggeman and D J Danka, Light Metal (1990)203
46) A Valles and V Lenis, Light Metal (1995)305
47) Per Utne, Light Metal, (19)359
48) W E Haupin JOM, Jul (1971)41
49) J W Evans, Y Zundelevich, and D Sharma, Met Trans B, 12B Jun (1981) 353
50) R Moreau and J W Evans, J Electrochem Soc , 131(1984)2251
51) S K Banerjee, PhD Thesis, Univ of California, USA
52) J J Brown Jr , S S Lee, K S Lei and P Xu, Light Metals, (1984) 841
53) H C Lee, C Vives and J W Evans, Met Trans B, 15B(1984) 734
54) S K Banerjee and J W Evans, Met Trans B, 21B Feb (1990) 59

MME-1998-M-SRI-EXP